UNIVERSIDAD AUTÓNOMA CHAPINGO

POSGRADO EN INGENIERÍA AGRÍCOLA Y USO INTEGRAL DEL AGUA

MEDICIONES CON UN DENDRÓMETRO PARA OPTIMIZAR EL USO DEL AGUA Y DETECCIÓN DE ENFERMEDADES EN ÁRBOLES DE MANGO

TESIS DE GRADO

COMO REQUISITO PARCIAL PARA OBTENER EL GRADO DE:

MAESTRO EN INGENIERÍA AGRÍCOLA Y USO INTEGRAL DEL AGUA

PRESENTA:

JESÚS ANTONIO GARCÍA MARTÍNEZ

BAJO LA SUPERVISIÓN DE:

DR. FEDERICO FÉLIX HAHN SCHLAM

Chapingo, Estado de México, Diciembre del 2019

MEDICIONES CON UN DENDRÓMETRO PARA OPTIMIZAR EL USO DEL AGUA Y DETECCIÓN DE ENFERMEDADES EN ÁRBOLES DE MANGO

Tesis realizada por **JESÚS ANTONIO GARCÍA MARTÍNEZ** bajo la dirección del Comité Asesor indicado, aprobada por el mismo y aceptada como requisito parcial para obtener el grado de:

MAESTRO EN INGENIERÍA AGRÍCOLA

Y USO INTEGRAL DEL AGUA

DIRECTOR: ______________________________

DR. FEDERICO FÉLIX HAHN SCHLAM

ASESOR: ______________________________

DR. RAÚL NIETO ÁNGEL

ASESOR: ______________________________

DR. RAMÓN ARTEAGA RAMÍREZ

,

CONTENIDO

ÍNDICE DE CUADROS

CAPÍTULO DOS

CAPÍTULO CUATRO

CAPÍTULO CINCO

CAPÍTULO SEIS

ÍNDICE DE FIGURAS

CAPÍTULO DOS

CAPÍTULO TRES

CAPÍTULO CUATRO

CAPÍTULO CINCO

CAPÍTULO SEIS

ANEXOS

ACRÓNIMOS

AS: Pendiente de la tarde
CO_2: Dioxido de carbono
DAF:. Días posteriores a la floración
ET: Evapotranspiración
ETc: Evapotranspiración máxima en condiciones estándar del cultivo
ETo: Evapotranspiración de referencia
k_c: Coeficientes de cultivo
MCD: Crecimiento diario del tronco
MERRA-2: Modern-Era Retrospective Analysis for Research and Applications version 2
MND: Mínima contracción diaria
MS: pendiente de la mañana
MXD: Máxima contracción diaria
NS: Pendiente de la noche
PRD: Secado parcial de la zona radicular
RDC: Riego deficitario controlado
SINA: Sistema nacional de información del agua

DEDICATORIAS

A mis padres, Antonio Garcia Martínez e Imelda Martinez Cuevas

A mis hermanos, Raúl y Naomi

À ma copine Fannie

A mi director y amigo, el Dr. Federico F. Hahn S.

A mis amigos y compañeros de la maestría, en especial a:

Carlos, Gama, Juan, David, Raúl y Ricardo

Por todo su apoyo

Muchas gracias

Chuy

AGRADECIMIENTOS

Al Consejo Nacional de Ciencia y Tecnología (CONACyT) por el apoyo económico para desarrollar mis estudios de posgrado y estancia académica en el Instituto Valenciano de Investigaciones Agrarias (IVIA).

A la Universidad Autónoma Chapingo y al Posgrado en Ingeniería Agrícola y Uso Integral del Agua (IAUIA), por darme la oportunidad de realizar mis estudios de posgrado.

A mis asesores, por su valioso tiempo en la revisión y aprobación del proyecto, y en especial al Dr. Federico Félix Hahn S. por todo su tiempo brindado en apoyo de la realización de este proyecto; aportando conocimiento sabiduría y experiencia.

DATOS BIOGRÁFICOS

Datos personales

Nombre: Jesus Antonio García Martínez

Fecha de nacimiento: 7 de abril de 1993

Lugar de nacimiento: Minatitlán, Veracruz

CURP: GAMJ930407HVZRRS08

Profesión: Ingeniero Mecánico

Cedula Profesional: 10927280

Desarrollo académico

Bachillerato: COBAEV Plantel 08, 2008-2011 Cosoleacaque

Licenciaturas:

Ingeniería Mecánica, UV, 2011-2016, Coatzacoalcos

Ingeniería en sistemas de producción agropecuarios, UV, 2013-2016, Acayucan

RESUMEN GENERAL

Mediciones con un dendrómetro para optimizar el uso del agua y detección de enfermedades en árboles de mango

El dendrómetro es un instrumento que registra variaciones compuestas por ritmos diurnos de contracción y expansión en el tallo del árbol. Las variables obtenidas por el dendrómetro son la máxima contracción diaria (MXD), mínima contracción diaria (MND), pendiente de la mañana (MS), pendiente de la tarde (AS), pendiente de la noche (NS) y crecimiento diario del tronco (MCD). Un dendrómetro capaz de detectar el estado hídrico del árbol de mango fue diseñado con un microcontrolador que optimiza el consumo energético. El experimento se ejecutó del 20 de abril al 20 de agosto del 2019, donde se monitoreo las variaciones en el tronco durante la floración y fructificación ante diferentes tratamientos de riego (riego al 100%, estrés, y riego deficitario). Así mismo, se evaluaron las mediciones del dendrómetro en árboles infectados por Fusarium en brotes e inflorescencias y su respuesta después de aplicar una solución de jabón con azufre a los árboles. El dendrómetro mostró ser eficiente utilizando rutinas de ahorro de energía, brindando 8 días de autonomía; al censar cada 10 minutos con 10 repeticiones por ciclo. Al comunicarse con una App celular, permite la transmisión del dendrómetro, la cual gráficamente indica si es necesario regar los árboles. El experimento de riego demostró que al regar un día y suspender el siguiente, el MXD y el MND no presentan diferencias estadísticas con la evapotranspiración (ET) de los árboles y durante el riego deficitario controlado (RDC). Durante el estrés, las mediciones de MXD y MND mostraron correlaciones exitosas con algunas variables climáticas. La aplicación de la solución de azufre más jabón en polvo fue eficaz durante las temporadas de riego y lluvia, pero pobre para los árboles bajo condición de estrés. Los valores MXD y MND mostraron cambios en la salud del árbol.

Palabras clave: Dendrómetro, déficit de irrigación, micro aspersión, aplicación de teléfono inteligente, Cámara térmica, Ahorro energético, Fusarium.

Tesis de Maestría en Ingeniería, Posgrado en Ingeniería Agrícola y Uso integral del Agua, Universidad Autónoma Chapingo

Autor: Jesús Antonio García Martínez
Director: Dr. Federico Félix Hahn Schlam

GENERAL ABSTRACT

Measurements with a dendrometer to optimize water use and disease detection in mango trees

The dendrometer is an instrument that variations composed of diurnal rhythms of contraction and expansion in the stem of the tree. The variables obtained by the dendrometer are the maximum daily contraction (MXD), minimum daily contraction (MND), morning slope (MS), afternoon slope (AS), night slope (NS) and daily trunk growth (MCD). A dendrometer capable of detecting the water state of the mango tree was designed with a microcontroller that optimizes energy consumption. The experiment was run from April 20 to August 20, 2019, where the variations in the trunk were monitored during flowering and fruiting before different irrigation treatments (100% irrigation, stress, and deficit irrigation). Likewise, the measurements of the dendrometer in trees infected by Fusarium in shoots and inflorescences and their response after applying a solution of soap with sulfur to the trees were evaluated. The dendrometer showed to be efficient using energy saving routines, providing 8 days of autonomy; when censoring every 10 minutes with 10 repetitions per cycle. When communicating with a cellular App, it allows the transmission of the dendrometer, in which it graphically indicates if it is necessary to water the trees. The irrigation experiment showed that when watering one day and suspending the next, the MXD and the MND do not present statistical differences with the evapotranspiration (ET) of the trees and during the controlled deficit irrigation (RDC). During stress, the MXD and MND measurements showed successful correlations with some climatic variables. The implementation of the solution of sulfur soap powder was effective during seasons of irrigation and rain, but poor for trees under condition of stress. The values MXD and MND showed changes in tree health.

Keywords: Dendrometer, irrigation deficit, micro spray, smartphone application, Thermal camera, Energy saving, Fusarium

Engineering Master Thesis, Postgraduate in Agricultural Engineering and Integrated Water Use, Autonomous University Chapingo.
Author: Jesús Antonio García Martínez
Thesis Advisor: Dr. Federico Félix Hahn Schlam

1 INTRODUCCIÓN GENERAL

La producción mundial de mango es superior a las 40 millones de toneladas (Mitra, 2016). México en el 2018 logro posicionarse como el quinto productor de mango a nivel mundial, produciendo 1.8 millones de toneladas (Srivastava, 2018). Otros países productores de mango son India (40%), China (11%), Kenia (7%), Tailandia (6%), Indonesia (6%), Pakistán (6%), México (5%), Brasil (3%), y Bangladesh (2%). Además, las plantaciones de mango cultivadas con técnicas orgánicas en México buscan satisfacer el mercado de consumidores que están en busca de productos sin químicos y que protegen al medio ambiente. Es estimado que más de 110 000 agricultores utilizan prácticas orgánicas en el país, por encima de cualquier otro país del mundo (Alberts-Organics, 2016).

En las plantaciones de mango normalmente se siembran entre 100 y 200 árboles por hectárea, y los árboles crecer hasta 10 m de altura en ambientes adecuados, produciendo entre 4 y 9 toneladas por hectárea. Existe un gran interés en introducir de plantaciones de hasta 4000 árboles por hectárea para aumentar la productividad de 12 a 22 toneladas por hectárea (Menzel & Le Lagadec, 2017).

La programación del riego implica determinar con precisión tanto la temporización del riego y la cantidad de agua a aplicar, guardando una relación entre el riego y la productividad (Jensen, Robb, & Franzoy, 1970). El uso de estrategias de ahorro de agua son una alternativa para escenarios con escasez de agua (Caspari, Neal, & Alspach, 2004). El suministro de agua es crítico durante la floración, hasta la etapa de cosecha de la fruta. Debido a esto el cultivo de mango se riega en exceso para evitar la deshidratación, promoviendo el crecimiento de las plantas. Sin embargo, esta práctica puede provocar ataque de hongos (Gamliel-Atinsky et al., 2009), pudrición del tallo (Johnson, Cooke, Mead, & Wells, 1991) y estrés anaeróbico en las raíces (Rao, Laxman, & Shivashankara, 2016). Por otro lado el déficit de agua podría provocar una absorción deficiente de nutrientes (Shaaban & Shaaban, 2012), crecimiento inhibido, un estado fenológico perturbado, una tasa de fotosíntesis deprimida, lo cual reduce la producción final de frutos (Durán et al., 2018).

Ante esta problemática, investigadores recomiendan aplicar estrategias de riego conducentes a una agricultura de precisión, como son las técnicas micro-riego por aspersión (Koumanov, Hopmans, Schwankl, Andreu, & Tuli, 1997), riego por desecación parcial del sistema radicular (Dry, Loveys, & During, 2000) o riego deficitario controlado (Fukuda et al., 2013); Estas técnicas pueden proporcionar un 50% de ahorro en el consumo de agua (Nortes, 2008). Aunque las estrategias de riego deficitario implican que el agua suministrada sea reducida a una fracción de la evapotranspiración potencial (Rodríguez et al., 2018), en determinados períodos del ciclo del cultivo, la producción y calidad de las cosechas se ven poco afectadas (Chenafi et al., 2016).

Uno de los principales problemas de las zonas productoras de mango es la escoba de bruja (Michel et al., 2013), causada por los hongos *Fusarium oxysporum* y *F. subglutinans* (Freeman, Maimon, & Y., 2000). Además, una nueva especie reportada como *Fusarium mangiferae*, está relacionada con las cepas que eran previamente identificados como *F. subglutinans* (Britz et al., 2002). En México existe en todos los estados productores y puede reducir en un 60% la productividad (Noriega et al., 2005). Los síntomas de la enfermedad incluyen la pérdida de la dominancia apical, hinchazón de las yemas vegetativas, falta de cuajado de los frutos, extenso aborto de la fruta y en las panículas se observan respuestas de estrés del árbol.

El estado hídrico del árbol puede obtenerse a través de mediciones directas e indirectas. los métodos indirectos estiman las necesidades hídricas del cultivo basándose en la evapotranspiración de referencia (ETo) y en la utilización de coeficientes de cultivo (k_c) (Kamienski et al., 2018). La precisión con la que se obtiene la ETo a partir de los diferentes modelos, se relaciona estrechamente con el tipo de cultivo, la precisión y la resolución de los sensores utilizados (Ahmadpari, Shokoohi, Lalabadi, Gerdini, & Ebrahimi, 2019). En consecuencia, la mayoría de los modelos meteorológicos están desarrollados para cultivos de cobertura, presentando problemas de representatividad para frutales (Mbangiwa, Savage, & Mabhaudhi, 2019). Las plantas son un indicador directo de su estado hídrico y fisiológico, porque en ellas integran efectos del abasto de agua que va desde el suelo hasta que sale a la atmosfera (Galindo, 2015). Estas mediciones presentan una relación directa con la productividad de los cultivos (Goldhamer & Fereres, 2001).Así mismo, (Gil & Maldonado, 2012) han confirmado la respuesta al estrés hídrico a través de las contracciones y las dilataciones diarias del diámetro del tronco.

Los dendrómetros son instrumentos que a través del cambio en el recorrido de un vástago miden el diámetro del tronco de un árbol, obteniendo la evaluación diaria del estado hídrico del tallo y su respuesta a diferentes condiciones ambientales (Giovanelli et al., 2007). Este tipo de datos son útiles para la programación del riego, la evaluación de la calidad del sitio, y el desarrollo de modelos (Drew & Downes, 2009). Ante la necesidad de contar con un dendrómetro sensible debe ser capaz de detectar el estado hídrico del árbol de mango en respuesta a distintas estrategias de riego y la presencia anticipada de escoba de bruja se abordaron los siguientes objetivos: Diseñar y construir un dendrómetro de fácil instalación en aboles frutales, alimentado por un sistema panel solar-batería capaz de proporcionar una autonomía de un año. Diseñar una

App con el fin de que un productor pueda usar los resultados obtenidos del dendrómetro en forma práctica con la finalidad de conocer el estado hídrico de los árboles de mango; Obtener conocimiento para evaluar los datos obtenidos por el dendrómetro bajo estrés, riego normal y riego deficitario correlacionados contra variables climáticas; Evaluar las curvas diarias obtenidas por el dendrómetro durante el periodo de floración y fructificación para arboles afectados por escoba de bruja (F. oxysporum) ante diferentes cantidades de riego.

El presente trabajo está conformado por 6 capítulos: una introducción general, una revisión de literatura y 4 artículos científicos enviados para su publicación en diferentes revistas científicas nacionales e internacionales:

Capítulo 1, se presenta la introducción general del proyecto planteándose el problema de estudio y su importancia.

Capítulo 2, se aborda información referente al problema de investigación, induciendo a conceptos y las diferentes metodologías que se encuentran para darle mayor comprensión.

Capítulo 3, consta del primer artículo presentado en el congreso de la ASABE titulado "Smartphone warns producers when to irrigate mango trees". Proporciona gráficamente el comportamiento de los arboles debido a la información proporcionada por el dendrómetro. Este captura los datos proporcionados por un sensor lineal, los cuales se almacenan en una memoria SD y pueden ser transmitidos a través de bluethooth. El sistema está configurado para monitorear las variaciones del tamaño del tronco cada 10 minutos. La aplicación de un teléfono inteligente, permite la activación de transmisión del dendrómetro, en la cual se indica si es necesario regar los árboles.

Capítulo 4, consta del segundo artículo titulado "Manejo autónomo de baterías de litio usadas por dendrómetros instalados en bosques o huertas remotas". Se realizó el manejo autónomo de baterías de litio usadas por el dendrómetro evaluando la eficiencia del hardware y la programación del microcontrolador para optimizar el consumo energético del dendrómetro.

Capítulo 5, consta del tercer artículo enviado a revisión titulado "Mango dendrometeter response under different irrigation regimes". Se evaluaron variables como; la pendiente de la mañana (MS), la pendiente de la tarde (AS), la máxima contracción del diámetro (MCD) y la mínima contracción del diámetro (MND). Estas variables se utilizaron para analizar las diferentes respuestas producidas por el mango, con diferentes tratamientos de riego

Capítulo 6, consta del cuarto artículo enviado a revisión titulado “Plant based sensors detect F. oxyporum on mango trees”. Se compararon sensores de plantas tales como dendrómetros, sondas magnéticas de las hojas, termómetro de temperatura por infrarrojos y fotografías térmicas. Siendo utilizados para detectar la infección por Fusarium en un huerto de mango. Los sensores ayudaron a obtener una comprensión más profunda de cómo el agua se mueve dentro del árbol y cómo la evapotranspiración se lleva a cabo en virtud de la infección por Fusarium.

1.1 Referencias

Ahmadpari, H., Shokoohi, E., Lalabadi, N. M., Gerdini, M. S., & Ebrahimi, M. (2019). Assessment of Potential Evapotranspiration Estimation Methods in the Fasa Region. *Specialty Journal of Agricultural Sciences*, *5*(2), 56–66. Recuperado de https://sciarena.com/storage/models/article/b9MK5taJsrPhp5Irh7lXqmgI58R7FlFRIQFXOyz6mHJUkPpnbP8AKUIbzxgl/assessment-of-potential-evapotranspiration-estimation-methods-in-the-fasa-region.pdf

Alberts-Organics. (2016). Organic Produce from Mexico. Recuperado de http://albertsorganics.com/resources/merchandising-tips/organic-produce-mexico.

Britz, H., Steenkamp, E. T., Coutinho, T. A., Wingfield, B. D., Marasas, W. F. O., & Wingfield, M. J. (2002). Two new species of Fusarium section Liseola associated with mango malformation. *Mycologia*, *38*(1), 109–114. https://doi.org/doi:10.1080/15572536.2003.11833199.

Caspari, H. W., Neal, S., & Alspach, P. (2004). Partial Rootzone Drying - A new deficit irrigation strategy for apple? En *Acta Horticulturae* (Vol. 646, pp. 93–100). International Society for Horticultural Science. https://doi.org/10.17660/ActaHortic.2004.646.10

Chenafi, A., Monney, P., Arrigoni, E., Boudoukha, A., Carlen, C., & . (2016). Influence of irrigation strategies on productivity, fruit quality and soil-plant water status of subsurface drip-irrigated apple trees, *71*(2). https://doi.org/10.1051/fruits/2015048

Drew, D. M., & Downes, G. M. (2009). The use of precision dendrometers in research on daily stem size and wood property variation: A review. *Dendrochronologia*, *27*(2), 159–172. https://doi.org/10.1016/j.dendro.2009.06.008

Dry, P. R., Loveys, B. R., & During, H. (2000). Partial drying of the rootzone of grape. II. Changes in the pattern of root development. *VITIS-GEILWEILERHOF*, *39*(1), 9-12. Recuperado de https://pdfs.semanticscholar.org/2e8c/09690dd07d5936c3290b4fb301270fc38d6b.pdf

Durán, V. H. Z., Cárceles, B. R., Rodríguez, C. R. P., García, I. F. T., Franco, D. T., Gálvez, B. R., & Francia, J. R. M. (2018). Irrigation Strategies for Mango (Mangifera indica L.) Under Water-Scarcity Scenario in the Mediterranean Subtropical Environment. *Water Scarcity and Sustainable Agriculture in Semiarid Environment*, 299–316. https://doi.org/10.1016/b978-0-12-813164-0.00013-2

Fereres, E. C., & Goldhamer, D. A. (2000). Avances recientes en la programación de los riegos. *Ingeniería del agua*, *7*(1), 47. https://doi.org/10.4995/ia.2000.2836

Freeman, S., Maimon, M., & Y., P. (2000). Etiology of mango malformation disease using GUS transformants of Fusarium subglutinans. *Acta Horticulture*, *509*, 731–758. https://doi.org/doi:10.17660/ActaHortic.2000.509.88.

Fukuda, S., Spreer, W., Yasunaga, E., Yuge, K., Sardsud, V., & Müller, J. (2013). Random Forests modelling for the estimation of mango (Mangifera indica L . cv . Chok Anan) fruit yields under different irrigation regimes. *Agricultural Water Management*, *116*, 142–150. https://doi.org/10.1016/j.agwat.2012.07.003

Galindo, A. (2015). Programación del riego con sensores de diámetro del tronco. En *V Congreso Nacional - IV Congreso Iberoamericano de Riego y Drenaje*.

Gamliel-Atinsky, E., Sztejnberg, A., Maymon, M., Vintal, H., Shtienberg, D., & Freeman, S. (2009). Infection dynamics of Fusarium mangiferae, causal agent of mango malformation disease. *Phytopathology*, *99*(6), 775–781. https://doi.org/10.1094/PHYTO-99-6-0775

Gil, P. M., & Maldonado, P. (2012). SENSITIVITY AND VARIABILITY OF TWO PLANT WATER STRESS INDICATORS : EXPLORING CRITERIA FOR CHOOSING A PLANT, *72*(September), 379–387.

Giovanelli, A., Deslauriers, A., Fragnelli, G., Scaletti, L., Castro, G., Rossi, S., & Crivellaro, A. (2007). Evaluation of drought response of two poplar clones (Populus?canaden- sis Mo¨nch ‘I-214’ and P. deltoides Marsh.‘Dvina’) through high resolution analysis of stem growth. *Journal of Experimental Botany*, *58*, 2673–2683.

Goldhamer, D., & Fereres, E. (2001). Irrigation scheduling protocols using continuously recorded trunk diameter measurements. *Irrig Sci*, *20*, 115–125. https://doi.org/10.1007/s002710000034

Jensen, M. E., Robb, D. C. N., & Franzoy, C. E. (1970). Scheduling Irrigations Using Climate-Crop-Soil Data.

Johnson, G. I., Cooke, A. W., Mead, A. J., & Wells, I. A. (1991). STEM END ROT OF MANGO IN AUSTRALIA: CAUSES AND CONTROL. *Acta Horticulturae*, (291), 288–295. https://doi.org/10.17660/actahortic.1991.291.32

Kamienski, C., Soininen, J.-P., Taumberger, M., Fernandes, S., Toscano, A., Cinotti, T. S., … Neto, A. T. (2018). SWAMP: an IoT-based Smart Water Management Platform for Precision Irrigation in Agriculture. En *2018 Global Internet of Things Summit (GIoTS)* (pp. 1–6). IEEE. https://doi.org/10.1109/GIOTS.2018.8534541

Koumanov, K. S., Hopmans, J. W., Schwankl, L. J., Andreu, L., & Tuli, A. (1997). Application efficiency of micro-sprinkler irrigation of almond trees. *Agricultural Water Management*, *34*(3), 247–263. https://doi.org/10.1016/S0378-3774(97)00030-9

Mbangiwa, N. C., Savage, M. J., & Mabhaudhi, T. (2019). Modelling and measurement of water productivity and total evaporation in a dryland soybean crop. *Agricultural and Forest Meteorology*, *266–267*, 65–72. https://doi.org/10.1016/J.AGRFORMET.2018.12.005

Menzel, C. M., & Le Lagadec, M. D. (2017). Can the productivity of mango orchards be increased by using high-density plantings? *Scientia Horticulturae*, *219*, 222–263. https://doi.org/10.1016/j.scienta.2016.11.041

Michel, A. C., Sánchez, M. A., Díaz, A., Martínez, R. D., Ariza, R., & Barrios, A. (2013). Biocontrol de la "Escoba de Bruja" del Mango, con Trichoderma spp., en Condiciones de 709 Campo. *Revista mexicana de fitopatología*, *31*(1), 1–12.

Mitra, S. K. (2016). Mango production in the world - Present situation and future prospect. En *Acta Horticulturae* (Vol. 1111, pp. 287–296). International Society for Horticultural Science. https://doi.org/10.17660/ActaHortic.2016.1111.41

Noriega, N., Ruben, J., ZaValeta, N., Izquierdo, C., Rubén Nava Noriega, J., Nava Zavaleta, J., & Córdova Izquierdo, A. (2005). Alimento balanceado-forraje verde idropónico en la alimentación de conejos criollos (oryctolagus cuniculus). *Revista Electrónica de Veterinaria REDVET*, *VI*. Recuperado de http://www.veterinaria.org/revistas/redvet

Nortes, P. A. T. (2008). *Respuesta Agronómica y Fisiológica del Almendro al Riego Deficitario. Indicadores de Estrés Hídrico*. Universidad Politécnica de Cartagena. Recuperado de http://repositorio.upct.es/bitstream/handle/10317/971/Pant.pdf?sequence=1&isAllowed=y

Rao, N. K. S., Laxman, R. H., & Shivashankara, K. S. (2016). Physiological and morphological responses of horticultural crops to abiotic stresses. En *Abiotic Stress Physiology of Horticultural Crops* (pp. 3–18). Springer India. https://doi.org/10.1007/978-81-322-2725-0_1

Rodríguez, C. R. P., Gálvez, B. R., García, I. F. T., Franco, D. T., Gutiérrez, S. G., & Durán, V. H. Z. (2018). Estrategias De Adaptación a La Escasez De Agua De Riego En Plantaciones De Mango De Clima Mediterráneo Subtrop Ical (pp. 1–1). https://doi.org/10.25028/cnriegos.2018.a24-p

Shaaban, S. H. A., & Shaaban, M. M. (2012). *Impact of the Nutritional Status on Yield of Nine Mango Cultivars Grown Under Farm Conditions at Giza Governorate, Egypt*. *Journal of American Science* (Vol. 8). Recuperado de http://www.americanscience.orghttp//www.americanscience.orgeditor@americanscience.org304http://www.americanscience.org.38

Srivastava, G. (2018). Effect of marketing channel on perishable goods. *Journal of Global Information and Business Strategy*, *10*(1), 84–89. Recuperado de http://www.indianjournals.com/ijor.aspx?target=ijor:jgibs&volume=10&issue=1&article=010

2 REVISIÓN DE LITERATURA

2.1 Situación del agua en la agricultura

El Agua es un elemento fundamental para la producción agrícola en México, cumpliendo una funcion fundamental en la seguridad alimentaria del país. El sistema nacional de información del agua (SINA), en sus clasificaciones de usos de agua en el 2016 menciona que en México, el 77% del agua se utiliza para sostener la agricultura; el 14%, en el abastecimiento público; el 5%, en las termoeléctricas y el 4%, en la industria (Conagua, 2018). Actualmente el 16% de la superficie continental de México se destina a la producción agrícola, donde el 79% está destinada a una agricultura de temporal y el otro 21% a cultivos con riego (INEGI, 2017). La agricultura es quien posee el consumo más alto de agua en el país, esto debido a la falta de modernización, donde casi el 50% del agua usada para riego se desperdicia (Santacruz & Santacruz, 2019). Se estima que a través de la reparación y modernización de los sistemas de riego, la producción rural de alimentos podría duplicarse (Luna & Grieger, 2015).

Actualmente se busca reducir el uso de agua para fines agrícolas y aumentar las superficies regadas, a través de técnicas de riego controlado, sin descuidar la sostenibilidad de la producción agrícola. El Aumento de la eficiencia en el consumo de agua depende de mejorar las explotaciones agrícolas a través de transferencia tecnológica, siendo una opción el aumento de la superficie física regada en el país (ver Figura 1). Donde los estados norteños como Sinaloa y Sonora representan, el 27% y 15% respectivamente de la superficie total de regadío (CONAGUA, 2013).

.

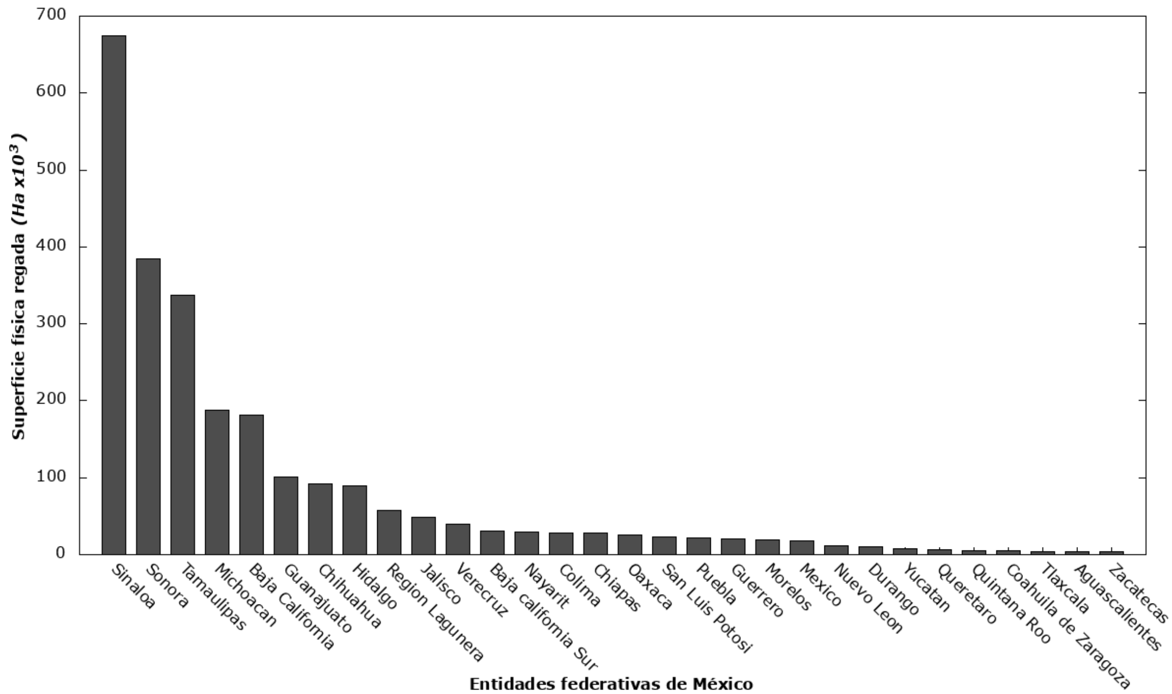

Figura 1 Superficie física regada por entidad federativa en México (CONAGUA, 2013).

2.2 Estrategias de riego para optimizar el uso del agua

La agricultura de riego pasa por un desequilibrio, su demanda hídrica va en aumento y la oferta de recursos hídricos va en declive (Perry, 2011). Ante estas limitaciones se emprenden acciones dirigidas al incremento de la producción, siendo prioridad el aumento de la eficiencia y el ahorro de agua (Pagán, 2012). A través de la adopción de tecnologías de ahorro de agua, como el secado parcial de la zona radicular (PRD) y el riego deficitario controlado (RDC), se proporciona suministro constante de agua en la zona de la raíz del cultivo, alto nivel de control sobre las aplicaciones de agua, utilización de bajos volúmenes de agua, y nula escorrentía superficial. Estas tecnologías se basan en cubrir la demanda y reducir los aportes hídricos en períodos fenológicos no críticos para el cultivo (Geerts & Raes, 2009). Además, debido a un área húmeda reducida, se pierde menos agua por evaporación (Madramootoo & Morrison, 2013). A través del uso de estas tecnologías se logra una reducción del 50% en las pérdidas debidas a la percolación y la evaporación (Namara, Nagar, & Upadhyay, 2007).

El PRD, es una estrategia basada en el riego de la mitad del sistema radicular en la cual se deja en desecación mediante alternancia del riego. Las raíces debajo del suelo seco activan un mecanismo de señalización basado en señales químicas que se transportan a las hojas a través de transpiración y de señales hidráulicas. Este sistema de riego ocasiona un cierre parcial de estomas y la transpiración de la hoja disminuye sin limitar la asimilación de CO_2. Las pérdidas de transpiración, no afectan la fotosíntesis (Romero, Kusakabe, & Melgar, 2014). Esta técnica ha demostrado tener el potencial de ahorrar agua en un 50% sin reducir el rendimiento (Zegbe, Behboudian, Lang, & Clothier, 2003). Independiente de la estrategia de riego utilizada, (Liao et al., 2019) demostraron el efecto que hay en los cerezos al suministrar agua a la zona radicular, garantizando el crecimiento y desarrollo del cultivo. Sin embargo, el tratamiento de microirrigación por anillo de goteo y el riego tradicional por inundación de surcos, no presentaron diferencias ($P<0.05$) en el rendimiento y calidad del fruto, pero si en el uso eficiente del agua. Sin embargo se puede reducir un 15% la tasa de expansión foliar, en relación con el control (Dry, Loveys, & During, 2000). De acuerdo con (Nunes et al., 2015), la disminución en un 50% de la disponibilidad de agua del suelo causó una disminución significativa en la producción de masa seca en todos los órganos de la papaya, así como el volumen de la raíz en comparación con el control. Al reducir el agua de forma moderada no hubo una reducción significativa en el rendimiento

Se han evaluado los efectos de la producción en manzanos ante sistemas de riego por goteo: al modificar los patrones de humectación en el suelo y la temperatura, promovían un menor crecimiento en los frutos pero un mayor crecimiento vegetativo (Osroosh, Peters, Campbell, & Zhang, 2016).

Por otro lado, (Girona, Mata, & Marsal, 2005) usaron un sistema de riego por microaspersión, el cual humedecía una fracción significativa de la superficie del suelo. Dicho aumento (100-130%) de agua en el cultivo no mostró diferencias significativas en los rendimientos. Aunque las reducciones de rendimiento fueron significativas a partir de 80% con respecto al 100%, al limitar al 60% de agua se promovió el uso del RDC en zonas donde la disponibilidad de agua es baja.

El RDC requiere conocimiento detallado de la respuesta fisiológica del cultivo sobre factores como estrés hídrico y tolerancia a la sequía; variando según el genotipo y etapa fenológica. Para la elaboración de estrategias de RDC debe atenderse el periodo específico del crecimiento del cultivo, por que debido al estrés causado se pueden provocar cambios favorables (Lagos et al., 2017). Tal es el caso de la aplicación de RDC en melocotoneros, donde se aplica en la fase de endurecimiento del hueso y la fase de crecimiento expansivo, debido a que no provoca cambios significativos en la calidad del fruto (Girona et al., 2003). En el caso de árboles de mango se demostró el efecto de diferentes niveles de riego en diferentes etapas fenológicas, observando la sensibilidad del mango al riego deficitario tanto en el crecimiento final de la fruta como en la etapa de post-cosecha (Levin et al., 2018). Siendo, el estrés hídrico responsable de un número inferior de frutos en Tailandia (Spreer, Müller, Hegele, & Ongprasert, 2009). por el contrario, en Málaga España (Durán, Rodríguez, & Franco, 2011) reportan 18.4 ton ha^{-1} de mango, con una eficiencia en la utilización del agua de 7.14 kg m^{-3} obteniendo mayor calidad de frutas con riego deficitario.

2.3 Importancia del uso de indicadores de estrés hídrico en la programación de riego

2.3.1 Métodos climáticos

Los métodos climáticos evalúan las necesidades hídricas del cultivo basándose en el cálculo de la ETo y en la utilización de coeficientes de cultivo (Kamienski et al., 2018). La FAO (Food and Agriculture Organization) define la ETo como la tasa de evapotranspiración de un cultivo hipotético de una superficie estándar afectado por un coeficiente de cultivo empírico (k_c) apropiado (Varmaghani, Eichinger, & Prueger, 2019). La estimación precisa de la ETo es importante para el cálculo de las necesidades de agua de riego, para optimizar la programación del riego, la calidad del cultivo y la productividad (Kisi & Alizamir, 2018).

Cuadro 1 Técnicas comúnmente usadas para la eficiencia en el uso del agua en diferentes frutales. Riego deficitario controlado(RDC), máxima contracción del diámetro (MCD).

Frutal	Riego	Temporizacion	Resultados	Autor
Aguacate Hass	Riego por goteo. Goteros compensados por presión	(1) Riego por pulsos (10-20 min cada 30 min) (2) Riego por la noche hasta la mañana (3) Riego cada dos días	El numero de frutos fue 75, 30, 27 para R1, R2 y R3 respectivamente. El estrés hídrico atenuó el crecimiento del tronco	(Silber et al., 2012)
Mandarina	Riego por goteo	*Control: ET = 100% *Tratamiento: ET = 10 a 20%	Permite un ahorro de agua del 12 a 18% sin reducción de rendimiento y peso de la fruta	(Velez, Intrigliolo, & Castel, 2007)
Almendros	microaspersor	*Control: ET = 100% *RDC =Practica de *agricultor *SIMDS=-10<ET<10%	La ahorro de agua fue de 55% y la producción disminuye en el 2009 entre 3-9% y el 2010 un 17% con respecto al control	(Puerto, Domingo, Torres, Pérez, & García, 2013)
Manzana	Goteo	Cantidad de agua en el suelo: *50% *62.5% *Convencional	El riego convencional no presento diferencia significativa en el rendimiento la transpiración de la planta se redujo en un 15% para el riego parcial	(Du, Kang, Li, & Du, 2017)
Mango	Microaspersores y mangueras de agua colocadas manualmente debajo de los árbole	*Control: ET=100% *DI: ET=50% *Experiencia del agricultot	DI aumento del 31% en las frutas de primera clase fueron mayores a 300 g	(Schulze, Spreer, Keil, Ongprasert, & Müller, 2013)

La selección del método depende de la disponibilidad de variables climáticas observadas, como la temperatura del aire, la humedad relativa, la velocidad del viento y la radiación solar. Actualmente, el método más completo, aceptado y recomendado para la determinación de la ETo es el de Penman-Moteith (Kovoor & Nandagiri, 2018). La principal desventaja de este método es que necesita una gran cantidad de datos climáticos que pueden no estar disponibles, siendo necesarios enfoques alternativos que requieran menos aportes climáticos (Yassin, Alazba, & Mattar, 2016).

Recientemente, investigadores utilizan herramientas tecnológicas para modelar y predecir con mayor fiabilidad los ciclos de carbono y de agua, la medición de la absorción de contaminantes, y la parametrización de las interacciones tierra-atmósfera para los modelos climáticos. Una técnica utilizada se llama covarianza de torbellinos (eddy covariance), basándose en la medición de flujos turbulentos de agua que viajan verticalmente a través de porciones de aire, esto permite conocer el flujo calor sensible y calor latente. A través de un anemometre sónico tridimensional se mide la velocidad vertical del viento. Por otro lado, con un higrómetro de respuesta rápida se obtiene la densidad de vapor de agua. Otro factor que afecta la estimación de los flujos de calor es la altura y la distancia de los sensores (Lee, 2018).

Además se han desarrollado muchas estimaciones de ETo, una de las cuales es el que propone un balance de energía en conjunto con la relación de Bowen (Yunusa, Walker, & Lu, 2004). Este método se basa en el balance de energía que ocurre en la superficie vegetal, la cual a través de los gradientes verticales de temperatura del aire y vapor de agua se puede determinar la tasa de transpiración (Savage, Everson, & Metelerkamp, 2009). Sin embargo, se deben hacer mediciones simultáneas de la temperatura, humedad del aire, la velocidad del viento y radiación neta a diferentes alturas (Nanda, Giri, & Bera, 2018). Por otro lado, este proceso es demasiado complejo para ser aplicado a nivel de agricultores.

La ET es un fenómeno complejo y no lineal, la exactitud de los diferentes modelos depende de la precision y la resolución que los sensores de humedad, temperatura y radiación (Ahmadpari, Shokoohi, Lalabadi, Gerdini, & Ebrahimi, 2019). La mayoría de los modelos micrometeorológicos están desarrollados para cultivos de cobertura total (Mbangiwa, Savage, & Mabhaudhi, 2019). En cultivos como frutales implicaria problemas de representatividad debido a la discontinuidad de cobertura, hetereogenidad de microclimas, rugosidad de superficie. Para ello, hay que considerar que el suelo y los arboles están perdiendo agua de forma diferente debido a la incidencia de la radiación en ellos, esto debido a que existen diferencias entre zonas de evaporación y superficies de intercambio de calor sensible (Cassardo, Andreoli, Spanna, Ferrarese, & Picco, 2018). Debido a ello, es necesario obtener la evapotranspiración máxima en condiciones estándar del cultivo (ETc). Aplicando coeficientes de ajuste para las diferentes especies vegetales de mango (ver Tabla 2). factores como el tipo de suelo y el volumen de cubierta pueden integrarse en un único Kc el cual se determina experimentalmente.

Cuadro 2 Evapotranspiración máxima en condiciones estándar y coeficientes de ajuste para mango en diferentes países tropicales y subtropicales. Días posteriores a la floración (DAF), evapotranspiración de referencia (ETo), coeficiente de cultivo (Kc).

País	ETc (mm)	Kc	Autor
Brasil	4.4	$K_c=0.36+0.009*(DAF)-4\times10^{-5}*(DAF)^2$ r^2= 0,79	(De Azevedo, Da Silva, & Da Silva, 2003)
Brasil	4.27	0.85	(Teixeira et al., 2008)
Tailandia	4.41	0.8	(Schulze et al., 2013)
Tailandia	K_c*ET_o	0.8	(Spreer et al., 2007)
Ecuador	1.8	0.6	(Proaño & Correa, 2006)
Trópicos	4-5	0.65-1.05	(Carr, 2019)
México	K_c*ET_o	0.85	(Pérez et al., 2012)

México tiene un kc=0.85, valor aproximado a los otros países que se encuentran entre los trópicos. Por otro lado, se tiene que considerar que México presenta variabilidad entre superficies y climas, es por ello que la evapotranspiración va de 460 hasta 2130 mm anuales (Ismael et al., 2016). Cabe señalar, que separar la evaporación de la transpiración es complicado dando un margen de error en el cálculo de las necesidades de riego. Siendo necesario para este error una calibración local que determine el exceso o déficit de las necesidades hídricas de los cultivos

2.3.2 Mediciones continúas

Con el procesamiento de la información continua del estado hídrico de la planta en un microcontrolador o su posterior análisis, los datos se recopilan continuamente durante la temporada de cultivo, y las mediciones se realizan día y noche, sin importar las inclemencias del tiempo. Los sensores instalados en una ubicación fija, aseguran la consistencia en las mediciones. Además, se puede automatizar el riego utilizando las variables climáticas reinantes que predicen la demanda evaporativa del ambiente y la condición directa del árbol. Entre estos métodos se distinguen:

2.4 Temperatura de la hoja

El monitoreo del estado hídrico de la planta es crítico para la detección temprana del estrés y la aplicación de técnicas de riego deficitario (E. Fereres & Soriano, 2006). Además, la apertura estomática de un cultivo en cualquier momento depende, entre otras cosas, de la disponibilidad de humedad en el suelo, la temperatura del aire y la temperatura de la hoja. Siendo afectada la producción por altas temperaturas y por el déficit de humedad (Boyle, McAinsh, & Dodd, 2016).

La temperatura del dosel se usa como indicador del estado hídrico de la planta. A través de la transpiración la cual promueve un descenso de la temperatura foliar con respecto a la del aire. Durante un déficit hídrico los estomas se cierran, se reduce el enfriamiento por evaporación y se produce un aumento de la temperatura foliar que puede ser detectado con un termómetro infrarrojo (Calderón, 2013). Sin embargo, la termometría infrarroja o la imagen térmica podrían ser una técnica útil para monitorear la conductancia estomática mostrando que la diferencia de temperatura del dosel y del aire están relacionada con el déficit de presión de vapor de aire, un parámetro que refleja la respuesta estomática al estrés hídrico (Wang & Gartung, 2010).

Los indicadores térmicos pueden adquirirse de forma remota mediante teledetección. No obstante, las imágenes térmicas satelitales disponibles están limitadas a los sensores Landsat TM y ASTER , con un rendimiento de 120 m y 90 m, respectivamente, siendo solo adecuadas para escalas regionales (Moran, Clarke, Inoue, & Vidal, 1994). Por otro lado, los métodos de modelado satelital son realizados con simulaciones, demostrando grandes defectos debidos a los componentes del suelo y de las sombras en el píxel térmico, lo que dificulta para controlar los niveles de estrés (Sepulcre-Cantó et al., 2009)

Por otro lado, los indicadores puntuales generalmente evalúan el estado del agua a nivel de hoja y extrapolan esos valores a nivel de planta. La principal desventaja es que la caracterización de campo por indicadores puntuales lleva mucho tiempo y no representa bien la heterogeneidad del campo (Zarco, González, & Berni, 2012). A pesar de ello, el monitoreo del estado fisiológico de la planta a través de la temperatura de la hoja (Cuadro 3 Sensores comúnmente ocupados para el monitoreo del estado hídrico a través de la temperatura de las hojas), puede estimar una cantidad de agua disponible en la planta (Drechsler, Kisekka, & Upadhyaya, 2019).

Aunque la temperatura del dosel se ha propuesto para la detección del estrés hídrico, su uso podría ser más eficiente al permitir la detección directa de enfermedades. Las enfermedades foliares, del tallo y de las raíces tienden a modificar las relaciones hídricas de las plantas causando un déficit hídrico, que resulta de la pérdida acelerada de agua, interrupciones de la transpiración o daños en el sistema radicular (Burdon, 1987). Las plantas estresadas tienden a cerrar los estomas, lo que lleva a una menor transpiración, un aumento de temperatura de la hoja y una reducción de la tasa fotosintética (Hamlyn G. Jones, 1999). Las plantas enfermas generalmente muestran el aumento en los niveles de estrés; las áreas infectadas pueden experimentar la descomposición de los pigmentos, el desarmado del aparato fotosintético y el colapso de la pared celular, lo que eventualmente causa necrosis (Moshou et al., 2012). Por lo tanto, la temperatura de la hoja puede ser un indicador de enfermedades.

Cuadro 3 Sensores comúnmente ocupados para el monitoreo del estado hídrico a través de la temperatura de las hojas

Aplicación	Sensor	Uso	Autor

Cultivos	Cámara infrarroja. Lepton LWIR (FLIR Systems, Wilsonville, OR) y termistores (Rs-232)	Mide la temperatura del dosel de cultivos a una alta resolución temporal	(P. L. Drew, Sudduth, Sadler, & Thompson, 2019)
Olivar	Escáner hiperespectral aerotransportado (AHS)	Estudia la variabilidad espacial y diurna de la temperatura en función del estrés hídrico.	(Sepulcre-Cantó et al., 2006)
Mandarinas	Sensores de temperatura infrarroja (IRT) (Apogee, Utah, EE. UU.)	Evaluar el índice de estrés hídrico de los cultivos (CWSI)	(Gonzalez-Dugo, Zarco-Tejada, & Fereres, 2014)
Limones	sonda de fibra óptica de 200 μm para adquirir y pasar la luz al espectrómetro	valuar el potencial de la espectroscopía visible e infrarroja cercana (Vis / NIR) para la detección temprana de los limones dulces dañados por congelación	(Moomkesh, Mireei, Sadeghi, & Nazeri, 2017)
Vid	Generador de imágenes térmicas de onda larga SnapShot 225	Estudio de la conductancia estomática en el campo	(H. G. Jones, 2002)
Algodón y maíz	Termopares infrarrojos (Modelo IRt / c. 2 GK-80F / 20C, EXERGEN Corporation)	Usan la temperatura del dosel para desarrollar señales de riego	(Wanjura, Maas, Winslow, & Upchurch, 2004)
Hoja de menta	MB25 Basic Moisture Analyzers, OHAUS, Pine Brook, NJ, USA	Observar el efecto de la temperatura de secado	(Ertekin & Heybeli, 2014)
Maduracion de frutos	Emisor térmico IR, sistema microelectromecánico (MEMS)	Detección de etileno para la discriminación de la maduración de la fruta.	(Kathirvelan & Vijayaraghavan, 2017)
Mango	Sonda de reflectancia	evaluación de la calidad del mango	(Cort et al., 2017)

Por otra parte, la tecnología de la teledetección puede identificar por separado cualquier estrés provocado por tensiones abióticas (temperatura, agua, gases, minerales) y bióticas (inducidas por microorganismos, animales, plantas, etc.) que afectan el funcionamiento de las plantas, dando diferentes respuestas fisiológicas, mejorando el diagnóstico y cuantificación de la infección (Chaerle et al., 2009).

El *Fusarium oxusporum, F. subglutinans* y *Fusarium mangiferae* son hongos que causan un problema fitosanitario llamado "Escoba de bruja", que tiene una distribución en todo el territorio Mexicano (Michel et al., 2013). Tiene un impacto económico particularmente significativo, dando pérdidas estimadas en un 60% de la producción de mango (Noriega et al., 2005). Sin embargo, en el caso de la escoba de bruja, la infección a menudo solo es visible a partir de las etapas avanzadas de la epidemia. Sensores remotos podrían servir como un método para mapear el alcance y la gravedad de la enfermedad. Dicha información sobre la distribución espacial y la intensidad de la infección permitiría una planificación e implementación de contramedidas apropiadas y efectivas.

Se ha buscado el control de la escoba de bruja; sin embargo, un método único que consiga reducirla significativamente, no existe. Por lo que, Montes-García et al., (2008) recomiendan un manejo integrado, donde se incluya la fertilización del suelo y follaje, aspersiones de fungicidas, acariciadas, la poda fitosanitaria, reguladores de crecimiento. Así mismo, una manera para controlar el hongo es a través de su antagonista, el cual puede modificarse en términos de adaptación a las condiciones bióticas y abióticas específicas (Dennis & Webster, 1971).

2.5 Sonda ZIM

El grosor de las hojas también se usa como indicador del estrés hídrico y pueden proporcionar información para la programación del riego (Malone, 1993). Los dispositivos de monitoreo del grosor de la hoja no son invasivos y son adecuados para mediciones en línea, pero tienen la desventaja de que los cambios en el estado del agua con frecuencia no se reflejan de manera sensible en los cambios del grosor de la hoja (Zimmermann et al., 2008). La técnica de la sonda de presión o sistema ZIM, consta de una sonda de silicón miniaturizado integrado en una abrazadera de resorte que se sujeta a una hoja de planta. La sonda mide la respuesta de presión atenuada de la hoja tras la aplicación de una presión constante (Mitcham & Yahia, 2009). La sonda ZIM registra la presión de salida, una variable inversamente correlacionada con la presión de turgencia de la hoja. (Meinzer, Clearwater, & Goldstein, 2001) demostraron que esta nueva sonda puede detectar cambios en el régimen de riego y en el microclima de manera muy sensible. Por otra parte, observaron que el uso de varias sondas permitió el estudio del transporte diurno de agua a múltiples escalas desde hojas individuales a toda la planta. (Fernández et al., 2011) obtuvieron curvas de la presión de la hoja cuando los valores del potencial hídrico del tallo del mediodía cayeron por debajo de -1.7 MPa. La forma de las curvas volvió a la normalidad unos días después del riego, el número depende del nivel de estrés hídrico alcanzado anteriormente. La sonda de presión de la hoja es una herramienta prometedora para dilucidar el transporte de agua en una planta.

2.6 Trabajos de investigación con el uso de dendrómetros en cultivos frutícolas y hortícolas

Los monitoreos continuos y automáticos del árbol, utilizan dendrómetros, los cuales registran variaciones micrométricas compuestas por ritmos diurnos de agotamiento y reposición del almacenamiento de agua en el tallo (Deslauriers, Rossi, & Anfodillo, 2007). Actualmente se utilizan dendrómetros de banda y puntuales para la programación de riego. Sin embargo, el uso de estos sensores se ve afectado por la variabilidad del tronco (Corell et al., 2014), y la ubicación del sensor dentro del árbol (Offenthaler, Hietz, & Richter, 2001). (Cuevas et al., 2010), informaron que factores como la edad, el tamaño de la planta, los patrones estacionales y la carga de los cultivos, disminuyen la utilidad del instrumento como de los indicador del estrés hídrico

Los dendrómetros puntuales son considerados más precisos que los dendrómetros de banda, pero requieren de un mayor mantenimiento debido a la interferencia de insectos (D. M. Drew & Downes, 2009). A lo largo del día los dendrómetros registran las fluctuaciones en el diámetro del tronco, las cuales tienen una base fisiológica como consecuencia de cambios en el contenido hídrico del suelo, la temperatura del aire, la humedad, la precipitación y el déficit de presión de vapor (Urrutia-Jalabert, Rossi, Deslauriers, Malhi, & Lara, 2015). Cuando amanece se reduce el potencial hídrico de los conductos del xilema debido al desequilibrio entre la demanda climática y la capacidad absorbente de raíces, lo que favorece el movimiento lateral desde el floema al xilema, provocando que la planta comience a transpirar. Al final del día, la transpiración desciende, y el movimiento del agua va desde el xilema al floema, esto provoca el hinchamiento del tallo, donde la rehidratación de estos tejidos tiene lugar. Estos cambios de los tejidos del tronco debido a su contenido de agua son reversibles, los cuales causan fluctuaciones diarias en el diámetro del tronco (Pagán, 2012).

El registro continuo de las microvariaciones de tronco y ramas proporciona el crecimiento y estado hídrico de la planta (E. C. Fereres & Goldhamer, 2000). Los sensores LVDT o resistencias lineales detectan las fluctuaciones del diámetro del tronco para ser fácilmente automatizados y utilizados en la programación del riego (Moreno et al., 2015). (Goldhamer, Fereres, Cohen, Girona, & Mata, 2000) propusieron que al MCD como un índice para la programación del riego debido a su alta correlación al estrés hídrico de la planta. De ese modo se han descrito evaluaciones del MCD como índice en la programación de riego para diferentes frutales como: Limoneros (Alarcón et al., 2004; Moreno et al., 2007), cerezos (Blanco, Torres, Blaya, Pérez, & Domingo, 2019), olivas (Pastor et al., 1999), melocotoneros (Conejero et al., 2007; W. P. Conejero, 2008), almendros (García, Gutiérrez, Souza, Cuadros, & Durán, 2019), nectarinos (De la Rosa, Conesa, Domingo, & Pérez, 2014) y mango (Nadler, Raveh, Yermiyahu, & Green, 2006). La respuesta del tallo presenta variabilidad entre especies, dando la necesidad de estudiar por separado cada etapa fenológica.

Entre las cuestiones técnicas a considerar, al momento de utilizar un dendrómetro se encuentran: posición del árbol, modo de fijación, tiempos de muestreos y la precisión del sensor. En los estudios realizados por (Urrutia-Jalabert et al., 2015), se colocaron dendrómetros que median cada 15 minutos, en el lado norte de los troncos, a 0.6 m del suelo, en lugares libres de cicatrices. El punto de contacto de cada dendrómetro se pegó a la superficie del tallo. Por otro lado, (Jiménez, Navarro, Sánchez-Miranda, & Ripoll, 2019) utilizaron dendrómetros de punto, con una precisión de ±2 μm con un rango de 15 mm y registrando los datos cada 30 min, tomando como indicador el MCD. En la investigación hecha por (Cuevas et al., 2010) el punto de contacto de cada dendrómetro se pegó a la superficie de los tejidos vivos de la corteza con una masilla estándar para cubrir las heridas, almacenando los promedios cada 15 minutos. Sin importar el intervalo de tiempo. En cada artículo se mencionaron las variaciones del tallo durante el periodo de estudio. Por otro lado, hacen énfasis en el cuidado de la posición del sensor.

2.7 Desarrollo de aplicaciones agrícolas para teléfonos inteligentes

Las tecnologías avanzadas pueden aportar beneficios a la mayoría de las personas. En los últimos años las tecnologías de teléfonos inteligentes (Smartphone) ha comenzado a tener un papel importante en la vida cotidiana. En el 2017, el 73,5% de la población de México utiliza teléfonos celulares (INEGI, 2019). Esto ha llevado a un aumento de las herramientas móviles, que ayudan a los pequeños agricultores con tareas cotidianas como educación, finanzas y servicios agrícolas (Baumüller, 2013). Desarrollándose en mayor medida aplicaciones que se basan en herramientas visuales y que funcionan con datos adquiridos por sensores incorporados, siendo útiles para usuarios con bajos niveles de alfabetización (Daum, Buchwald, Gerlicher, & Birner, 2018). Por ejemplo, (Muangprathub et al., 2018) desarrollaron redes de sensores inalámbricos para optimizar el riego en la agricultura, mediante la gestión de los datos a través de teléfonos inteligentes y aplicaciones web. Además, (Daum et al., 2018) desarrollaron una aplicación de aspecto socioeconómico en Zambia para la recolección de datos en los sistemas agrícolas pequeños, analizando los efectos de la mecanización agrícola y su efecto a largo plazo. También se pueden utilizar los sensores propios del teléfono inteligente, como: el GPS, el barómetro, el giroscopio, el sensor de luz ambiental y la cámara. Tal es el caso de Cubero et al. (2018), que desarrollaron una App Android para estimar el índice de color de los cítricos en ambientes exteriores e interiores, obteniendo valores de R^2 de 0.854 y 0.881 respectivamente. Novas *et al*. (2018) desarrollaron una App para teléfonos inteligentes que evalúa las lesiones por frio en calabacín, variando ligeramente de los métodos estándares de evaluación. Estos ejemplos muestran el potencial que está al alcance de los agricultores a través de las aplicaciones.

2.8 Referencias

Ahmadpari, H., Shokoohi, E., Lalabadi, N. M., Gerdini, M. S., & Ebrahimi, M. (2019). Assessment of Potential Evapotranspiration Estimation Methods in the Fasa Region. *Specialty Journal of Agricultural Sciences*, *5*(2), 56–66. Retrieved from https://sciarena.com/storage/models/article/b9MK5taJsrPhp5Irh7lXqmgI58R7FlFRIQFXOyz6mHJUkPpnbP8AKUIbzxgl/assessment-of-potential-evapotranspiration-estimation-methods-in-the-fasa-region.pdf

Alarcón, J. J., García-Orellana, Y., Ruiz-Sánchez, M. C., Conejero, W., Ortuño, M. F., Nicolás, E., & Torrecillas, A. (2004). Evaluación del uso de la máxima contracción diaria del tronco para la programación del riego en limonero. *Congreso Albacete*, *2*, 1–6.

Baumüller, H. (2013). Facilitating Agricultural Technology Adoption Among the Poor: The Role of Service Delivery Through Mobile Phones. *SSRN Electronic Journal*. https://doi.org/10.2139/ssrn.2237987

Blanco, V., Torres, R. S., Blaya, P. J. R., Pérez, A. P., & Domingo, R. (2019). Vegetative and reproductive response of ‘Prime Giant’ sweet cherry trees to regulated deficit irrigation. *Scientia Horticulturae*, *249*, 478–489. https://doi.org/10.1016/J.SCIENTA.2019.02.016

Boyle, R. K. A., McAinsh, M., & Dodd, I. C. (2016). Stomatal closure of Pelargonium × hortorum in response to soil water deficit is associated with decreased leaf water potential only under rapid soil drying. *Physiologia Plantarum*, *156*(1), 84–96. https://doi.org/10.1111/ppl.12346

Burdon, J. J. (1987). Effects of pathogens on individual plants. *Diseases and Plant Population Biology*, 8–27.

Calderón, R. A. C. (2013). *Uso de sensores infrarrojos para la deteccion temprana de Ralstonia solanacearum en plantas de tomate*. Universidad de costarrica. Retrieved from http://repositorio.sibdi.ucr.ac.cr:8080/jspui/bitstream/123456789/2505/1/36373.pdf

Carr, M. K. V. (2019). THE WATER RELATIONS AND IRRIGATION REQUIREMENTS OF MANGO (Mangifera indica L.): A REVIEW, *50*(1), 1–23. https://doi.org/10.1017/S0014479713000288

Cassardo, C., Andreoli, V., Spanna, F., Ferrarese, S., & Picco, S. (2018). Climatology of phenological and other micrometeorological variables parameters in regional vineyard ecosystem in Piedmont (Italy). *20th EGU General Assembly, EGU2018, Proceedings from the Conference Held 4-13 April, 2018 in Vienna, Austria, p.13897*, *20*, 13897. Retrieved from http://adsabs.harvard.edu/abs/2018EGUGA..2013897C

Chaerle, L., Lenk, S., Leinonen, I., Jones, H. G., Van Der Straeten, D., & Buschmann, C. (2009). Multi-sensor plant imaging: Towards the development of a stress-catalogue. *Biotechnology Journal*, *4*(8), 1152–1167. https://doi.org/10.1002/biot.200800242

CONAGUA. (2013). Estadísticas agrícolas de los distritos de riego. Retrieved from https://www.gob.mx/cms/uploads/attachment/file/147019/ea2011-2012.pdf

Conagua. (2018). *Estadísticas del agua en México*. Mexico. Retrieved from http://sina.conagua.gob.mx/publicaciones/EAM_2018.pdf

Conejero, W., Alarcón, J. J. ., García, Y. O., Abrisqueta, J. M., & Torrecillas, A. (2007). Daily sap flow and maximum daily trunk shrinkage measurements for diagnosing water stress in early maturing peach trees during the post-harvest period. *Tree Physiology*, *27*(1), 81–88. https://doi.org/10.1093/treephys/27.1.81

Conejero, W. P. (2008). *Programación del riego en melocotonero mediante el uso de sensores del diámetro del tronco*. Universidad Politécnica de Cartagena.

Corell, M., Girón, I. F., Galindo, A., Torrecillas, A., Torres-Sánchez, R., Pérez-Pastor, A., … Moriana, A. (2014). Using band dendrometers in irrigation scheduling Influence of the location inside the tree and comparison with point dendrometer. *Agricultural Water Management*, *142*, 29–37. https://doi.org/10.1016/j.agwat.2014.04.005

Cort, V., Blanes, C., Blasco, J. E., Ortíz, C., Aleixos, N., Mellado, M., … Talens, P. (2017). Integration of simultaneous tactile sensing and visible and near-infrared reflectance spectroscopy in a robot gripper for mango quality assessment. https://doi.org/10.1016/j.biosystemseng.2017.08.005

Cubero, S., Albert, F., Manuel Prats-Moltalb an, J., Fern andez-Pacheco, D. G., Blasco, J., & Aleixos, N. (2018). Application for the estimation of the standard citrus colour index (CCI) using image processing in mobile devices. https://doi.org/10.1016/j.biosystemseng.2017.12.012

Cuevas, M. V., Torres-Ruiz, J. M., Álvarez, R., Jiménez, M. D., Cuerva, J., & Fernández, J. E. (2010). Assessment of trunk diameter variation derived indices as water stress indicators in mature olive trees. *Agricultural Water Management*, *97*(9), 1293–1302. https://doi.org/10.1016/j.agwat.2010.03.011

Daum, T., Buchwald, H., Gerlicher, A., & Birner, R. (2018). Smartphone apps as a new method to collect data on smallholder farming systems in the digital age: A case study from Zambia. https://doi.org/10.1016/j.compag.2018.08.017

De Azevedo, P. V, Da Silva, B. B., & Da Silva, V. P. R. (2003). Water requirements of irrigated mango orchards in northeast Brazil. *Agricultural Water Management*, *58*, 241–254. https://doi.org/https://doi.org/10.1016/S0378-3774(02)00083-5

De la Rosa, J. M. S., Conesa, M. del R. S., Domingo, R. M., & Pérez, A. P. (2014). Contracción temprana de diámetro del tronco. Un nuevo indicador altamente sensible al estrés hídrico en nectarinos extratempranos, 143–146. Retrieved from http://repositorio.upct.es/handle/10317/4892

Dennis, C., & Webster, J. (1971). Antagonistic properties of species-groups of Trichoderma. *Transactions of the British Mycological Society*, *57*(1), 25-IN3. https://doi.org/10.1016/S0007-1536(71)80077-3

Deslauriers, A., Rossi, S., & Anfodillo, T. (2007). Dendrometer and intra-annual tree growth: What kind of information can be inferred? *Dendrochronologia*, *25*, 113–124. https://doi.org/10.1016/j.dendro.2007.05.003

Drechsler, K., Kisekka, I., & Upadhyaya, S. (2019). A comprehensive stress indicator for evaluating plant water status in almond trees. *Agricultural Water Management*, *216*, 214–223. https://doi.org/10.1016/j.agwat.2019.02.003

Drew, D. M., & Downes, G. M. (2009). The use of precision dendrometers in research on daily stem size and wood property variation: A review. *Dendrochronologia*, *27*(2), 159–172. https://doi.org/10.1016/j.dendro.2009.06.008

Drew, P. L., Sudduth, K. A., Sadler, E. J., & Thompson, A. L. (2019). Development of a multi-band sensor for crop temperature measurement, 269–280. https://doi.org/10.1016/j.compag.2019.04.007

Dry, P. R., Loveys, B. R., & During, H. (2000). Partial drying of the rootzone of grape. II. Changes in the pattern of root development. *VITIS-GEILWEILERHOF*, *39*(1), 9-12. Retrieved from https://pdfs.semanticscholar.org/2e8c/09690dd07d5936c3290b4fb301270fc38d6b.pdf

Du, S., Kang, S., Li, F., & Du, T. (2017). Water use efficiency is improved by alternate partial root-zone irrigation of apple in arid northwest China. *Agricultural Water Management*, *179*, 184–192. https://doi.org/10.1016/j.agwat.2016.05.011

Durán, V. H. Z., Rodríguez, C. R. P., & Franco, D. T. (2011). Impact of sustained-deficit irrigation on tree growth, mineral nutrition, fruit yield and quality of mango in Spain. Impact of sustained-deficit irrigation on tree growth, mineral nutrition, fruit yield and quality of mango in Spain, *66*(4), 257–268. https://doi.org/10.1051/fruits/2011038

Ertekin, C., & Heybeli, N. (2014). Thin-Layer Infrared Drying of Mint Leaves. *Journal of Food Processing and Preservation*, *38*(4), 1480–1490. https://doi.org/10.1111/jfpp.12107

Fereres, E. C., & Goldhamer, D. A. (2000). Avances recientes en la programación de los riegos. *Ingeniería Del Agua*, *7*(1), 47. https://doi.org/10.4995/ia.2000.2836

Fereres, E., & Soriano, M. A. (2006). Deficit irrigation for reducing agricultural water use. *Journal of Experimental Botany*, *58*(2), 147–159. https://doi.org/10.1093/jxb/erl165

Fernández, J. E., Rodriguez, C. . D., Perez, M. A., Zimmermann, U., Palomo, M. M. J., Torres, J. M. R., … Ehrenberger, W. (2011). Online-monitoring of tree water stress in a hedgerow olive orchard using the leaf patch clamp pressure probe. *Agricultural Water Management*, *100*, 25–35. https://doi.org/doi:10.1016/j.agwat.2011.08.015

García, I. F. T., Gutiérrez, S. G., Souza, L., Cuadros, S. T., & Durán, V. H. Z. (2019). Fostering sustainable water use in almond (Prunus dulcis Mill.) orchards in a semiarid Mediterranean environment. *Archives of Agronomy and Soil Science*, *65*(2), 164–181. https://doi.org/10.1080/03650340.2018.1492113

Geerts, S., & Raes, D. (2009). Deficit irrigation as an on-farm strategy to maximize crop water productivity in dry areas. *Agricultural Water Management*, *96*, 1275–1284. https://doi.org/10.1016/j.agwat.2009.04.009

Girona, J. ., Mata, M., Arbonès, A., Alegre, S., Rufat, J., & Marsal, J. (2003). Peach Tree Response to Single and Combined Regulated Deficit Irrigation Regimes under Shallow Soils. *American Society for Horticultural Science*, *128*(3), 432–440.

Girona, J., Mata, M., & Marsal, J. (2005). Regulated deficit irrigation during the kernel-filling period and optimal irrigation rates in almond. *Agricultural Water Management*, *75*(2), 152–167. https://doi.org/10.1016/j.agwat.2004.12.008

Goldhamer, A., Fereres, E., Cohen, M., Girona, J., & Mata, M. (2000). COMPARISON OF CONTINUOUS AND DISCRETE PLANT-BASED MONITORING FOR DETECTING TREE WATER DEFICITS AND BARRIERS TO GROWER ADOPTION FOR IRRIGATION MANAGEMENT. *Acta Horticulturae*, (537), 431–445. https://doi.org/10.17660/ActaHortic.2000.537.51

Gonzalez-Dugo, V., Zarco-Tejada, P. J., & Fereres, E. (2014). Applicability and limitations of using the crop water stress index as an indicator of water deficits in citrus orchards. *Agricultural and Forest Meteorology*, *198*, 94–104. https://doi.org/10.1016/j.agrformet.2014.08.003

INEGI. (2017). Encuesta Nacional Agropecuaria. Retrieved from https://www.inegi.org.mx/temas/agricultura/default.html#Informacion_general

INEGI. (2019). *COMUNICADO DE PRENSA NÚM. 179/19*.

Ismael, A., Rivas, M., David, J., Díaz, G., Rafael, A., Romero, A., … Gayosso, L. (2016). EVAPOTRANSPIRACIÓN DE REFERENCIA (ET0) Y CAMBIO CLIMÁTICO EN MÉXICO COMO HERRAMIENTA DE PLANEACIÓN DE LA ADAPTACIÓN. https://doi.org/10.14198/XCongresoAECAlicante2016-52

Jiménez, M. N., Navarro, F. B., Sánchez-Miranda, A., & Ripoll, M. A. (2019). Using stem diameter variations to detect and quantify growth and relationships with climatic variables on a gradient of thinned Aleppo pines. https://doi.org/10.1016/j.foreco.2019.03.061

Jones, H. G. (2002). Use of infrared thermography for monitoring stomatal closure in the field:

application to grapevine. *Journal of Experimental Botany*, *53*(378), 2249–2260. https://doi.org/10.1093/jxb/erf083

Jones, Hamlyn G. (1999). Use of infrared thermometry for estimation of stomatal conductance as a possible aid to irrigation scheduling. *Agricultural and Forest Meteorology*, *95*(3), 139–149. https://doi.org/10.1016/S0168-1923(99)00030-1

Kamienski, C., Soininen, J.-P., Taumberger, M., Fernandes, S., Toscano, A., Cinotti, T. S., … Neto, A. T. (2018). SWAMP: an IoT-based Smart Water Management Platform for Precision Irrigation in Agriculture. In *2018 Global Internet of Things Summit (GIoTS)* (pp. 1–6). IEEE. https://doi.org/10.1109/GIOTS.2018.8534541

Kathirvelan, J., & Vijayaraghavan, R. (2017). An infrared based sensor system for the detection of ethylene for the discrimination of fruit ripening. https://doi.org/10.1016/j.infrared.2017.07.022

Kisi, O., & Alizamir, M. (2018). Modelling reference evapotranspiration using a new wavelet conjunction heuristic method: Wavelet extreme learning machine vs wavelet neural networks. *Agricultural and Forest Meteorology*, *263*, 41–48. https://doi.org/10.1016/j.agrformet.2018.08.007

Kovoor, G. M., & Nandagiri, L. (2018). Sensitivity Analysis of FAO-56 Penman–Monteith Reference Evapotranspiration Estimates Using Monte Carlo Simulations (pp. 73–84). Springer, Singapore. https://doi.org/10.1007/978-981-10-5801-1_6

Lagos, L. O., Lama, W., Hirzel, J., Souto, C., & Lillo, M. (2017). Regulated deficit irrigation evaluation on kiwi (actinidia deliciosa) production. *Agrociencia*, *51*(4), 359–372. Retrieved from http://www.scielo.org.mx/pdf/agro/v51n4/1405-3195-agro-51-04-00359.pdf

Levin, A. G., Peres, M., Noy, M., Love, C., Gal, Y., & Naor, A. (2018). The response of field-grown mango (cv. Keitt) trees to regulated deficit irrigation at three phenological stages. *Irrigation Science*, *36*(1), 25–35. https://doi.org/10.1007/s00271-017-0557-5

Liao, R., Wu, W., Hu, Y., Xu, D., Huang, Q., & Wang, S. (2019). Micro-irrigation strategies to improve water-use efficiency of cherry trees in Northern China. *Agricultural Water Management*, *221*, 388–396. https://doi.org/10.1016/j.agwat.2019.05.017

Luna, O. P., & Grieger, C. E. (2015). *El agua en México*. Mexico. Retrieved from https://backend.aprende.edu.mx/media/uploads/resources/el_agua_en_mexico_124e215f.pdf

Madramootoo, C. A., & Morrison, J. (2013). Advances and challenges with micro-irrigation. *Irrigation and Drainage*, *62*(3), 255–261. https://doi.org/10.1002/ird.1704

Malone, M. (1993). Rapid Inhibition of Leaf Growth by Root Cooling in Wheat: Kinetics and Mechanism. *Journal of Experimental Botany*, *44*(11), 1663–1670. https://doi.org/10.1093/jxb/44.11.1663

Mbangiwa, N. C., Savage, M. J., & Mabhaudhi, T. (2019). Modelling and measurement of water productivity and total evaporation in a dryland soybean crop. *Agricultural and Forest Meteorology*, *266–267*, 65–72. https://doi.org/10.1016/J.AGRFORMET.2018.12.005

Meinzer, F. C., Clearwater, M. J., & Goldstein, G. (2001). *Water transport in trees: current perspectives, new insights and some controversies*. *Environmental and Experimental Botany* (Vol. 45). Retrieved from www.elsevier.com/locate/envexpbot

Michel, A. C., Sánchez, M. A., Díaz, A., Martínez, R. D., Ariza, R., & Barrios, A. (2013). Biocontrol de la “Escoba de Bruja” del Mango, con Trichoderma spp., en Condiciones de 709 Campo. *Revista Mexicana de Fitopatología*, *31*(1), 1–12.

Mitcham, E., & Yahia, E. (2009). *Alternative Treatments to Hot Water Immersion for Mango*.

Montes-García, N., Williams-Alanís, H., Prom, L., Isakeit, T., Odvody, G., Narro-Sánchez, J., & Ronney, W. (2008). Disease Severity and Susceptibility of Sorghum [Sorghum bicolor (L.)

Moench.] to Infection by Claviceps africana Frederickson, Mantle and de Milliano in Mexico and the United States of America. *Revista Mexicana de Fitopatología*.

Moomkesh, S., Mireei, S. A., Sadeghi, M., & Nazeri, M. (2017). Early detection of freezing damage in sweet lemons using Vis/SWNIR spectroscopy. https://doi.org/10.1016/j.biosystemseng.2017.10.009

Moran, M. S., Clarke, T. R., Inoue, Y., & Vidal, A. (1994). Estimating crop water deficit using the relation between surface-air temperature and spectral vegetation index. *Remote Sensing of Environment*, *49*(3), 246–263. https://doi.org/10.1016/0034-4257(94)90020-5

Moreno, F. ., Ortuño, M. F. ., García, Orellana, Y. ., Alarcón, J. J. ., Conejero, W. ., Nocilás, E. ., … Torrecillas, A. . (2007). Estado actual de la rogramación del riego en Limonero mediante medidas del estado hídrico. *Ingeniería Del Agua*, *14*(3), 215–222. https://doi.org/10.4995/ia.2007.2913

Moreno, F., Girón, I., Corell, M., Moriana, A., Galindo, A., & Torrecillas, A. (2015). Programación del riego deficitario controlado en aceituna de mesa empleando la dendrometría . In *ACTAS DE LAS IV JORNADAS DE INGENIERÍADEL AGUA: La precipitación y los procesos erosivos*. Retrieved from isbn: 978-84-608-3043-6

Moshou, D., Gravalos, I., Kateris, D., Bravo, C., Oberti, R., West, J. S., & Ramon, H. (2012). Multisensor fusion of remote sensing data for crop disease detection. In *Geospatial Techniques for Managing Environmental Resources* (Vol. 9789400718586, pp. 201–219). Springer Netherlands. https://doi.org/10.1007/978-94-007-1858-6_13

Muangprathub, J., Boonnam, N., Kajornkasirat, S., Lekbangpong, N., Wanichsombat, A., & Nillaor, P. (2018). IoT and agriculture data analysis for smart farm. https://doi.org/10.1016/j.compag.2018.12.011

Nadler, A., Raveh, E., Yermiyahu, U., & Green, S. (2006). Stress Induced Water Content Variations in Mango Stem by Time Domain Reflectometry, 510–520. https://doi.org/10.2136/sssaj2005.0127

Namara, R. E., Nagar, R. K., & Upadhyay, B. (2007). Economics, adoption determinants, and impacts of micro-irrigation technologies: Empirical results from India. *Irrigation Science*, *25*(3), 283–297. https://doi.org/10.1007/s00271-007-0065-0

Nanda, M. K., Giri, U., & Bera, N. (2018). Canopy Temperature-Based Water Stress Indices: Potential and Limitations. In *Advances in Crop Environment Interaction* (pp. 365–385). Singapore: Springer Singapore. https://doi.org/10.1007/978-981-13-1861-0_14

Noriega, N., Ruben, J., ZaValeta, N., Izquierdo, C., Rubén Nava Noriega, J., Nava Zavaleta, J., & Córdova Izquierdo, A. (2005). Alimento balanceado-forraje verde idropónico en la alimentación de conejos criollos (oryctolagus cuniculus). *Revista Electrónica de Veterinaria REDVET*, *VI*. Retrieved from http://www.veterinaria.org/revistas/redvet

Novas, N., Alvarez-Bermejo, J. A., Valenzuela, J. L., Azquez, J. A. G., & Manzano-Agugliaro, F. (2019). Development of a smartphone application for assessment of chilling injuries in zucchini. Biosystems Engieenering, 181, 114–127. https://doi.org/10.1016/j.biosystemseng.2019.03.009

Nunes, R. S. de L., de Assis Figueiredo, F. A. M. M., Martins, A. O., de Deus, B. C. da S., Ferraz, T. M., Gomes, M. de M. de A., … Campostrini, E. (2015). Partial rootzone drying (PRD) and regulated deficit irrigation (RDI) effects on stomatal conductance, growth, photosynthetic capacity, and water-use efficiency of papaya. *Scientia Horticulturae*, *183*, 13–22. https://doi.org/10.1016/j.scienta.2014.12.005

Offenthaler, I., Hietz, P., & Richter, H. (2001). Wood diameter indicates diurnal and long-term patterns of xylem water potential in Norway spruce. *Trees - Structure and Function*, *15*(4), 215–221. https://doi.org/10.1007/s004680100090

Osroosh, Y., Peters, R. T., Campbell, C. S., & Zhang, Q. (2016). Comparison of irrigation automation algorithms for drip-irrigated apple trees. *Computers and Electronics in Agriculture*, *128*, 87–99. https://doi.org/10.1016/j.compag.2016.08.013

Pagán, E. R. (2012). *Uso de Indicadores del Estado Hídrico de la Planta para la Optimización del Riego en Cultivos Leñosos*. UNIVERSIDAD POLITÉCNICA DE CARTAGENA.

Pastor, M., Castro, J., Mariscal, M. J., Vega, V., Orgaz, F., Fereres, E., & Hidalgo, J. (1999). RESPUESTAS DEL OLIVAR TRADICIONAL A DIFERENTES ESTRATEGIAS Y DOSIS DE AGUA DE RIEGO. *Nvest. Agr.: Prod. Prot. Veg*, *14*(3). Retrieved from https://helvia.uco.es/bitstream/handle/10396/2398/fererescastiel4.pdf?sequence=1&isAllowed=y

Pérez, M., Puche, M., Soto, E., Figueroa, R., Gutierrez, M., & Avilán, L. (2012). El régimen hídrico como determinante ambiental en la iniciación floral de los cultivares de mango (Mangifera indica L.) Haden y Edward en condiciones tropicales. *Revista Científica UDO Agrícola*, *12*(4), 770–778.

Perry, C. (2011). Accounting for water use: Terminology and implications for saving water and increasing production. *Agricultural Water Management*, *98*, 1840–1846. https://doi.org/10.1016/j.agwat.2010.10.002

Proaño, J., & Correa, M. (2006). *"DETERMINACIÓN DE LA PROGRAMACIÓN DEL RIEGO Y LA FERTIRRIGACIÓN EN EL CULTIVO DEL MANGO (Mangífera indica)*. Ecuador. Retrieved from www.uagraria.edu.ec

Puerto, P., Domingo, R., Torres, R., Pérez, A. P., & García, M. R. (2013). Remote management of deficit irrigation in almond trees based on maximum daily trunk shrinkage. Water relations and yield. *Agricultural Water Management*, *126*, 33–45.

Ravazzani, G. (2016). Open hardware portable dual-probe heat-pulse sensor for measuring soil thermal properties and water content. https://doi.org/10.1016/j.compag.2016.12.012

Romero, A. C., Kusakabe, A., & Melgar, J. C. (2014). Physiological responses of citrus to partial rootzone drying irrigation. *Scientia Horticulturae*, *169*, 234–238. https://doi.org/10.1016/j.scienta.2014.02.022

Santacruz, E. E. D. L., & Santacruz, G. D. L. (2019). Análisis Crítico del Consumo de Agua en Establecimientos Hoteleros de México. *ROSA DOS VENTOS - Turismo e Hospitalidade*, *11*(3). https://doi.org/http://dx.doi.org/10.18226/21789061.v11i3p664

Savage, M. J., Everson, C. S., & Metelerkamp, B. R. (2009). Bowen ratio evaporation measurement in a remote montane grassland: Data integrity and fluxes. *Journal of Hydrology*, *376*, 249–260. https://doi.org/10.1016/j.jhydrol.2009.07.038

Schulze, K., Spreer, W., Keil, A., Ongprasert, S., & Müller, J. (2013). Mango (Mangifera indica L. cv. Nam Dokmai) production in Northern Thailand-Costs and returns under extreme weather conditions and different irrigation treatments. *Agricultural Water Management*, *126*, 46–55. https://doi.org/10.1016/j.agwat.2013.04.010

Sepulcre-Cantó, G., Zarco-Tejada, P. J., Jiménez-Muñoz, J. C., Sobrino, J. A., De Miguel, E., & Villalobos, F. J. (2006). Detection of water stress in an olive orchard with thermal remote sensing imagery. *Agricultural and Forest Meteorology*, *136*, 31–44. https://doi.org/10.1016/j.agrformet.2006.01.008

Sepulcre-Cantó, G., Zarco-Tejada, P. J., Sobrino, J. A., Berni, J. A. J., Jiménez-Muñoz, J. C., & Gastellu-Etchegorry, J. P. (2009). Discriminating irrigated and rainfed olive orchards with thermal ASTER imagery and DART 3D simulation. *Agricultural and Forest Meteorology*, *149*(6–7), 962–975. https://doi.org/10.1016/j.agrformet.2008.12.001

Silber, A., Israeli, Y., Levi, M., Keinan, A., Shapira, O., Chudi, G., … Assouline, S. (2012). Response of “Hass” avocado trees to irrigation management and root constraint. *Agricultural Water Management*, *104*, 95–103. https://doi.org/10.1016/j.agwat.2011.12.003

Silber, A., Naor, A., Israeli, Y., & Assouline, S. (2013). Combined effect of irrigation regime and fruit load on the patterns of trunk-diameter variation of “Hass” avocado at different phenological periods. *Agricultural Water Management*, *129*, 87–94. https://doi.org/10.1016/j.agwat.2013.07.015

Spreer, W., Müller, J., Hegele, M., & Ongprasert, S. (2009). Effect of deficit irrigation on fruit growth and yield of mango (mangifera indica l.) in Northern Thailand. In *Acta Horticulturae* (Vol. 820, pp. 357–364). International Society for Horticultural Science. https://doi.org/10.17660/ActaHortic.2009.820.41

Spreer, W., Nagle, M., Neidhart, S., Carle, R., Ongprasert, S., & Mu, J. (2007). Effect of regulated deficit irrigation and partial rootzone drying on the quality of mango fruits (Mangifera indica L ., cv . ‘ Chok Anan ’), *88*, 173–180. https://doi.org/10.1016/j.agwat.2006.10.012

Teixeira, A. H. d. C., Bastiaanssen, W. G. M., Moura, M. S. B., Soares, J. M., Ahmad, M. D., & Bos, M. G. (2008). Energy and water balance measurements for water productivity analysis in irrigated mango trees, Northeast Brazil. *Agricultural and Forest Meteorology*, *148*(10), 1524–1537. https://doi.org/10.1016/j.agrformet.2008.05.004

Urrutia-Jalabert, R. B., Rossi, S. B., Deslauriers, A. B., Malhi, Y. A., & Lara, A. (2015). *Environmental correlates of stem radius change in the endangered Fitzroya cupressoides*. *Environmental correlates Agricultural and Forest Meteorology* (Vol. 200).

Varmaghani, A., Eichinger, W. E., & Prueger, J. H. (2019). Modification of FAO Penman–Monteith equation for minor components of energy. *Hydrology Research*, *50*(2), 607–615. https://doi.org/10.2166/nh.2018.093

Velez, J. E., Intrigliolo, D. S., & Castel, J. R. (2007). Scheduling deficit irrigation of citrus trees with maximum daily trunk shrinkage. *Agr i c Ultural Water Management*, *90*, 197–204. https://doi.org/10.1016/j.agwat.2007.03.007

Wang, D., & Gartung, J. (2010). Infrared canopy temperature of early-ripening peach trees under postharvest deficit irrigation. *Agricultural Water Management*, *97*(11), 1787–1794. https://doi.org/10.1016/j.agwat.2010.06.014

Wanjura, D. F., Maas, S. J., Winslow, J. C., & Upchurch, D. R. (2004). Scanned and spot measured canopy temperatures of cotton and corn. *Computers and Electronics in Agriculture*, *44*(1), 33–48. https://doi.org/10.1016/j.compag.2004.02.005

Yassin, M. A., Alazba, A. A., & Mattar, M. A. (2016). Artificial neural networks versus gene expression programming for estimating reference evapotranspiration in arid climate. *Agricultural Water Management*, *163*, 110–124. https://doi.org/10.1016/j.agwat.2015.09.009

Yunusa, I. A. M., Walker, R. R., & Lu, P. (2004). Evapotranspiration components from energy balance, sapflow and microlysimetry techniques for an irrigated vineyard in inland Australia. *Agricultural and Forest Meteorology*, *127*, 93–107. https://doi.org/10.1016/j.agrformet.2004.07.001

Zarco, P. J. T., González, V. D., & Berni, J. A. J. (2012). Fluorescence, temperature and narrow-band indices acquired from a UAV platform for water stress detection using a micro-hyperspectral imager and a thermal camera. *Remote Sensing of Environment*, *117*, 322–337. https://doi.org/10.1016/j.rse.2011.10.007

Zegbe, J. A. D., Behboudian, M. H., Lang, A., & Clothier, B. E. (2003). Deficit irrigation and partial rootzone drying maintain fruit dry mass and enhance fruit quality in “Petopride” processing tomato (Lycopersicon esculentum, Mill.). *Scientia Horticulturae*, *98*(4), 505–510. https://doi.org/10.1016/S0304-4238(03)00036-0

Zimmermann, D., Reuss, R., Westhoff, M., Geßner, P., Bauer, W., Bamberg, E., … Zimmermann, U.

(2008). A novel, non-invasive, online-monitoring, versatile and easy plant-based probe for measuring leaf water status. *Journal of Experimental Botany*, *59*(11), 3157–3167. https://doi.org/10.1093/jxb/ern171

3 SMARTPHONE WARNS PRODUCERS WHEN TO IRRIGATE MANGO TREES

2950 Niles Road, St. Joseph, MI 49085-9659, USA
269.429.0300 fax 269.429.3852 hq@asabe.org www.asabe.org

An ASABE Meeting Presentation

DOI: https://doi.org/10.13031/326.201900596

Paper Number: 1900596

Smartphone warns producers when to irrigate mango trees

Federico Hahn[1], Jesús García[2]

[1]Irrigation Dept., Universidad Autonoma Chapingo, Texcoco, Edo. México. Email: fedhahn@gmail.com

[2]IAUIA, Universidad Autonoma Chapingo, Texcoco, Edo. México.

Written for presentation at the
(2019-326 in Apps Agriculture Applications)
Sponsored by ASABE
(Boston, Massachusetts)
(July 7-10, 2019)
[Click here to mention other presentations of this paper (optional)]

Abstract. *The dendrometer has become essential equipment for predicting controlled deficit irrigation (CDI) in precision agriculture. The information provided by the instrument is proportional to the tree behavior, surpassing algorithms using soil moisture sensors and evapotranspiration. The dendrometer installed in mango tree stems, captures the data provided by a linear sensor, stores them in an SD memory and transmits them via bluetooth. The acquisition system must monitor the variations of the trunk size every 10 minutes with 10 repetitions per cycle to obtain an accurate knowledge of the tree behavior. The greatest difficulty found by producers in using dendrometers lies in interpreting data together with its statistical management. The application of a smartphone allows the activation of the dendrometer bluetooth to transmit data to the cell phone and indicate if it is necessary to irrigate the trees. Bluetooth high energy consumption causes battery energy decay; so it is advisable to use a switch activated by the producer. Also, another screen shows environmental (temperature, RH) and dendrometer variables such as battery status and memory load. The system has already been used successfully in Guerrero Mexico.*

.

Keywords: *Bluetooth, deficit irrigation, dendrometer, smartphone application.*

3.1 Introduction

Water demand will increase due to population growth and food demand (De Fraiture and Wichelns, 2010). 70% of fresh water is used in agriculture as the main consumer (FAO, 2014).

Irrigation programming can be achieved using equipment that is monitored in real time at the site of interest, such as weather stations that provide data used to estimate ET or the use of soil moisture sensors (SWS). The use of ET requires measuring the demand for water in the atmosphere and in the soil to be able to recommend automated irrigation programs, which are adapted to the hydric needs of the crop. Regional weather networks that provide environmental measurements (i.e., temperature, solar radiation, relative humidity, wind speed, and rainfall) They are climate variables available in meteorological stations that are commonly used for the development of irrigation programs that are based on ET (Pavan et al., 2011; Dukes, 2012). Currently there are tools for irrigation programming in which data from meteorological stations are integrated in a practical way, which data is provided in real time. On the other hand, these tools use simple models for water balance. (Morgan et al., 2006).

However, in practice the use of prediction models is limited to the need for the use of computers, causing the difficulty of poor interaction between user and tool. on the other hand, the use of smartphones offers real-time data, greater versatility and a continuous interaction between the user and the tool. ones and the availability of meteorological data have resulted in an ideal situation to design and implement smartphone applications for irrigation programming (Bartlett et al., 2015; Migliaccio et al., 2016). Using this concept, several Smart Irrigation apps were developed. In Italy, a new smartphone application, called Bluleaf®, was developed and tested showing its capacity to save water and energy with respect to traditional irrigation practices (Todorovic et al.,2016). Bluleaf® provided daily customized irrigation scheduling using local meteorological data on a real-time basis, obtaining water saving of at least 1000 m^3/ha (Abi Saab et al. 2019). This tool constitutes a promising solution for irrigation scheduling by maintaining a very good soil water balance in the root zone.

In this way, the methods that involve discrete measurements of the hydric state of the plant have limitations such as: the need for field trips to make measurements, intensive and relatively cumbersome work. On the other hand, techniques that use real-time sensors such as sap flow and stem diameter, immediate, consistent and reliable measures of the tree's response to water deficit (Goldhamer et al. 1999, Ortuño et al. 2004). That is why, it is sought to evaluate the use of automatic indicators of the hydraulic systems that are evaluated in the plants themselves for their irrigation programming. (Fernández et al. 2001).

In this project an application was developed in order that a normal producer can apply the results of a recently built dendrometer. Dendrometer present excellent data in water stress detection but its difficulty appears during its interpretation

3.2 Materials and methods

The dendrometer is an apparatus that measures the axial variations and the thickness of the trunk, these variations in the diameter have a physiological basis, showing an imbalance between transpiration and water absorption during the day. The linear displacement sensor used to measure this variation is a resistance (model 9605R1.7KL2.0, BEISensors, 1% linearity, USA), providing an analog voltage variation, which is acquired by a port of the AVR microcontroller (Atmega 328P, Microchip, USA) of the NANO card. The NANO system is connected to a real time card (RTC) to program the acquisition times, a module reading the temperature and the relative humidity of the day were monitored through DHT sensors (model DHT22 with precision of 0.5 ° C, 2-5% for humidity), the temperature of the sheet was measured through infrared sensors (MELEXIS, model MLX90614 of resolution of 0.02 ° C and an accuracy of 0.5 ° C) which were installed at 1.5 m, at the main sheets, and an MSD module to store the information in memory.

In the same way, the device is provided by a Bluetooth module for wireless transmission of the data that allows to communicate it with an intelligent device such as a smartphone, a tablet or a laptop, where an application is executed that shows the results of the data processing sensed the water conditions of the trees during a time interval and instructs the operator (producers) the actions to be executed through simple instructions or intuitive graphics and easy interpretation.

3.2.1 Dendrometer load analysis

The electrical demand of the dendrometer depends on the energy consumption of each component of the system and is analyzed during a period of one hour. A resistance connected in series between the negative pole and the circuit provides a voltage drop proportional to the current used by the circuit and which is acquired by a datalogger (NOVUS, model LogBox-AA) every second for one hour.

To achieve the goal of low consumption of the device, you have to use the sleep mode of the microcontroller. The possibility of replacing the switch with a latching type relay (NAIS, model DS2E-M2-DC5V) or in better case with a Mosfet N channel (VISHAY, IRF720) was evaluated. Using these power cut-off devices, it is achieved that the other modules (such as the clock, the SD, the temperature sensors) make use of the energy in idle mode. The Mosfet is ideal for making the system work automatically, and you can activate the sensors whenever you want. That's why the board has the normal line of GND to power the processor and then a switched line of GND called GND_2.

3.2.2 Data processing

The data raised by the sensors are processed by the microcontroller and stored in the MSD memory; the system includes an intelligent electronic device selected from a tablet, a cell phone or a computer where an application is housed with which the system acquires the data, the graphics, and indicates to the producer without values (numbers) if the tree requires irrigation. The data of the three environmental sensors (leaf temperature, air temperature and RH) are interpreted to help make decisions in case of rain, cloudy days and phenological stages of the crop.

3.2.3 Dendrometer system

The data acquisition process is programmed the sampling time of 10 minutes executed by the microcontroller of the system to determine the water condition of the trees of an orchard. In this program the variables of the minimum and maximum contraction MIN and MAX of the trunk. The program acquires digital or analog signals from the temperature, humidity and linear displacement sensors. 10 measurements per sensor are acquired continuously, and stored in the MSD memory. It is determined if the value obtained is greater than the MAX maximum, always looking for the highest value stored to calculate the GCF; if it is larger, the value in the memory is saved in MAX; if it is not, it is determined if the obtained value is lower than the MIN minimum and if it is it is stored in the MIN memory and the MCD is calculated from there. The calculated values (MCD) as well as the MIN and MAX are stored in the MSD memory.

that illustrates a block diagram of the process from the data transmission circuit of the electronic device of the system to determine the water condition of the trees, in this figure 1 the process starts and first asks and waits to see if the Bluetooth is activated, what which is generated when the switch is activated. If it is not active the action is repeated; if it is active or linked then it waits for the signal from the smartphone, then it acquires the "x" character of the smartphone's input and asks to determine if the "x" character is in the database, if it is not found then it does not exist

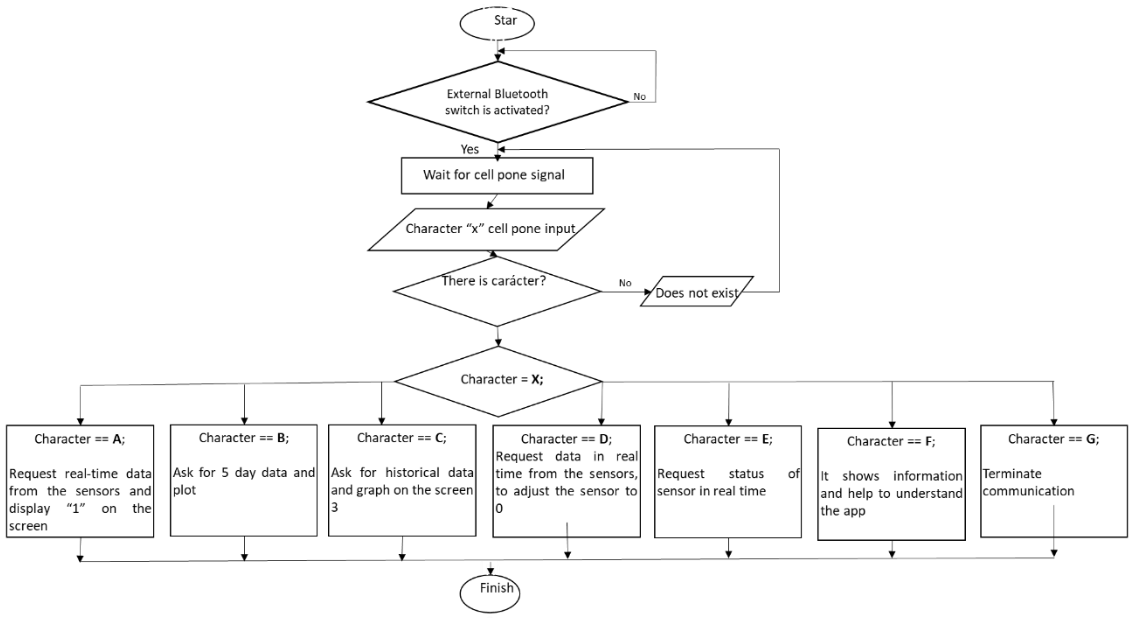

Figure 1 Process from the data transmission circuit of the electronic device of the system to determine the water condition of the trees. The "character A" obtains the real-time information from the sensors data and shows on a first screen; while the "character B" asks for the data of the last three days and graphs on a second screen. The "C character" requests the historical data and graphs in a third screen; while the "character D" requests the real-time values of the sensors obtained during the calibration and is shown in a fourth screen to adjust the linear displacement sensor to calibrated zero value. The "E character" asks for the status of each sensor in real time, while the "F character" provides help to the user. Finally, the "G character" ends with the transmission operation.

3.2.4 Intelligent device system

With reference to Figure 2 showing a block diagram of the operation process of the application running on the smart mobile device, it shows its start on the screen to be introduced and later it is analyzed if the Bluetooth is on, if it is then it determines if you want to deactivate and disconnect the Bluetooth, later the data reading clock must be disabled and the exit button must be enabled, if the exit button is pressed then it ends operation. If the Bluetooth is not active then it asks if you want to activate it, if you do not want to activate it then it is channeled; but if you want to activate it then the button to connect Bluetooth must be enabled and the clock disabled, and then in the next step the Bluetooth and the data reading clock enabled; then an action must be performed if you want to select a screen and data reception is implemented. At the end of the data reception, you wait again if you want to select a different screen. If a screen is selected then "character A" sensors, "character B" graphs, "C character" historical graphs, "character D" calibration, "Character" sensor status "E" character and "F character" information can be selected. In all cases, the "x" character is sent from the screen.

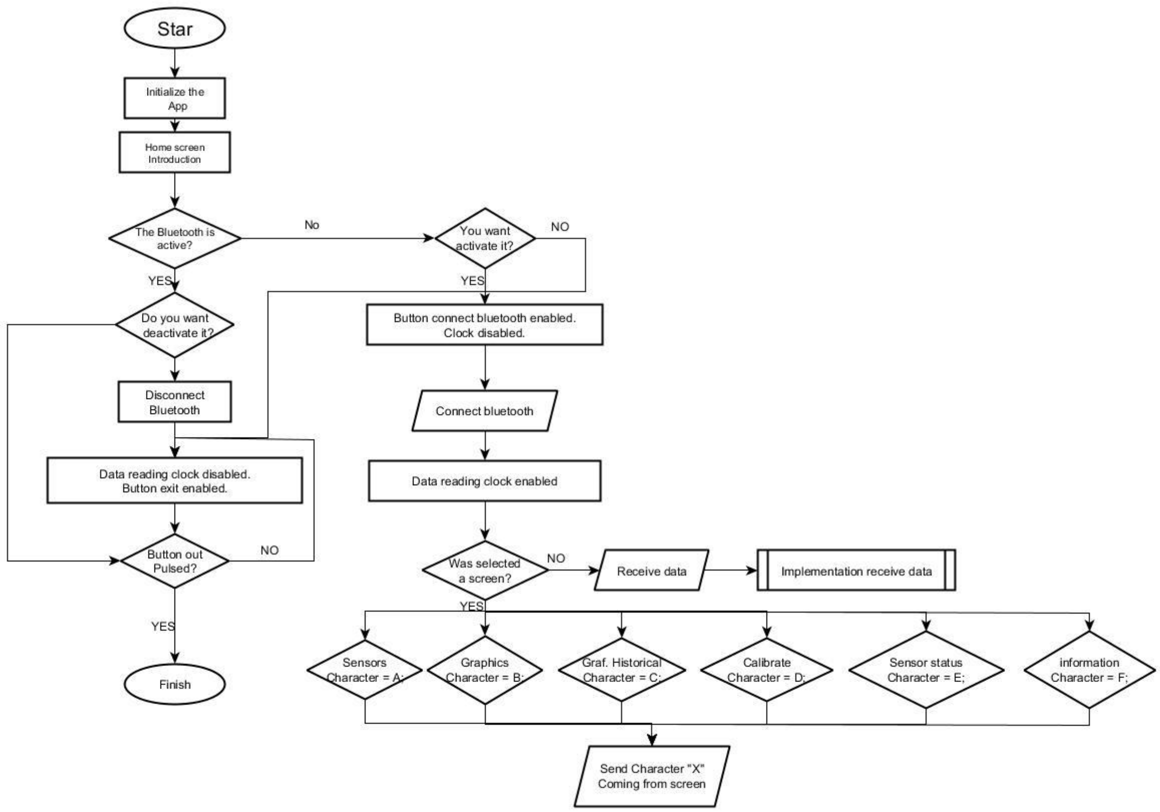

Figure 2 Process of data acquisition by the system to determine the water condition of the trees

3.3 Discussion and results

3.3.1 Load analysis of the dendrometer

The energy that the circuit consumes in its entirety was calculated to be 60 mAh. By partially disconnecting components such as bluetooth by means of a switch it was observed that this device consumes 33 mAh. The Bluetooth card which is the transmission device and the most current consumes, comprises an external switch in the electronic device to turn it on when you want to get the information read or a

Mosfet to activate the Bluetooth card from the microcontroller which decreased the total consumption by 55%.

The tests of the Sleep mode in the microcontroller manage to go down from a general consumption of 20 mAh (33.4%) to only 4 mA, achieving significant energy consumption for the suspension phase. The tests show that the real time it takes to take data is 5 seconds, and the consumption rises to 43 mA, this consumption is obtained during the measurement, every 10 minutes.

Analyzing the graphic publications, you can deduce that the developed automatic control system works acceptably. It can be seen in figure 3 the shape of the sensors have been able to measure the trunk variations required by the control system to keep its value close to the water deficit required for the phenological stage. In some sectors of the graphs disturbances are observed, these disturbances were due to power cuts. Verify, in the graphs that the controller is able to regain control once the disturbance was eliminated

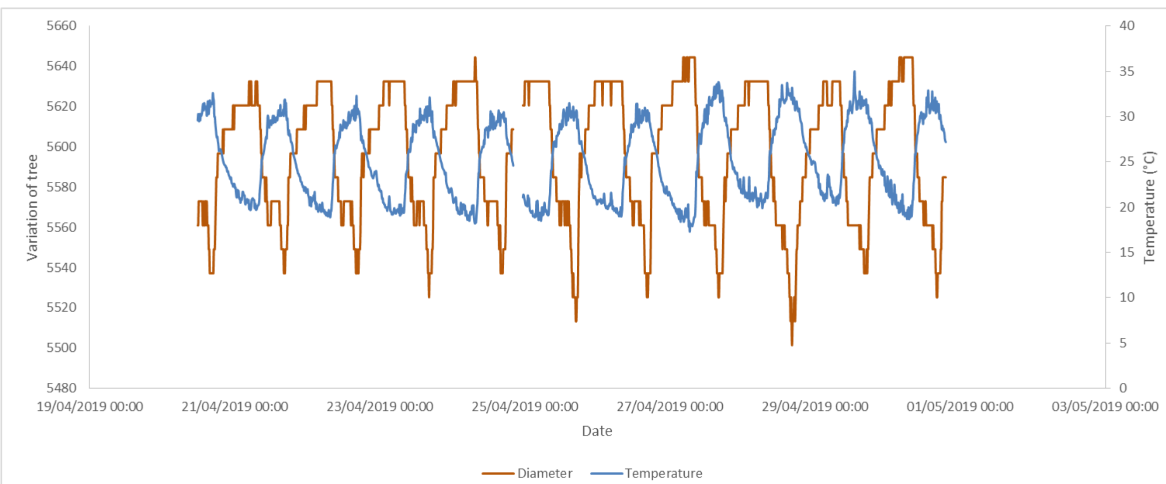

Figure 3 Trunk variations during five days of control

The use of a more elaborate control algorithm will allow the variation of the water deficit of the trunk to be approached with smaller variations to the reference, achieving greater productivity in irrigation.

The screens allow to observe different application functionalities, as shown in figure 4a, which shows a general menu, where it houses 6 main screens: sensors screen (figure 4b), which shows in real time the measurement made by the sensors; the status screen (figure 4c), where it shows if any sensor is not recognized or has a malfunction; calibration screen, where the aim is to calibrate the sensor of the trunk diameter to a reference value; help screen (figure 5), which gives the farmer the option to contact the programmer in case there are problems with the sensors; graphic screen (figure 6), where trunk variations are shown on a daily, weekly or historical basis, providing help and recommendation for future risks.

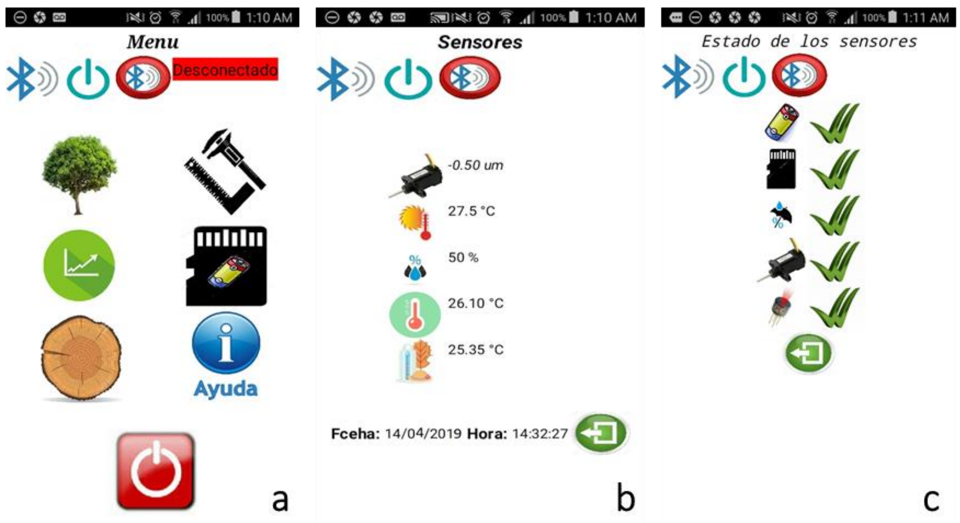

Figure 4 Application screens.

Figure 5 Help screen

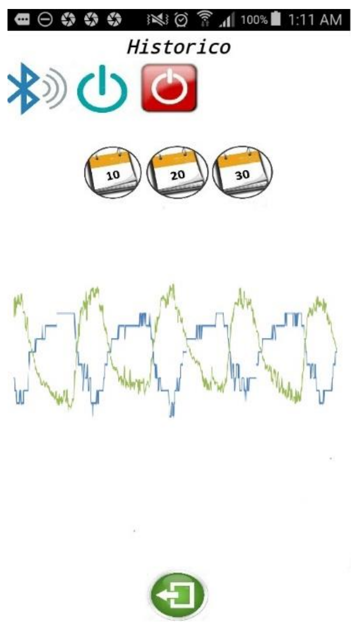

Figure 6 Graphic screen

3.4 Conclusion

The equipment has been tested with many producers and even those that cannot read have been able to get profits from their farms. Although one of the main problems is to maintain the cells charged work has been carried to include solar cells in the future. Cloud-web management and introducing data ibn internet are the new proposals for the next funding. Companies are using our system as nodes and they are providing gateway equipment for national management.

3.5 Acknowledgments

I will like to thank the University authorities for their help and all the producers that open their doors to our research.

3.6 References

Abi Saab, MT., Jomaa, I., Skaf, S., Fahed, S., Todorovic, M. (2019) Assessment of a Smartphone Application for Real-Time Irrigation Scheduling in Mediterranean Environments. *Water*, *11*, 252. https://doi.org/10.3390/w11020252.

Bartlett, AC., Andales, AA., Arabi, M., Bauder, TA. (2015) A smartphone app to extend use of a cloud-based irrigation scheduling tool. Comput. Electron. Agric., 111, 127–130.

Dukes, MD. (2012) Water conservation potential of landscape irrigation smart controllers. *Trans. ASABE, 55*(2), 563-569.

De Fraiture, C., & Wichelns, D. (2010). Satisfying future water demands for agriculture. *Agric. Water Mgmt., 97*(4), 502-511. http://dx.doi.org/10.1016/j.agwat.2009.08.008.

FAO. (2014). Water uses website. Rome, Italy: United Nations FAO. Retrieved from www.fao.org/nr/water/aquastat/water_use/index.stm.

Fernández, JE., Palomo, M.J., Díaz-Espejo, A., Clothier, BE., Green, SR. Girón, IF., Moreno, F. (2001). Heat-pulse measurements of sap flow in olives for automating irrigation: tests, root flow and diagnostics of water stress. Agric. Water Manage. 51:99–123.

Goldhamer, DA., Fereres, E., Mata, M., Girona, J., Cohen, M. (1999). Sensitivity of continuous and discrete plant and soil water status monitoring in peach trees subjected to deficit irrigation. J. Am. Soc. Hortic. Sci. 124:437–444.

Migliaccio, KW., Morgan, KT., Vellidis, G., Zotarelli, L., Fraisse, C., Zurweller, BA., Andreis, JH.; Crane, JH., Rowland, D.L. (2016) Smartphone APPS for irrigation scheduling. ASABE, 59, 291–301.

Morgan, KT., Obreza, TA., Scholberg, JM., Parsons, LR., Wheaton, TA. (2006) Citrus water uptake dynamics on a sandy Florida entisol. SSSA J., 70, 90–97.

Ortuño, MF., Alarcón, JJ., Nicolás, E. Torrecillas, A. (2004) Interpreting trunk diameter changes in young lemon trees under deficit irrigation. Plant Sci. 167:275–280.

Pavan, W., Fraisse, CW., & Peres, NA. (2011). Development of a web-based disease forecasting system for strawberries. *Comput.Elec. Agric., 75*(1), 169-175.

Todorovic, M., Riezzo, EE., Buono, V., Zippitelli, M., Galiano, A., Cantore, V. (2016) Hydro-Tech: An automated smart-tech Decision Support Tool for eco-efficient irrigation management. Int. Agric. Eng. J., 25, 44–56.

4 MANEJO AUTÓNOMO DE BATERÍAS DE LITIO USADAS POR DENDRÓMETROS INSTALADOS EN BOSQUES O HUERTAS REMOTAS

4.1 Resumen

Introducción: Equipos de monitoreo remoto donde el personal no tiene acceso y requiere de sistemas autónomos de energía. El dendrómetro captura la variación de crecimiento en ramas del árbol con un sensor lineal, almacenando los datos en una memoria SD, y transmitiéndolos por bluetooth.

Objetivos: Evaluar el consumo energético (corriente y voltaje) de cada componente electrónico de un dendrómetro, para determinar la cantidad de baterías de litio requeridas para proporcionar dos días de mediciones continuas en huertas remotas.

Materiales y métodos: La optimización del consumo energético del dendrómetro analiza el número de muestreos por hora (5, 10, 15, 30 minutos) y el número de repeticiones por muestreo (5, 10, 15, 25). La resolución de las curvas obtenidas no debe perderse al reducirse el número de repeticiones adquiridas. Las curvas características de carga y descarga de las baterías de litio se obtuvieron con un datalogger simulando la carga del instrumento con una resistencia. Se construyó un controlador de carga fotovoltaico (550 mA) que utiliza circuitos TP4056 para cargar automáticamente baterías de litio. La aplicación de la rutina de modo suspensión aplicada en software, alarga la vida útil de las baterías brindando más días de autonomía.

Resultados y discusión: El conocimiento del comportamiento del árbol por el dendrómetro requiere de monitoreos cada 10 minutos con 10 repeticiones por ciclo. El consumo es de 26.4 mAh y la duración de una batería ICR18650 es de 48 horas. El controlador fotovoltaico que opera con una eficiencia del 95% realiza la carga de la batería con corriente constante en 3 horas durante un día soleado y durante 4 horas en un día nublado. La rutina de modo de suspensión, demostró tener un consumo de 4 mAh con una autonomía de 8 días

Conclusiones: Independientemente de las condiciones ambientales el sistema operó sin ningún contratiempo por 4 meses. Las baterías de litio demostraron tener alta densidad energética y eficiencia.

Palabras claves: Optimización energética/ monitoreo del crecimiento del tronco/ recarga solar automática/ ICR18650.

4.2 Abstract

Introduction: Remote monitoring equipment where humans do not have access requires autonomous power systems. The dendrometer captures the growth variation of tree branches with a linear sensor, storing the data in a SD memory, and transmitting them by bluetooth.

Objectives: Evaluate the energy consumption (current and voltage) of the electronic components of the dendrometer, to determine the quantity of lithium batteries required to provide two days of continuous measurements in remote orchards.

Materials and methods: The optimization of the energy consumption of the dendrometer analyzes the number of samples per hour (5, 10, 15, 30 minutes) and the number of repetitions per sample (5, 10, 15, 25). The resolution of the obtained curves should not be lost by reducing the number of repetitions acquired. The characteristic charge and discharge curves of the lithium batteries were obtained with a datalogger simulating the loading of the instrument with a resistance. A photovoltaic charge controller (550 mA) was built using TP4056 circuits to automatically charge lithium batteries. The application of the sleep mode routine applied in software, extends the life of the batteries providing more days of autonomy.

Results and discussion: Accurate knowledge of tree behavior by the dendrometer requires monitoring every 10 minutes with 10 repetitions per cycle. The consumption is 26.4 mAh and each ICR18650 battery lasts 48 hours. The photovoltaic controller that operates with an efficiency of 95% carries out the charging of the battery with constant current in 3 hours during a sunny day, increasing to 4 hours in a cloudy day. The routine of sleep mode, showed to have a consumption of 4 mAh with an autonomy of 8 days

Conclusions: Regardless of the environmental conditions, the system operated without any setback for 4 months. The lithium batteries allowed to have high energy density and efficiency.

Keywords: Energy optimization/ trunk growth monitoring/ automatic solar recharge/ ICR18650.

HIGHLIGHTS:

Sistemas electrónicos autónomos usan baterías de litio.

Autonomous electronic systems use lithium batteries.

Consumo de energía depende de tiempo de muestreo y repetividad.

Energy consumption depends on sampling time and repeatability.

Carga automática de baterías con panel solar.

Automatic charging of batteries with solar panel.

Carga independiente de condiciones ambientales.

Nondependent battery charging due to environmental conditions.

4.3 Introducción

Actualmente el 70% de agua consumida en México se utiliza para regar cultivos agrícolas (Luna & Grieger, 2015; Vélez & Saez, 2012), además en muchos lugares incluyen técnicas de gravedad, inundación y sistemas de presurización. Aunque estos últimos incluyen goteros y aspersores, el agua utilizada para regar cultivos debe adaptarse a las variaciones del cambio climático (Galindo et al., 2018). En el sector agrícola y en particular los árboles frutales, el manejo del agua es de gran importancia para optimizar y maximizar su producción (Blanco-Cipollone et al., 2017; Garcia-Tejera et al., 2015). Actualmente, en la agricultura de precisión se utilizan sensores para el control de riego eficiente (Schugurensky & Capraro, 2018).

Los sensores más importantes implementados para monitorear los flujos de agua en la interacción suelo-planta-atmósfera, son los sensores capacitivos de humedad del suelo (Kizito et al., 2008; Schugurensky & Capraro, 2018; Seyfried & Murdock, 2004), sensores de medición de flujo de savia (James, et al., 2002; López-López, et al., 2013; LU, Urban, & Zhao, 2004), y dendrómetros que tienen el principio de operación de medir variaciones de crecimiento del tallo del árbol (Intrigliolo y Castel, 2007; Drew & Downes, 2009). Los dendrómetros proporcionan una señal del comportamiento fisiológico del tallo a lo largo del día (De Swaef et al., 2015; Fernández, 2017; Hall, et al., 1978), por lo tanto, es un método excelente para el control del riego, para las necesidades hídricas de la misma planta (Miralles et al., 2016; Fereres & Soriano, 2007; Sheil, 2003), y además garantiza una respuesta rápida a los cambios en el árbol.

Los paneles solares dan solución al abastecimiento de energía en lugares remotos (Chung, et al., 2003; Feron, 2016), pero se requiere optimizar la etapa de almacenamiento de energía (Raghunathan et al., 2005). La demanda eléctrica proporcionada por las baterías es una parte fundamental en los circuitos electrónicos autónomos (Al-Shorman et al., 2018; Lawder et al., 2016, Li et al., 2011), y debe considerarse su operación en función del tiempo (Botero, 2012). La operación eficiente de un sistema remoto no debe requerir de personal para el intercambio de baterías en los equipos montados en huertas y bosques. Las baterías de litio-ion proporcionan un largo ciclo de vida, alta densidad energética, baja toxicidad, bajas fugas propias de descarga y alta eficiencia (Saw et al., 2016; Scrosati & Garche 2010). Para la carga de baterías de iones de litio, se han reportado diferentes técnicas de carga (Hussein y Batarseh, 2011; Chen, 2007; Tsang y Chan, 2011), tales como el de corriente constante y voltaje constante (CC / CV), el algoritmo de carga por pulsos, y los algoritmos de carga de corriente de etapas múltiples (MSCC).

Un dendrómetro fue diseñado y construido en el posgrado en Ingeniería Agrícola de la Universidad Autonoma Chapingo (Hahn & García, 2018). Al evaluarlo y probarlo en una huerta de mango se encontró que era fundamental que la alimentación del equipo fuera autónomo y no requiriera de cambios continuos de batería. En este trabajo se recolectaron datos del consumo energético de los circuitos del dendrómetro, así como la evaluación de las consecuencias que tienen los intervalos de medición, y la repetitividad de las mediciones realizadas. Los datos de carga y descarga (voltaje y corriente) recolectados de la batería de Li-ion permiten determinar su tamaño para obtener al menos dos días de autonomía. La energía proporcionada por un panel solar fue utilizada para cargar óptimamente las baterías y obtener una mayor eficiencia en su operación. Una autonomía total se obtendría usando dos baterías en paralelo, en donde una se carga mientras la otra alimenta al dendrómetro. El intercambio de baterías debe realizarse de forma automática cuando la carga almacenada en la batería que alimenta al dendrómetro cae por debajo del 35%.

Se optimizó la descarga del sistema utilizando una rutina de modo de suspensión, para asegurar que el tiempo de descarga aumente arriba de 8 días.

4.4 Materiales y métodos

El dendrómetro es un aparato que mide las variaciones axiales en el grosor del tronco o rama durante el transcurso del día. El sensor utilizado para medir dicha variación es una resistencia (modelo 9605R1.7KL2.0, BEISensors, USA), proporcionando una variación de voltaje analógico, el cual es adquirido por un puerto del microcontrolador AVR (Atmega 328P, Microchip, USA) de la tarjeta NANO. El sistema NANO se conecta a una tarjeta de tiempo real (RTC) para programar los tiempos de adquisición, a un módulo MSD para almacenar la información en memoria y a un módulo Bluetooth para la transmisión inalámbrica de los datos. Todos estos módulos se encuentran dentro del rectángulo punteado y mostrados en el diagrama a bloques de la figura 1.

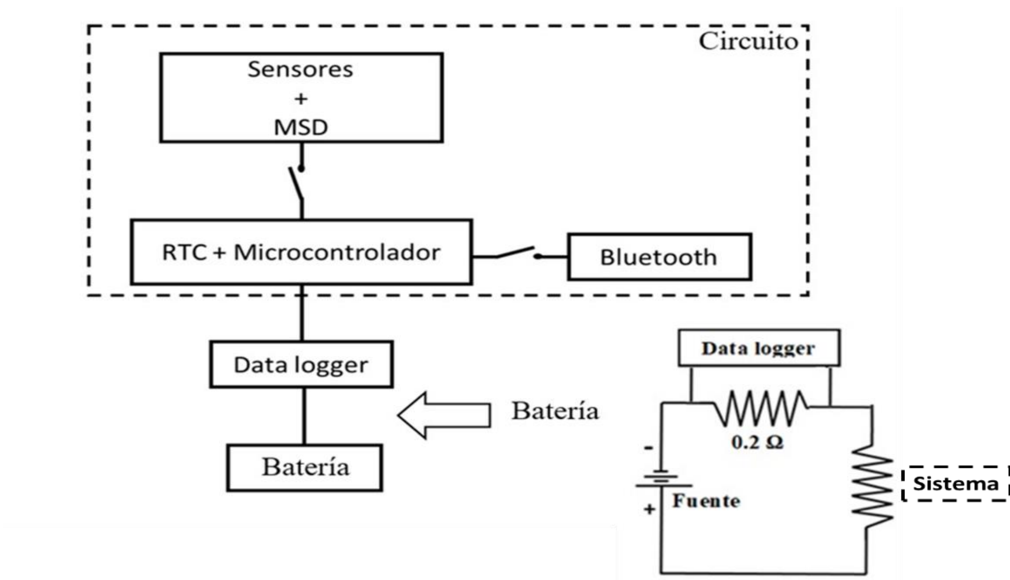

Figura 1 Diagrama de conexión del dendrómetro y del datalogger

4.4.1 Análisis de la carga del dendrómetro

La demanda eléctrica del dendrómetro dependió del consumo energético de cada componente del sistema y se analizó durante un período de una hora. Una resistencia de 0.2 Ω (Figura 1) conectada en serie entre el polo negativo y el circuito proporciono una caída de voltaje proporcional a la corriente utilizada por el sistema y el cual es adquirido por un datalogger cada segundo durante una hora. Para controlar los consumos por módulos, se usaron dos interruptores uno antes del bluetooth y otro antes de los sensores (Di Nisio et al., 2016).

Además, se evaluó el efecto del consumo energético al sustituir el interruptor por un relevador, en función del número de muestreos por hora. Un relevador es ideal para que el sistema trabaje de forma automática, activando los sensores cuando se desee. Por esta razón se adquirieron consumos energéticos del desplazamiento de la resistencia, en funcion al número de mediciones realizadas por hora.

La optimización del consumo energético del dendrómetro, considera el número de muestreos por hora (cada 5, 10, 15, 20 y 30 minutos) y el número de repeticiones por muestreo (5, 10, 15, 20 y 25). Al ser menor el tiempo entre mediciones, la curva de comportamiento de los flujos de agua en el árbol es más precisa, pero su consumo energético mayor. El segundo parámetro evaluó el promedio con mínima varianza de la variable estudiada basado en la cantidad de repeticiones. Una mayor longevidad en la carga almacenada en la batería es deseada y se obtuvo reduciendo el número de repeticiones.

4.4.2 Evaluación de carga y descarga de baterías

La elaboración de las curvas características de carga y descarga de las baterías ICR18650 tipo Li-ion de 3.7 V a 2200 mAh, se obtuvieron a través de un datalogger (mod LogBox-AA, NOVUS, Brasil). Las baterías fueron cargadas usando un cargador inteligente de baterías (Schumacher 1.5A), que aporto una corriente lineal máxima entre 20 y 30 mA de manera constante. El datalogger (Figura 2a) adquirió el amperaje y el voltaje de carga en la batería cada segundo (Di Nisio et al., 2016).

El datalogger se sustituyó por un celular SAMSUNG utilizando una aplicación que se comunicó con el microcontrolador, del cual obtuvo el estado de la carga, que la contabilizo precisamente. La alarma del sistema permitió que al llegar la energía almacenada (SoC) a un 15%, se activó una alarma y con ella se inició la recarga automática del sistema.

Las curvas de descarga de la batería se obtuvieron utilizando cuatro resistencias de diferentes valores (30, 50, 57 y 130 Ω). Estas resistencias simularon el consumo que proporciona el dendrómetro en condiciones variables de muestreo y de número de repeticiones. La resistencia se colocó en serie durante cada prueba. Posteriormente, se tomaron mediciones de corriente y voltaje cada segundo durante 34 horas (Figura 2b). A partir de las curvas de descarga de la batería y el consumo energético requerido por el dendrómetro, se obtuvieron diferentes tiempos de resoluciones del flujo del agua en el tallo. Además, se calcularon el número de baterías requerida para dos días de autonomía.

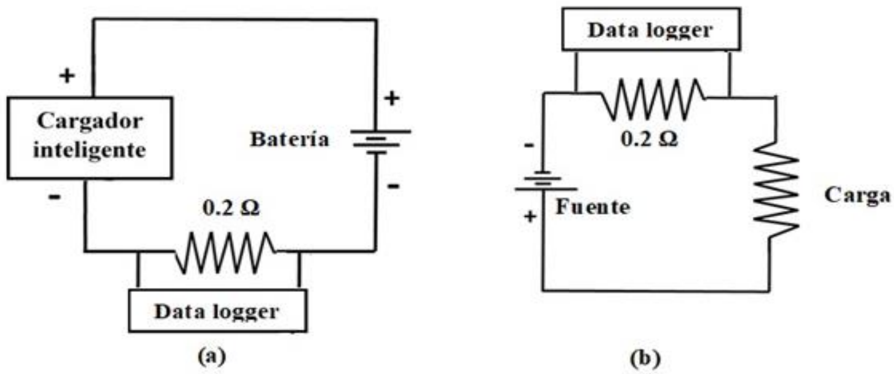

Figura 2 Diagrama del circuito para obtener las curvas de (a) carga y (b) descarga

4.5 Sistema fotovoltaico

El sistema fotovoltaico cargo automáticamente las baterías, de este modo, se seleccionaron dos celdas de 5W a 9V y 556 mA cada una (modelo KS-Q280G, China Solar Ltd., China). Se utilizaron dos pares de dos baterías en serie para proporcionar los 7.4 a 8.4 V requeridos por el dendrómetro y las otras dos baterías son simultáneamente cargadas por proceso de recarga a través del panel solar (Figura 3).

El cargador electrónico basado en el controlador TP4056 (NanJing Top Power, 2016) permitió programar la carga a corriente constante o la carga a voltaje constante. La carga a corriente constante realizada a una corriente de 0.2 a 0.7 de la capacidad de carga de la batería (440 mA a 1540 mA) finalizó cundo el voltaje de la batería alcanzó un valor de 4.2 V. Este periodo de carga se alcanzó en una hora utilizando una carga de 1 A. La carga a voltaje constante (4.2 V) se realizó hasta que la corriente de la batería disminuyo a 250 mA.

El microcontrolador NANO requiere de un voltaje superior a los 8 volts para operar satisfactoriamente si la señal proviene de un rectificador y se conecta a su terminal de alimentación (V_{in}) que tiene un regulador interno. Al provenir el voltaje de las baterías, la alimentación carece de rizo y el voltaje puede ser de 7 V.

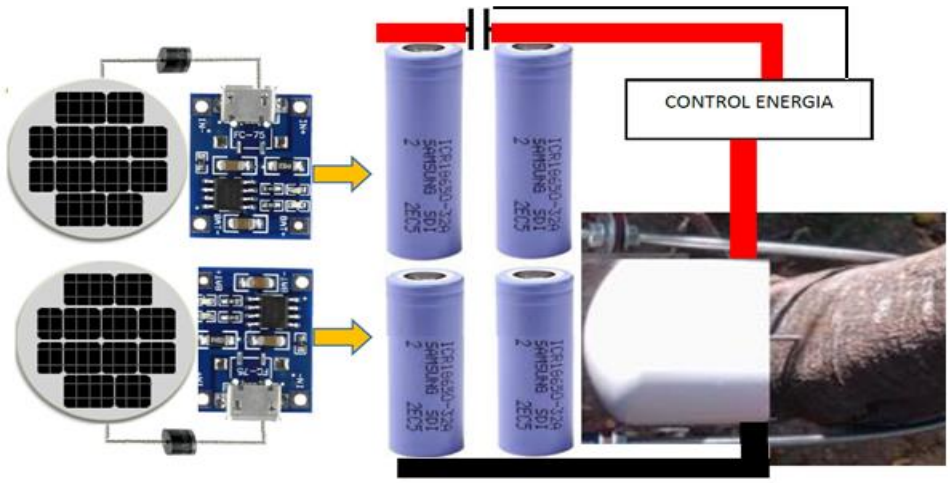

Figura 3 Sistema de carga y alimentación usado para la operación de dendrómetros.

El control de energía realiza tres operaciones fundamentales: muestreo de la carga en la batería, intercambio de baterías y finalmente carga de las baterías (figura 4a). La operación de estas rutinas no interfiere entre ellas y se realizan de forma independiente. En el monitoreo del estado de carga se mide la caída de voltaje en las pilas y cuando estas caen debajo de 7.5 V es necesario empezar la etapa de recarga. Si esto ocurre entre 6:00 y 11:00 AM conviene mantenerlas en uso hasta las 11:00 AM, puesto que el arreglo de baterías tiene una carga remanente de energía que puede durar hasta las horas de optima radiación, que ocurren regularmente a partir de las 11:00 AM, es en ese momento donde se hace el cambio de batería para recarga. Sin embargo, si ocurre en la noche se debe realizar el cambio de batería y empezar la recarga igualmente a las 11:00 AM.

El controlador de energía, desconecta las baterías descargadas. La batería superior empieza a cargarse al conectarle el circuito TP4056 a través de los contactos de relevador SW2 y SW3. La batería inferior se carga a través de los contactos SW5 y SW6 (Figura 4 b). El controlador de energía usa el microcontrolador Atmega 328P para activar tres relevadores. El primero activa los contactos SW1-3, el segundo activa al contacto SW4, mientras el tercero acciona los contactos SW5-7.

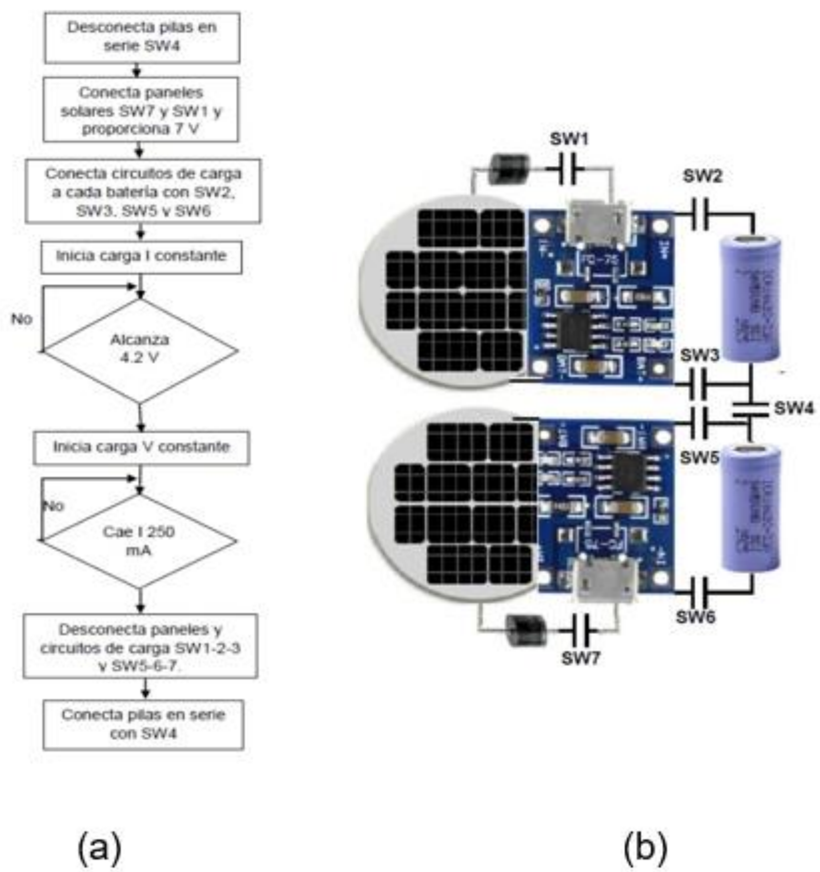

Figura 4 Operación del controlador de energía mostrando (a) el diagrama a bloques del circuito de carga y (b) la conexión de relevadores del mismo.

Cada panel se conectó a la entrada de la tarjeta controladora de carga, que contiene dos circuitos TP4056. El panel proporciono 9 V y mediante diodos reduce el voltaje a 7 V manteniendo la corriente en 550 mA. Esta tarjeta se programó para trabajar bajo el régimen de corriente constante o voltaje constante. Para iniciar la carga se conectan los contactos SW1 y SW7 entre la tarjeta de carga y la salida del diodo en serie del panel solar. La fase de carga con corriente constante duro hasta que la batería se carga a 4.2 V y de allí paso a la etapa de voltaje constante y terminó cuando la carga cae a 250 mA (Figura

4 a). La energía requerida para la operación de las tarjetas controladoras de energía y las tarjetas de carga es proporcionada por el panel solar antes de entrar al diodo.

4.6 Discusión y resultados

4.6.1 Análisis de la carga del dendrómetro

La energía que el circuito consume fue de 60 mAh. Al desconectar mediante un interruptor el bluetooth se observó que este dispositivo consume 33 mAh, lo cual representa el 55% del consumo energético total del circuito. El consumo de los sensores fue de 7 mAh (11.6%) y el del microcontrolador 20 mAh (33.4%). Dudacek y Vavricka (2007) mencionaron que la energía requerida para ejecutar tareas por microcontroladores es un parámetro importante a considerar. En consecuencia, frecuencias de trabajo entre 4 y 8 MHz afectaron el consumo total de energía. Al tener el bluetooth un consumo alto, se optó por instalar un interruptor para reducir el consumo total en un 55%. Este interruptor se sustituye por un relevador el cual se activa una vez al día cuando se transmitan los datos.

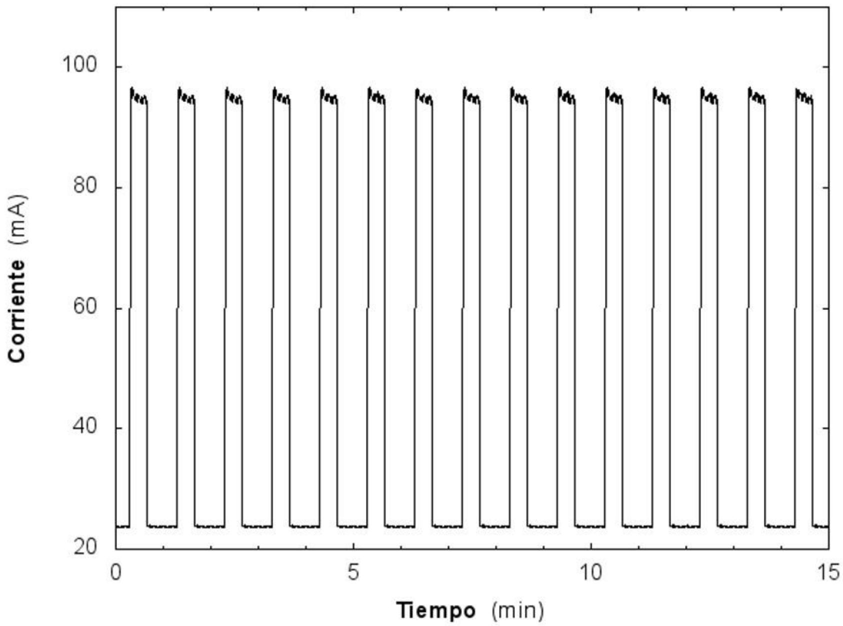

Figura 5 Consumo energético de accionar el relevador en intervalos de medición.

Un relevador conecta los sensores al microcontrolador cuando este lo requiere, por lo que los sensores solo se encienden durante las mediciones. La activación continua del relevador dentro del circuito presenta un consumo energético excesivo, el cual varía entre 90 y 95 mA (Figura 5). Teniendo en cuenta que el circuito sin relevador presenta un consumo total de 27 mAh, la activación del relé representa un aumento del 333%. Al variar los intervalos de muestreo durante una hora y la cantidad de mediciones hechas en cada intervalo, se ve afectado el consumo energético del sistema como se aprecia en la Tabla 1.

La diferencia en el consumo energético, se encuentra correlacionado directamente del tiempo que están encendidos los sensores y en particular el relevador. En otras palabras, aunque los sensores y el ARDUINO tengan consumos energéticos constantes, el consumo del dendrómetro depende de los tiempos de activación y de reposo del relevador. La sumatoria de consumos energéticos durante una hora de operación con sus respectivos ciclos se presentan en la tabla 1.

Cuadro 1 Consumo de corriente en función de muestreos por hora y número de mediciones por ciclo

periodo	muestreos por hora	Consumo mAh con diferentes repeticiones				
		5	10	15	20	30
5	12	26.4	52.8	79.4	106.1	158.8
10	6	13.2	26.4	39.7	53.0	79.4
15	4	8.8	17.6	26.4	35.4	53.0
20	3	6.6	13.2	19.9	26.4	39.7
30	2	4.4	8.8	13.2	17.7	26.4

Al incrementar el número de mediciones que hace el microcontrolador por hora, aumenta el tiempo en que el relevador permanece encendido consumiendo energía. Un alto consumo energético de 158.8 mAh se observa al adquirir 30 datos cada 5 minutos (Tabla 1). Sin embargo, si se mide dos veces por hora y se adquieren 5 datos por muestreo, el consumo energético se reduce a 4.4 mAh. El ahorro energético obtenido sería del 277%. Se puede apreciar en la Tabla 1, que todos los valores en la diagonal son de 26.4 mAh y los valores en la parte superior de esta diagonal muestran mayores consumos.

Los sensores presentan cierta incertidumbre a la hora de medir y para aumentar su confiabilidad deben utilizarse métodos estadísticos (Dudacek y Vavricka, 2007). En lo particular, el número de repeticiones por muestreo fue de 5, 10, 15, 20 y 30, los cuales fueron analizados y los valores almacenados en la memoria MSD. Por otra parte, en este dendrómetro se obtuvo una varianza alta al realizar 5 mediciones por muestreo. Sin embargo, a partir de 10 repeticiones no se observa efecto de forma significativa en la precisión del sensor ($P \leq 0.05$). Es decir, se puede prescindir de hacer un número elevado de mediciones para lograr un ahorro energético (Figura 6).

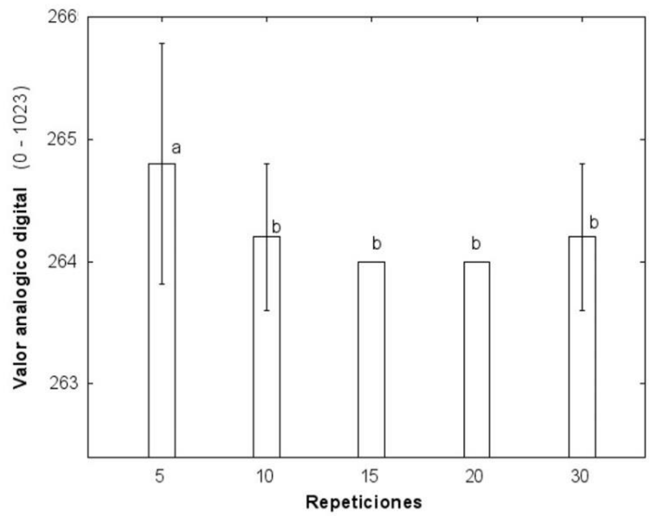

Figura 6 Variación en la medición del sensor resistivo lineal con 5, 10, 15, 20, 30 repeticiones después de pasar la conversión analógica digital de 10 bits en el Arduino NANO.

La precisión en la medición de la resistencia lineal no se ve afectado a partir de 10 repeticiones, aunque el consumo energético del dendrómetro aumenta con el número de repeticiones. Al obtener datos cada 10 minutos se obtiene informacion precisa del comportamiento del árbol, lo cual requiere de una memoria MSD para guardar el aumento del número de datos. El periodo de muestreo puede ser variable, sin embargo, Krepkowski *et al*., (2013) en sus estudios demostraron que no es necesario tener tanta resolución para describir la curva característica del flujo del agua en el tallo, reportado muestreos cada media hora. En cambio, Morandi et al., (2007) utilizaron resistencias variables conectadas a un datalogger CRX 10 para el muestreo del crecimiento de los tallos cada 12 minutos. En ambos casos, el muestreo presento el comportamiento del flujo de agua que atravesaba el tronco del árbol. Sin embargo, el sistema que se propone busca una mayor resolución para ser utilizado en los estudios de las principales causas de estrés en la planta.

La energía que la batería debe proporcionar para la medición de dos días utilizando mediciones cada 10 y 15 minutos y 10 repeticiones, es de 1333.2 y 910.8 mAh, respectivamente. Estos cálculos se obtienen de considerar un gasto horario de 26.4 mAh por adquisición y manejo de la información de una vez por día de 33 mAh para transmitir los datos. En una aplicación similar en donde se monitoreo en forma continua el metano en tiraderos de basura, donde se redujo el tamaño de la batería en un 50% después de reducir el número de repeticiones de 143 a 30 por muestreo (Fay et al., 2011). La adquisición de datos con un relevador debe considerar que este está diseñado para 100,000 contactos, por lo que considerando 10 muestreos por hora su vida es de 400 días y requiere de un cambio a menos que se sustituya por un relevador de estado sólido.

4.6.2 Carga y descarga de baterías

La capacidad de la batería depende significativamente de su estado de carga (SoC), la temperatura y la corriente de descarga (Waag et al., 2013). Chu et al., (2017) presentan en su modelo estrategias para la recuperación óptima de la carga en baterías, dando una reducción en el tiempo de carga de 5.56 a 2 h, usando velocidad de carga rápida sin deposición de litio. La batería Li-ion 18650 representa una solución factible a usuarios, ya que su tiempo de recarga requiere entre 2 a 2.5 h (Capasso y Veneri, 2014). Sin embargo, es recomendable solo descargar la carga de la batería a un máximo del 20% y el voltaje hasta 3.0 V, pues a partir de allí la vida útil de la batería decaerá drásticamente.

Capasso & Veneri (2014) evaluaron las características de carga, descarga y eficiencia en baterías de litio, demostrando que su capacidad real es cercana a su capacidad nominal, esto en comparación con baterías de plomo que muestran tan solo el 40% referido a su capacidad nominal. El fabricante de la batería ICR18650 recomienda que esta opere en un rango de temperatura de 20 y 60 °C, las cuales pueden existir en el circuito bajo ciertas condiciones a la intemperie.

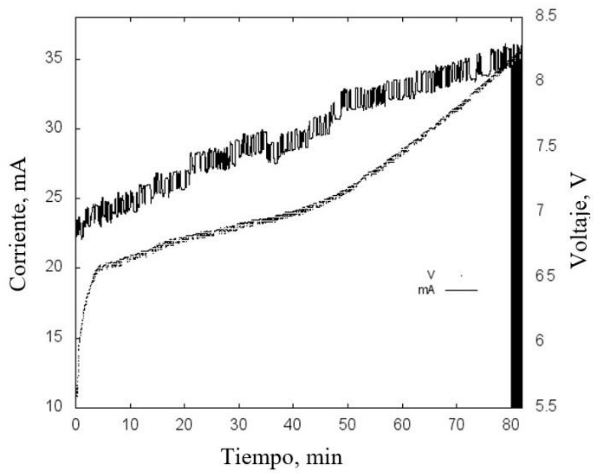

Figura 7 Curva de carga de Batería Li-ion 18650 utilizando un cargador inteligente.

En la figura 7 se aprecia como el datalogger tomó muestras del comportamiento de la carga lineal de la batería Li-ion 18650 alcanzando la carga completa en un tiempo de 2 horas con un cargador inteligente. El celular Samsung mostró que la carga total adquirida fue del 63%.

Las baterías de litio proporcionan una corriente constante hasta un voltaje de referencia, y a partir de allí la corriente aportada empieza a descender hasta el punto donde la carga de la batería se desvanece totalmente. Todas las baterías que aportan alto consumo, después de cierto tiempo descienden abruptamente. Las curvas de descarga de las baterías se obtuvieron utilizando diferentes resistencias, donde la resistencia de 130 Ω es equivalente a realizar un ciclo de mediciones de 10 minutos con 20 repeticiones. Por otro lado, se tiene una resistencia de 50 Ω y equivale a un ciclo de 5 minutos con 30 repeticiones aproximadamente. Esta resistencia simula la carga hipotética de la conexión de los diferentes módulos del circuito que consumen corriente. En figura 8a se observa que superando un consumo de 100 mA, el tiempo de descarga de la batería Li-ion 18650 se reduce a 13 horas. Sin embargo, cuando se producen consumos menores a 55 mA, la batería proporcionará 34 horas de autonomía antes de presentar la caída de tensión. Waag et al. (2013) explican que la batería funciona con alta eficiencia, pero el SoC disminuye debido al envejecimiento significativo que en ella ocurre debido al estado de la carga y la temperatura.

Al tener una carga de 26.4 mAh debido a los 10 muestreos por hora con 10 repeticiones (Tabla 1), la batería ICR18650 soportará 48 horas (figura 8 a) si no se enciende el bluetooth continuamente. Si este módulo se conecta de forma continua al funcionar en un área remota el consumo se incrementará a 60 mAh, lo cual reduce el tiempo que la batería puede proporcionar energía a 30 horas.

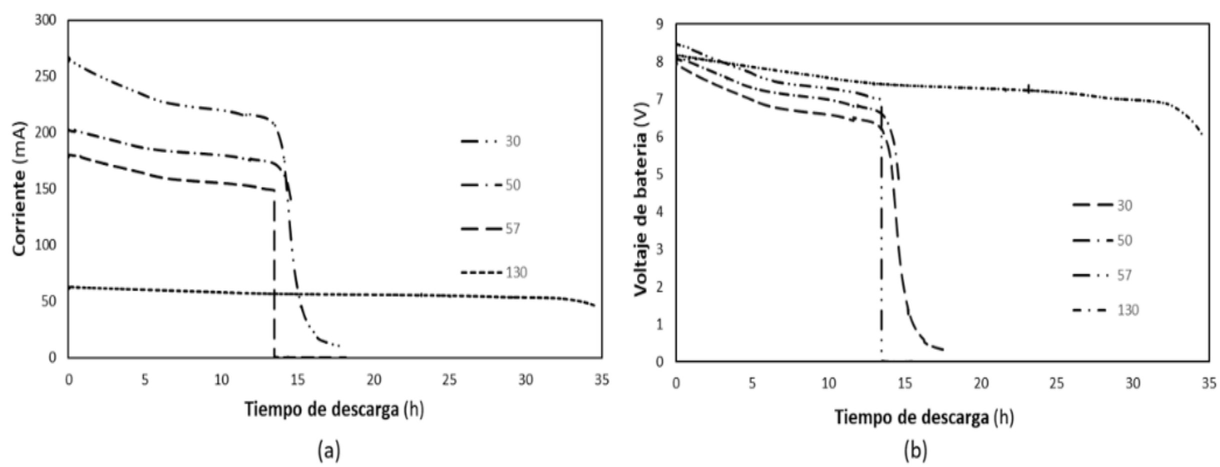

Figura 8 Perfil de descarga de (a) corriente y (b) voltaje de una batería Li-ion ICR18650 con diferentes cargas.

En huertas donde la descarga de datos es manual, el modulo del bluetooth solo se enciende cuando el productor adquiere los datos. Distribuyendo el consumo de energía de este módulo (33 mAh) en las 24 horas, incrementa el consumo horario por 1.38 mAh. Con una carga de 27.8 mAh, una sola batería proporcionará la corriente requerida por el dendrómetro para 2 días. El voltaje de las baterías en serie se debe mantener sobre 7 V, esto con el fin de evitar problemas de mal funcionamiento del NANO durante 30 horas para cargas similares de 130 Ω.

4.6.3 Panel fotovoltaico

La carga de la batería ICR18650 tipo Li-ion realizada mediante paneles solares permite autonomía total en localidades remotas. En un día totalmente soleado la carga con corriente constante utilizó 550 mA empezando a las 11:30 AM y finalizando tres horas después a las 14:30 PM (Figura 9 a). A partir de entonces el sistema entro al régimen de voltaje constante hasta que la corriente de carga cayó por debajo de 250 mA a las 15:40 PM (Figura 9 a).

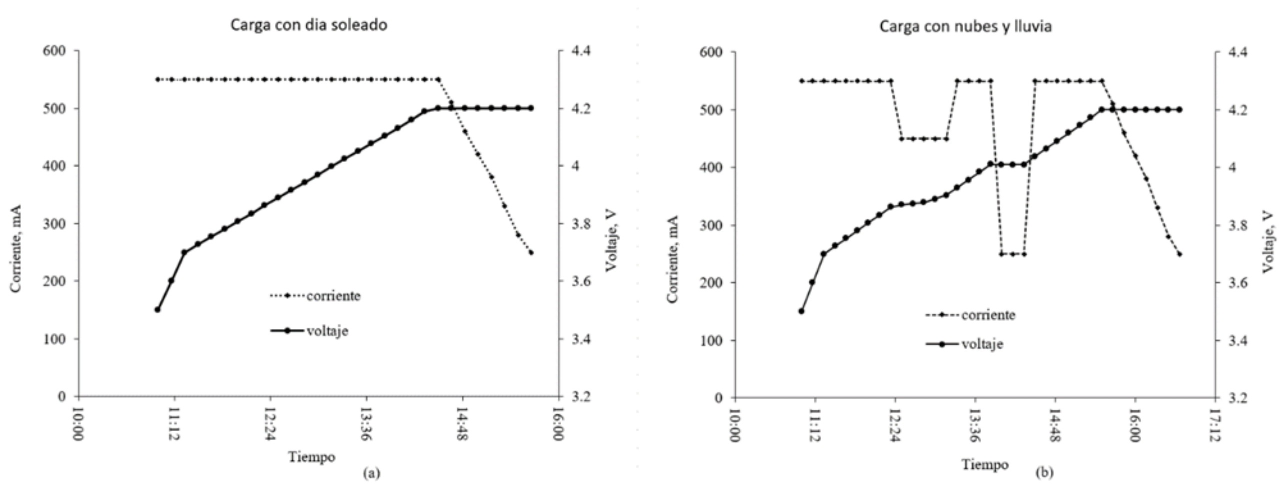

Figura 9 Carga de la batería de litio en día (a) soleado y (b) nublado.

En un día nublado (figura 9b) con radiación de 750 Wm^2 entre 12:30 y las 13:10 PM, las celdas solares proporcionaron 450 mA para cargar la batería; en este periodo el voltaje en la batería solo se incrementó de 3.87 a 3.9 V. El día volvió a estar soleado hasta las 13:55 PM y después comenzó a llover hasta las 14:30 PM reduciéndose la corriente de carga a 250 mA y el voltaje en la batería se mantuvo constante. El sol volvió a salir con plena intensidad y la batería se cargó a corriente constante (550 mA a 900 Wm^2) hasta las 15:30 PM cuando el voltaje en la batería alcanzó los 4.2 V. El sistema acabó de cargarse a voltaje constante a las 16:40 PM. Al comparar ambas figuras se aprecia un aumento en el tiempo de carga de una hora debido a las condiciones ambientales.

La radiación se reduce debajo de 400 Wm^2 después de las 18:00 PM, por lo que el sistema de carga se suspendió y continúo automáticamente a las 10:00 AM del siguiente día. Al finalizar la carga del par de baterías estas se conectan en serie y están listas para que el relevador las conecte al dendrómetro cuando la carga de las baterías que este usa están por debajo de 7.5 V.

El cargador con panel solar y circuitos electrónicos debe trabajar con el mayor grado de autonomía. El sistema de carga proporciona una eficiencia del 95% en la carga de las baterías y por ello incluyendo al bluetooth permitiría una autonomía de 75 horas (un poco más de tres días). Las recargas son recomendables cada 2 días por lo que en el momento de intercambiar el voltaje en la batería conectada en serie estaría en 7.2 V y con carga remanente del 35%. Al final del primer día de operación la carga remanente en la batería era del 67% y el voltaje de 7.8 V. Al iniciar con este estado de carga la batería alcanzaría su plena carga en un periodo de 2 horas.

La tarjeta que realiza la carga inteligente y acciona los relevadores es activada por el mismo panel solar por lo que no requiere de alimentación adicional y no influye en los consumos considerados en este estudio para el dendrómetro. Al analizar la operación del equipo intercambiando pilas durante 4 meses no hubo necesidad de tener personal y los datos fueron enviados diario a una central (Gateway) que los transmite del bosque o huerta a un sistema central por Ethernet. El utilizar un panel mayor permitirá cargar las baterías más rápidamente al aplicar una carga de corriente constante de 1 A. Sin embargo, no se necesita debido a los tiempos de carga. Por otra parte, aunque el panel sea más grandes si no hay sol, las baterías no se cargaran.

4.6.4 Optimización del software del microcontrolador

Independientemente que se tiene un panel solar y el sistema de carga de la batería esta automatizado, mediante software puede optimizarse el consumo energético para:

- Que el tiempo de descarga sea menor.
- Evitar que las baterías entren frecuentemente al SoC, para alargar su vida.
- Asegurar que las baterías tengan carga en probables eventos desfavorables donde no se tenga radiación solar.

El microcontrolador NANO utiliza instrucciones de programación, cuyos ciclos de trabajo dependen del oscilador, consumiendo 20 mAh de energía, únicamente por mantenerse en operación y activar el reloj de tiempo real. Se optimizó esta operación de tal manera que se alcanzó un consumo de 4 mAh, utilizando la rutina de “modo de suspensión (MS)” también conocido en programación como “Sleep Mode”. Con la cual se obtuvo una autonomía de 8 días. De ahí que, se obtengan días de reserva para cuando se presenten condiciones climáticas desfavorables.

Por lo general, el MS se encuentra en la mayoría de los circuitos integrados, el cual reduce el consumo de energía cuando no está en operación. La rutina MS se incluyó en la programación, para suspender funciones que consumen energía dentro del procesador. Esto consiste en verificar el estado actual de los sensores, adquiriendo el horario del reloj de tiempo real (RTC) y guardándolo en una variable “min” que indica intervalos de 10 minutos. Si no es el múltiplo de 10 minutos, un contador de 8 eventos se activa, siendo cada evento de 8 segundos que activa el MS, el cual espera una interrupción interna por watchdog. Si el contador llego a 0, se resetea y vuelve a realizarse la rutina principal. Por otro lado si la variable min tiene un múltiplo de 10, entra en la programación de adquisición y guardado de datos. Al acabar este código, entra nuevamente en la rutina de decremento y MS (Figura 10).

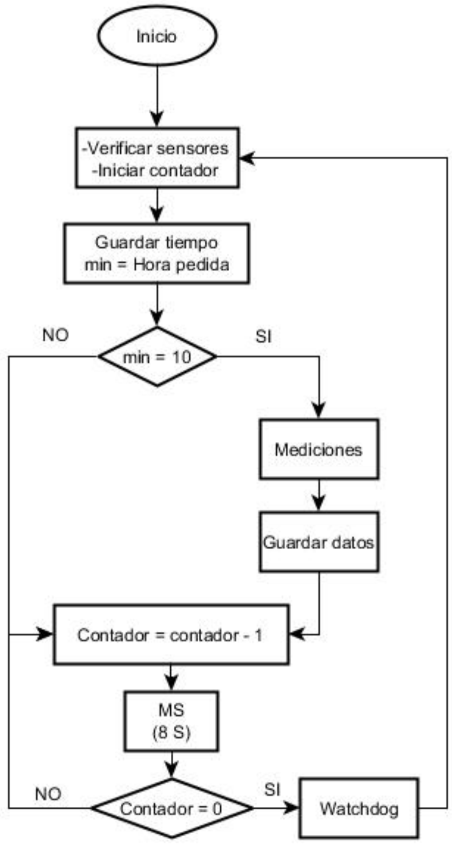

Figura 10 Diagrama de flujo de software modo suspensión

4.7 Conclusión

El dendrómetro instalado en una zona remota opera sin necesitar personal para su manejo, con transmisión inalámbrica de datos y uso de relevadores para la adquisición de los datos. Los resultados obtenidos indican que los monitoreos deben realizarse cada 10 minutos con 10 repeticiones cada uno para obtener una información con mayor resolución del comportamiento del flujo de agua en el árbol y reducir al mínimo el consumo energético. El gasto energético de este dendrómetro lo hace inviable para aplicaciones a distancia, es por ello que utilizar el modo suspensión es una solución para brindar autonomía al equipo.

Al utilizar baterías de litio permite tener alta densidad energética y eficiencia. En lugares remotos no se puede utilizar el cargador inteligente, el cual requiere de electricidad y su eficiencia de carga fue de solo 63%. El cargador con paneles solares propuesto obtuvo una eficiencia de carga del 95%, lo cual permite que el dendrómetro adquiera y transmita datos durante 8 días. Al estar en un bosque lejano, el sistema monitorea el estado de carga y utiliza otras baterías en paralelo previamente cargadas en caso de que la carga de las baterías alimentando al dendrómetro se reduzca al 35%. Un sistema automático cambia las pilas cargadas por las descargadas y en 4 meses de operación no se ha perdido un solo dato. El sistema de carga de las baterías opera aun en días nublados, aunque su recarga se alcanza en un tiempo mayor.

4.8 Bibliografía

Al-Shorman, M. Y., Al-Kofahi, M. M., & Al-Kofahi, O. M. (2018). A practical microwatt-meter for electrical energy measurement in programmable devices. *Measurement and Control*, *51*(9), 383–395. https://doi.org/10.1177/0020294018794350.

Blanco-Cipollone, F., Lourenço, S., Silvestre, J., Conceição, N., Moñino, M.J., Vivas, A., Ferreira, M.I. (2017). Plant Water Status Indicators for Irrigation Scheduling Associated with Iso- and Anisohydric Behavior: Vine and Plum Trees. *Horticulturae*, *3*, 47. https://doi.org/10.3390/horticulturae3030047

Botero, J.V. (2012). Characterization of Li-Ion Polymer battery to estimate the download time on systems with constant load. XVII Symposium of Image, Signal Processing, and Artificial Vision (STSIVA) pp. 128-131. doi: 10.1109/STSIVA.2012.6340569.

Capasso, C., & Veneri, O. (2014). Experimental analysis on the performance of lithium based batteries for road full electric and hybrid vehicles. *Applied Energy*, *136*, 921–930. doi.org/10.1016/j.apenergy.2014.04.013.

Chen, L.R. (2007). A design of an optimal battery pulse charge system by frequency-varied technique. *IEEE Trans. Ind. Electron*., 54, 398–405. *doi*:10.1109/TIE.2006.888796.

Chu, Z., Feng, X., Ouyang, M., Wang, Z., Lu, L., Li, J., & Han, X. (2017). Optimal charge current of lithium ion battery. *Energy Procedia*, *142*, 1867–1873. https://doi.org/10.1016/j.egypro.2017.12.577.

Chung, H. S. H., Tse, K. K., Hui, S. Y. R., Mok, C. M., & Ho, M. T. (2003). A novel maximum power point tracking technique for solar panels using a SEPIC or Cuk converter. *IEEE Transactions on Power Electronics*, *18*(3), 717–724. https://doi.org/10.1109/TPEL.2003.810841.

De Swaef, T., De Schepper, V., Vandegehuchte, M. W. & Steppe K. (2015). Stem diameter variations as a versatile research tool in ecophysiology. *Tree Physiology 35(10)*, 1047–1061. https://doi.org/10.1093/treephys/tpv080.

Di Nisio, A., Di Noia, T., Carducci, C. G. C., Spadavecchia, M. (2016). High Dynamic Range Power Consumption Measurement in Microcontroller-Based Applications. *IEEE Transactions on Instrumentation and Measurement*, 65(9), 1968-1976. *doi*: 10.1109/TIM.2016.2549818.

Drew, D. M., & Downes, G. M. (2009). The use of precision dendrometers in research on daily stem size and wood property variation: A review. *Dendrochronologia*, *27*(2), 159–172. https://doi.org/10.1016/j.dendro.2009.06.008

Dudacek, K., & Vavricka, V. (2007). Experimental evaluation of the MSP430 microcontroller power requirements. En Proc: *EUROCON 2007: International Conference on Computer as a Tool*, Sep 9-12, pp: 400–404. https://doi.org/10.1109/EURCON.2007.4400326.

Fay, C., Doherty, A.R., Beirne, S., Collins, F., Foley, C., Healy, J., Kiernan, B.M., Lee, H., Maher, D., Orpen, D., Phelan, T., Qiu, Z., Zhang, K., Gurrin, C., Corcoran, B., O'Connor, N.E., Smeaton, A.F., Diamond, D. (2011). Remote Real-Time Monitoring of Subsurface Landfill Gas Migration. *Sensors, 11(7)*: 6603–6628. doi: 10.3390/s110706603.

Fereres, E., & Soriano, M. A. (2007) Deficit irrigation for reducing agricultural water use. *J. Experimental Botany*, 58 (2), 147–159, https://doi.org/10.1093/jxb/erl165.

Fernández, J. E. (2017). Plant-Based Methods for Irrigation Scheduling of Woody Crops. *Horticulturae* 3, 35; doi:10.3390/horticulturae3020035.

Feron, S. (2016). Sustainability of Off-Grid Photovoltaic Systems for Rural Electrification in Developing Countries: A Review. *Sustainability 8*, 1326. https://doi.org/10.3390/su8121326.

Galindo, A., Collado González, J., Carbonell-Barrachina, A. A., Griñán, I., Hernández, F., Corell, M., Martín-Palomo, M. J., Moriana, A., Girón, I. F., Centeno, A., Memmi, H., López-Pérez, D., Rodríguez, P., Cruz, Z. N., & Torrecillas, A. (2018). Deficit irrigation and emerging fruit crops as a strategy to save water in Mediterranean semiarid agrosystems. Agricultural Water Management, 202, 311-324. https://doi.org/10.1016/j.agwat.2017.08.015.

García-Tejero, I.F., Hernández, A., Rodríguez, V.M., Ponce, J. R., Ramos, V., Muriel, J., & Durán Zuazo, V.H. (2015). Estimating Almond Crop Coefficients and Physiological Response to Water Stress in Semiarid Environments (SW Spain). *J. Agr. Sci. Tech., 17:* 1255-1266. http://jast-old.modares.ac.ir/article_13157.html

Hahn, F., & García, J.A. (2018). Sistema para determinar la condición hídrica de un huerto para ser usado por productores sin conocimiento en el área. IMPI. MX/a/2018/007965. 27/Jun/2018. Patente en trámite.

Hall, T. H., Layton, C. R., & Oxtoby, L. D. (1978). Electromechanical Dendrometer Band. *Enviroment Canada*. http://www.cfs.nrcan.gc.ca/pubwarehouse/pdfs/2007.pdf.

Hussein, A.A., Batarseh, I. (2011). A review of charging algorithms for nickel and lithium battery chargers. *IEEE Trans. Veh. Technology, 60*, 830–838. http://dx.doi.org/10.1109/TVT.2011.2106527.

Intrigliolo, D.S., Castel, J.R. (2007). Evaluation of grapevine water status from trunk diameter variations. *Irrigation Science, 26*: 49–59. https://doi.org/10.1007/s00271-007-0071-2

James, S. A., Clearwater, M. J., Meinzer, F. C., & Goldstein, G. (2002). Heat dissipation sensors of variable length to measure sap flow in trees. *Tree Physiology*, *22*(August), 227–283. https://www.ncbi.nlm.nih.gov/pubmed/11874724.

Kizito, F., Campbell, C. S., Campbell, G. S., Cobos, D. R., Teare, B. L., Carter, B., & Hopmans, J. W. (2008). Frequency, electrical conductivity and temperature analysis of a low-cost capacitance soil moisture sensor. *Journal of Hydrology*, *352*(3–4), 367–378. https://doi.org/10.1016/j.jhydrol.2008.01.021

Krepkowski J, Gebrekirstos A, Shibistova O, Bräuning A. (2013). Stable carbon isotope labeling reveals different carry-over effects between functional types of tropical trees in an Ethiopian mountain forest. New Phytol. 199(2):441-51. doi: 10.1111/nph.12266. Epub 2013 Apr 16.

Lawder, M. T., Viswanathan, V., & Subramanian, V. R. (2015). Balancing autonomy and utilization of solar power and battery storage for demand based microgrids. Journal of Power Sources, 279, 645-655. http://dx.doi.org/10.1016/j.jpowsour.2015.01.015.

Li, N., Chen, L., & Low, S. H. (2011). Optimal demand response based on utility maximization in power networks. *Power and Energy Society General Meeting*, 1–8. https://doi.org/10.1109/PES.2011.6039082

López-López, R., Ojeda-Bustamante, W., López Andrade, A. P., & Catalán-Valencia, E. A. (2013). Heat pulse method and sap flow for measuring transpiration in cacao. *Revista Chapingo Serie Zonas Áridas*, *XII*(2), 85–96. https://doi.org/10.5154/r.rchsza.2012.06.023

Lu, P., Urban, L., & Zhao, P. (2004). Granier's thermal dissipation probe (TDP) method for measuring sap flow in trees: theory and practice. *Acta Botanica Sinica-English Edition*, *46*(6), 631–646. https://doi.org/316-646.

Luna, O. P., & Grieger, C. E. (2015). *El agua en México*. pp.40. Secretaría de Medio Ambiente y Recursos Naturales, México, DF. https://www.gob.mx/semarnat.

Miralles, J., Franco, J.A., Sánchez-Blanco, M.J., Bañón, S. (2016). Effects of pot-in-pot production system on water consumption, stem diameter variations and photochemical efficiency of spindle tree irrigated with saline water. Agric. Water Management. http://dx.doi.org/10.1016/j.agwat.2016.01.022

Morandi, B., Manfrini, L., Zibordi, M., Noferini, M., Fiori, G., Grappadelli, L. (2007). A low-cost device for accurate and continuous measurements of fruit diameter. HortScience. 42. 1380-1382. http://hortsci.ashspublications.org/content/42/6/1380.full

Raghunathan, V., Kansal, A., Hsu, J., Friedman, J., & Srivastava, M. (2005). "Design Considerations for Solar Energy Harvesting Wireless Embedded Systems". *Proceedings of the 4th international symposium on Information processing in sensor networks*, *00*(C), 511. https://doi.org/10.1109/IPSN.2005.1440973.

Saw, L.H.; Ye, Y.; Tay, A.A. (2016). Integration issues of lithium-ion battery into electric vehicles battery pack. J. Clean. Prod., 113, 1032–1045. https://doi.org/*10.1016/j.jclepro.2015.11.011*

Schugurensky, C., & Capraro, F. (2018). Control automático de riego agrícola con sensores capacitivos de humedad de suelo. Aplicaciones en vid y olivo. http://www.fi.unsj.edu.ar/departamentos/DptoCivil/gcuencas/tercersemi/ACCA%2018_45.pdf

Scrosati, B.; Garche, J. Lithium batteries: Status, prospects and future. (2010). J. Power Sources, 195, 2419–2430. http://dx.*doi*.org/10.1016/*j*.jpowsour.2009.11.048.

Seyfried, M. S., & Murdock, M. D. (2004). Measurement of Soil Water Content with a 50-MHz Soil Dielectric Sensor. *Soil Science Society of America Journal*, *68*(2), 394. https://doi.org/10.2136/sssaj2004.0394

Sheil, D. (2003). Growth assessment in tropical trees: large daily diameter fluctuations and their concealment by dendrometer bands. *Canadian Journal of Forest Research*, *33*(10), 2027–2035. https://doi.org/10.1139/x03-121.

TP4056. (2016) 1A Standalone Linear Li-lon Battery Charger with Thermal Regulation in SOP-8. NanJing Top Power ASIC Corp.

Tsang, K., & Chan, W. (2011). Current sensorless quick charger for lithium-ion batteries. *Energy conversion and management, 52*, 1593-1595. doi: 10.1016/j.enconman.2010.08.011.

Vélez E.P., & Saez E.M. (2012). Water Use for Agriculture in Mexico. In: Oswald Spring Ú. (eds) Water Resources in Mexico. Hexagon Series on Human and Environmental Security and Peace, vol 7. Springer, Berlin, Heidelberg. https://doi.org/10.1007/978-3-642-05432-7_9.

Waag, W., Käbitz, S., & Sauer, D. U. (2013). Experimental investigation of the lithium-ion battery impedance characteristic at various conditions and aging states and its influence on the application. *Applied Energy*, *102*, 885–897. https://doi.org/10.1016/j.apenergy.2012.09.030

5 MANGO DENDROMETETER RESPONSE UNDER DIFFERENT IRRIGATION REGIMES

5.1 Abstract

Mexico has dominated the international mango trade and is doing research for optimizing water use without losing fruit quality and productivity. The use of soil, plant and environmental sensors helps to monitor plant water status. Linear resistance dendrometers were developed and installed in a high-density commercial mango orchard. Stem diameter variations were acquired every 10 minutes to obtain the maximum diameter (MXD), minimum diameter (MND), morning slope (MS) and afternoon slope (AS). Daily irrigation with 100% ET was applied to reference fruit-bearing trees and to others deprived of fruits. Also, reduced deficit irrigation (RDI) was applied watering the trees one day and keeping them without water the next. After comparing both treatments, daily stem changes (MXD and MND) were insignificant. Trees were stressed for 15 days without applying water during May, resulting in a drastic drop in MXD and MND measurements. The most successful correlations were obtained between MXD and Tmin and between MXD and daily average HR. On the other hand, all correlations against MND were poor. Although averaging 3-day trunk MXD variations, peaks are eliminated but correlations against environmental measurements do not get much better.

Keywords: Dendrometer, RDI, fruit-bearing tree, canopy-only tree, environmental correlations

5.2 Introduction

Mango is a popular product in tropical countries, but its global market has reached the last decade. Mango trade has increased significantly in both volume and geographic scope with the rapid expanding consumption in the US, China and the Netherlands. Mexico has dominated international mango trade from 2012-2016 with a 16% of market share, reaching US$328 million in 2015, four times higher than the fruit exported in 2005 (UNComtrade, 2016). However, 53% of world exports in 2015 are attributed to exporters such as Peru, Brazil, India, Thailand and Mexico. Mexico with an 8.98 MT/ha production is doing a good job of determining shifting market demands for different varieties that include Kent, Keitt, Tommy Atkins, Haden, Ataulfo, among others. An improved organic mango is offered, which satisfies a select group of consumers who are looking for healthy products, without chemicals and that protect the environment. More than 110,000 farmers in Mexico use organic practices, surpassing any other country in the world. (Alberts Organics, 2016).

Although mango trees are drought-tolerant plants they have to be irrigated mainly during the fruiting period. Water supply is critical during the first six weeks of the fruit developing process, and drought will induce late-stage fruit drop and reduced fruit mass (Singh, 2005). Effective water-saving irrigation techniques without affecting crop production are being developed. Micro-sprinkling irrigation can effectively reduce water consumption and has the advantages of both dripping and sprinkling irrigation (Wei *et al.*, 2017; Shah *et al.*, 2018; Levin *et al.*, 2018). A new method used commonly in trees is known as regulated deficit irrigation (RDI), where irrigation is withheld during certain growing stages of the plant. However, RDI requires a solid knowledge of the physiological response of the crop to water conditions and the levels of water stress of the plant throughout its entire cycle. (Fereres and Soriano, 2007; Fernandez, 2014). The water deficit can alter the vegetative growth and growth of the fruit in certain stages, such as hot flashes, and promote the growth of the fruit, at the same time, since the fruit represents the dominant sink in the tree (Naor, 2014; Bustan *et al*., 2016; Levin *et al*., 2018). In RDI fruit orchards, reduction of crop load is required to maintain marketable fruit size, despite reduced water applications (Neilsen, 2016; Naor *et al*., 2008).

The methods that are based on soil or climate for scheduling irrigation in fruit tree plantations are questionable. due to the non-uniform nature of the soils and limitations in monitoring the state of water. (Salgado and Cautín, 2008). The indirect connection between soil and climate based methods and fruit tree crop coefficients are very imprecise, generating differences between real and estimated water requirements (Goodwin *et al.*, 2006). A measurement of water status in the tree is affected by soil moisture and the demand for evaporation. A reliable index of plant water status can only be obtained from plant measurements (Naor *et al*., 2008; Ortuño *et al.*, 2004). Since plant water status controls many physiological processes and crop productivity, this information is fundamental for irrigation scheduling. Many researchers are focused in obtaining useful indicators based on stem diameter variations together with its threshold values for irrigation scheduling (Livellara *et al.*, 2011; Ortuño *et al.*, 2004; Conejero *et al.*, 2011; Goldhamer and Fereres, 2004; Moreno *et al.*, 2006).

Under the necessity of an efficient water management for complex soil-plant-water relationships in mango plantations, the primary objective was to obtain a sound knowledge of the dendrometer monitoring behavior under stress, normal irrigation and reduced deficit irrigation. The acquired information was going to be correlated against punctual and average environmental variables in order to predict mango tree water status and find a control signal for irrigation signaling.

5.3 Materials and methods

5.3.1 Field site for experiment trial

The experiment was established in a high density commercial mango orchard located at the town of Loma Bonita, Guerrero, Mexico (17° 25' 47" N, -101° 11' 19" W, 17 m ASL). The region is influenced by a subtropical arid climate, having the closest weather station at Petatlan (20 km north from the experimental site). The station recorded a mean annual rainfall of 1574 mm in 2018 and an average of 1470 mm during the last five years. The lowest rainfall typically occurs from January to May and the raining months from September to November.

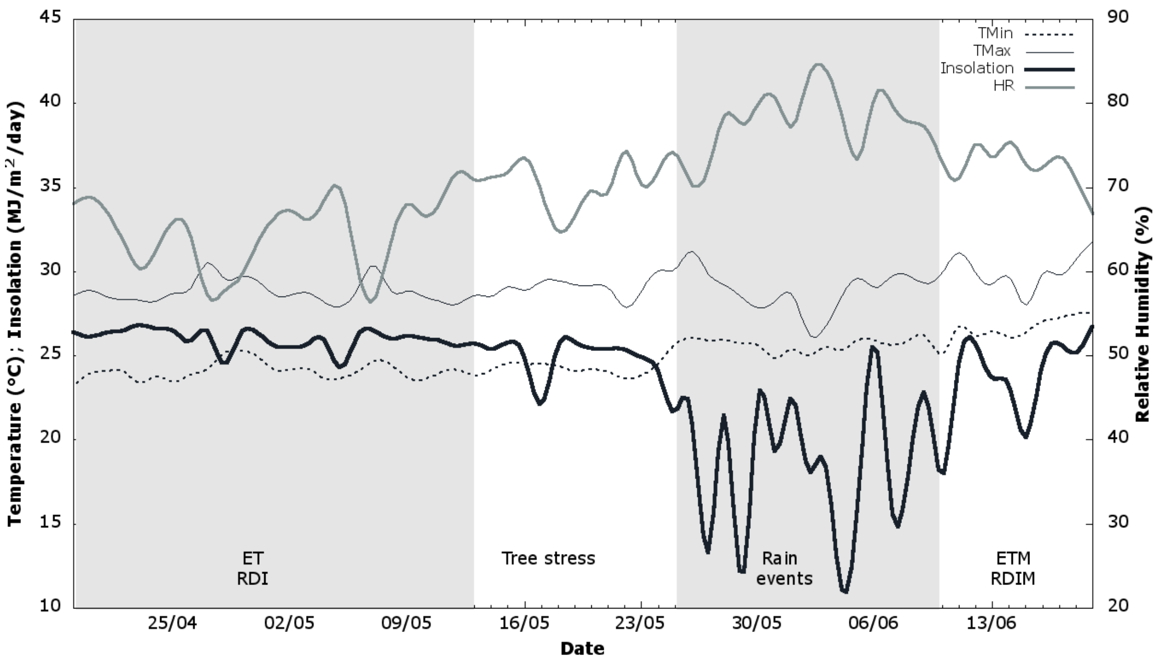

Figure 1 MERRA-2 season meteorological data (NASA).

Meteorological data from the experimental site were also obtained from NASA Modern-Era Retrospective Analysis for Research and Applications version 2 (MERRA-2). MERRA-2 (Bosilovich *et al.*, 2016) is produced with version 5.12.4 of the Goddard Earth Observing System 142 (GEOS-5.12.4) atmospheric data assimilation system and the 144 Gridpoint Statistical Interpolation (GSI) analysis scheme (Kleist *et al*., 2009)

The trial site is characterized by basaltic clay-loam red soil. Its bulk density was obtained from 30 soil cores taken randomly from 10 to 40 cm of depth, being its average density of 1.1 gcm^{-3}. A water retaining well with a 0.15 m depth was built beneath the trees canopy.

The well excavation presented a mount surrounding the trunk that avoided water contact with the trunk. During preliminary observational studies, soil moisture measurements indicated that watering with micro sprinklers maintained wet the soil beneath the trees. Farmer´s experience helped to select sunset as the better irrigation scheduling time. Three hours after irrigation stopped, water inside the well was still present, so null soil transpiration occurred. A number of excavations were done to visually assess the depth of tree roots. The highest root density was observed 0.4 m deep in the soil, with fewer roots observed at a maximum depth of 0.6 m. Plant roots were found to occupy space beneath trees canopy edges.

5.3.2 Tree selection and experimental treatment

The tree orchard was managed under the farmer's standard pruning, irrigation and fertilizer practices. The farmer's existing irrigation regime was applied according to his experience. From harvesting, watering was provided daily until pruning and fertilizers were also applied within this period. After pruning the tress were subjected to 3 months of stress until inflorescences appeared. After the stress period 5 different treatments were recommended to the farmer. Evapotranspiration (ET) and reduced deficit irrigation (RDI) common in worldwide modern orchard irrigation were the two techniques considered.

Irrigation was controlled by automatic timers set to run for 20 min at 18:00 just before sunset to avoid soil transpiration. Water was delivered via one 120 L h^{-1} micro sprinkler (Figure 2 points K&L) installed at a distance of 0.5 m from the tree trunk. Three treatments were applied throughout the field experiment:

1. ETo (100% replacement of crop water use)
2. Tree stress
3. RDI (one day 100% ETo, no irrigation the next).

According to tree size and age, 55 l day^{-1} were recommended. The experiment was run from the 20th of April 2019 to end of harvest on July 15th 2019. Five mango trees variety 'Kent' were selected within the same site having the same soil type for the study. The six-year-old mango trees had an 8 m between row and 4 m in-row spacing. Three trees (ETF, ETRC and ETLC) were selected for applying an ET period of 17 days followed by a twelve-day stress period (Figure 1). Stressed trees cycles resulted from withholding irrigation water until plants began to wilt. Another two trees (RDIF, RDIC) worked under reduced deficit irrigation (RDI) and stress treatments. The RDI treatment consisted of alternating one 100% ET irrigated day with a dry day (null watering). This RDI treatment started the 20th of April 2019 until May 13th, when stress started (Figure 1). After the stress period, a rainfall events occurred. The RDIM treatment consisted in applying water one day at 18:20 with 130% ET followed by two days with null watering. During the entire experiments trunk measurements were taken with dendrometers and ambient temperature with environmental sensors.

5.3.3 Tree topology

Mango tree is considered a woody trunk (A) plant with primary branches (B) departing at a certain height (D) from the main trunk (Figure 2). Secondary branches (C) grow from primary branches. The main trunk height (D) is measured from the soil to the first ramification. The dendrometer (F) was placed at a height (G) of 0.15 m below the main bifurcation with a N-S direction to avoid direct incidence from the sun. The initial diameter where the dendrometer was placed (E) was measured with a vernier. The amount of dark green leaves of the tree, were counted one by one. A temperature and humidity sensor (M) was placed just over the canopy of a second branch, approximately at a height of 1.5 m over the soil. The shaded canopy area (H) proportional to the amount of leaves (leaf area index), influences the amount of light that is transmitted through the tree canopy. The radius (K) is used to obtain the tree canopy and external well circumference. This area was obtained by measuring the diameter of the shaded area at the zenith of the solar day. The tree structure (Figure 2) was pruned and secondary branches strapped with threads (I) to soil-fixed tutors (J). Pruned trees with strapped secondary branches presented slower vegetative growth and higher fruiting rates. The micro sprinkler (L) was positioned just outside the well section (H) for water storage.

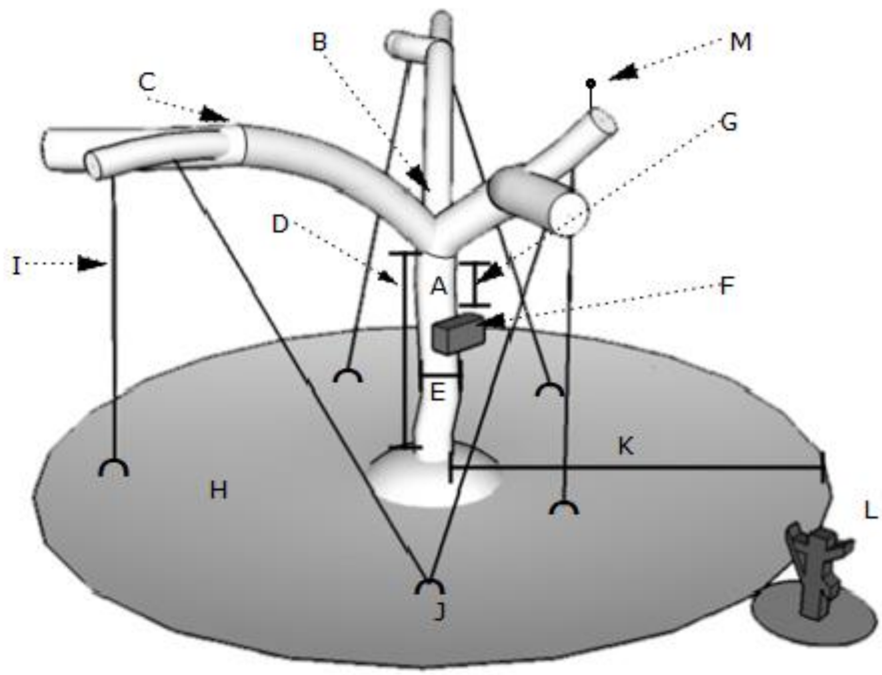

Figure 2 Topology of a mango tree consisting of a stem (A), bifurcated branch (B), secondary branches (C), stem height (D), stem diameter (E), dendrometer (F), dendrometer distance to stem ramification (G), canopy area (H), pruning threads (I), soil tutors (J), irrigation well radius (K), micro sprinkler (L), and temperature and RH sensor position (M).

Table 1 General dimensions of each mango treepresents the dimensions of each one of the trees selected. Two trees (ETF & RDIF) started inflorescence in May and continued fruit production during June and July. ETF is a tree with a height of 1.7 m, three branches and 1200 leaves. Its canopy diameter measures 3.37 m being almost twice its height. The main bifurcation was found at a height of 0.83 m and 0.15 below, its stem diameter was of 8.21 cm. Its name ETF comes from a fruit-bearing tree watered with ET treatments. The 2.1 m high RDIF tree produced fruits under RDI treatments. Four branches departed from the main trunk and presented 900 leaves at the beginning of the experiment, with a canopy diameter of 2.4 m. The diameter where the dendrometer was fixed was of 7.3 cm (Table 1). The other 3 trees did not produce fruits at all (ETRC, ETLC & RDIC). The ETRC (EvapoTranspiration Regular Canopy) tree presented a canopy diameter of 1.9 m, having 670 leaves shared within 3 branches. The 1.8 m high tree never showed vegetative growth and its diameter was of 8 cm. Both ETRC and ETLC trees were watered with ET treatments. The ETLC tree (EvapoTranspiration Large Canopy) was 1.9 m high, with a canopy diameter of 2.1 m and presented only two main branches. This tree presented a pivotal non-pruned branch which departs from the main branch and never showed vegetative growth. The total tree height considering the pivotal branch was of 3.2 m and the stem diameter where the dendrometer was installed was of 8.5 cm. A total of 810 leaves were counted within the canopy.

Table 1 General dimensions of each mango tree

	ETLC	ETRC	RDIC	RDIF	ETF
Tree height (cm)	190/320	180	160	210	170
Canopy diameter (cm)	210	190	185	240	337
Main junction height (cm)	90	110	100	120	83
Sensor height (cm)	75	95	85	105	68
Primary branches	2/3	3	3	4	3
Leaf number	810	670	660	900	1200
Main trunk diameter	85.47(±5.6)	79.8(±5.4)	75.7(±3.4)	73.3(±1)	82.1(±1. 9)

The RDIC (Reduced Deficit Irrigation only Canopy) tree never flowered. This 1.6 m high tree, presented 3 branches with a canopy diameter of 1.85 m and 660 leaves.

5.3.4 Dendrometer trunk measurements

Dendrometers take micrometric trunk diameter measurements using linear variable transducers attached to the trunk by a special bracket (Zweifel *et al*., 2000). A dendrometer was designed and used a linear resistor transducer to convert a linear displacement into a proportional electrical signal. A linear current source fed the resistance to avoid variations caused by the discharge of the lithium battery. A microcontroller with real time clock provided the exact timing for acquiring the voltage at the resistor pins. In order to optimize the energy stored in the battery ten measurements were acquired every ten minutes, averaged and the result saved in a MSD memory. Data was transmitted wirelessly and introduced to a computer resulting in a graph like the one showed in Figure 3.

MXD corresponds to the maximum trunk diameter, meanwhile MND the minimum trunk diameter after stem shrinkage (Figure 3). MXD and MND daily values occur just before sunrise and sometime during the afternoon, respectively. Ambient air temperature increases just after MXD, and as stomata open evapotranspiration (ET) starts. A trunk morning slope (MS) results from stem shrinkage, as water and carbon compounds stored in trunk cells flow upward. An afternoon slope (AS) results when stomata close and water gets stored in the trunk; this slope starts as air temperature decreases. Temperature continues dropping through the night and when the temperature slope changes, a new night slope (NS) is produced. The daily plot was centered at zero with the dendrometer value obtained at the irrigation time of 18:20. Values during shrinkage and expansion were obtained from this reference point.

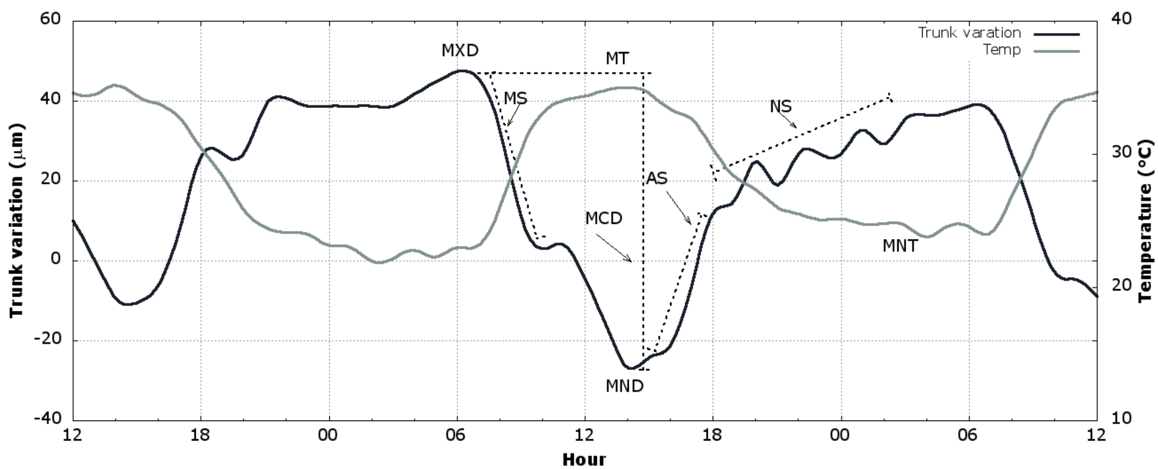

Figure 3 Daily temperature and stem growth variables plotted, being MXD the maximum diameter, MND the minimum diameter, MS the morning slope, AS the afternoon slope, NS the night slope, MCD the daily trunk growth, MT the maximum temperature, and MNT the minimum temperature.

5.3.5 Environmental measurements

Two sensors were used to monitor environmental variables. Air relative humidity and temperature were measured with a Sensirion DTH22 sensor. The CMOSens sensors, signal magnifier, A/D switch and 12C bus interface are integrated in one chip; This chip was installed by one side of the tree canopy (Figure 2, point M) and connected to the microcontroller. Data are collected every 10 minutes and saved in a MSD memory. The Apogee SP-110 pyranometer measures the total solar global irradiance both direct and diffuse in W m^{-2}. Values were acquired by the microcontroller system every ten minutes and saved in a MSD memory

5.3.6 Statistical analysis

Every tree provided a huge quantity of data as 144 measurements were taken daily. After a 30-day month 4320 stem diameter values were acquired and saved in the MSD. The same quantity of data was obtained from the air temperature and relative humidity sensor. A macro program in Excel was generated to obtain the MXD, MND, maximum and minimum air temperatures. Average daily air temperature and moisture were obtained also. Correlations of MXD and MND were carried out against the environment variables, grouped by irrigation treatment and tree phenological stage (fruit-bearing and only-canopy). After an initial study data with 70% variation from one day to the next were taken off and the correlation coefficients were obtained again. It is important to note that in a 3-day span irrigation changes cannot affect severely tree water status. Simple regression curves were adjusted using the least squares technique in order to correlate the trunk variables against environmental variables using software R.

5.4 Results

After comparing NASA measurements with tree temperature air and RH measurements in the trees it was encountered that daily maximum tree temperatures exceed by 22±5% the daily measurement provided by NASA (Figure 4). Minimum daily temperature differences were closer after May 23th, but in previous days an average difference of 19% was encountered.

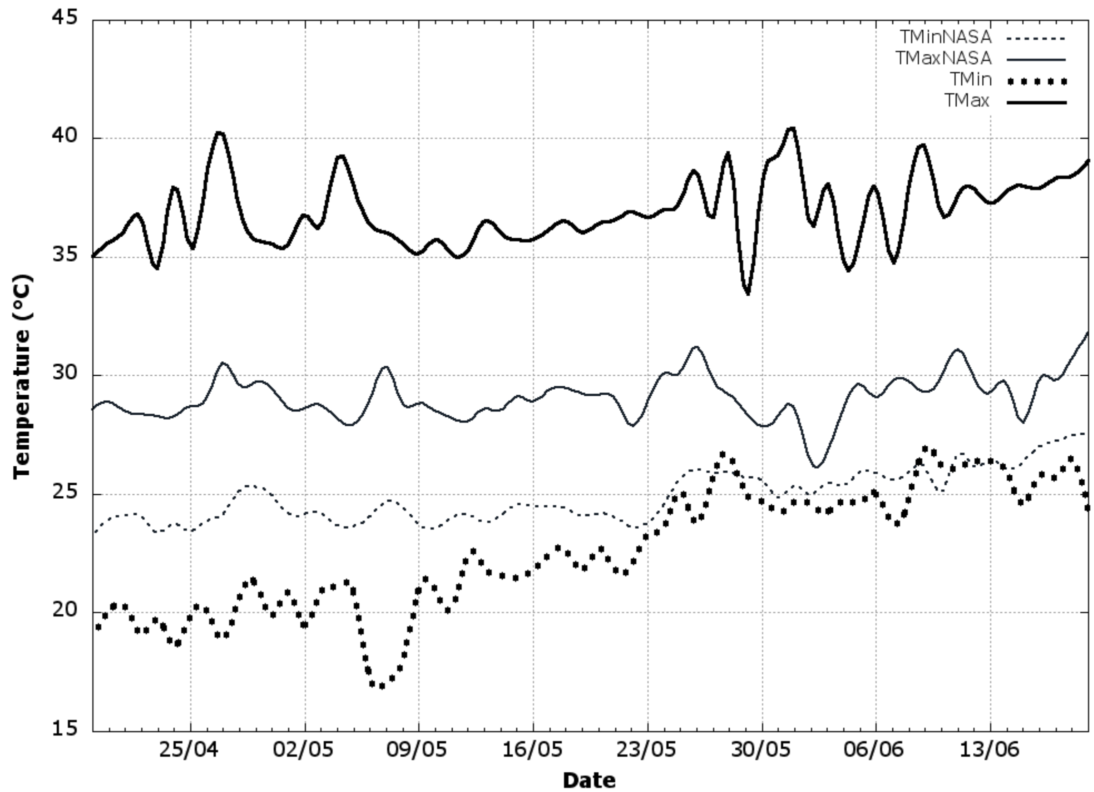

Figure 4 On site and NASA minimum and maximum daily temperatures.

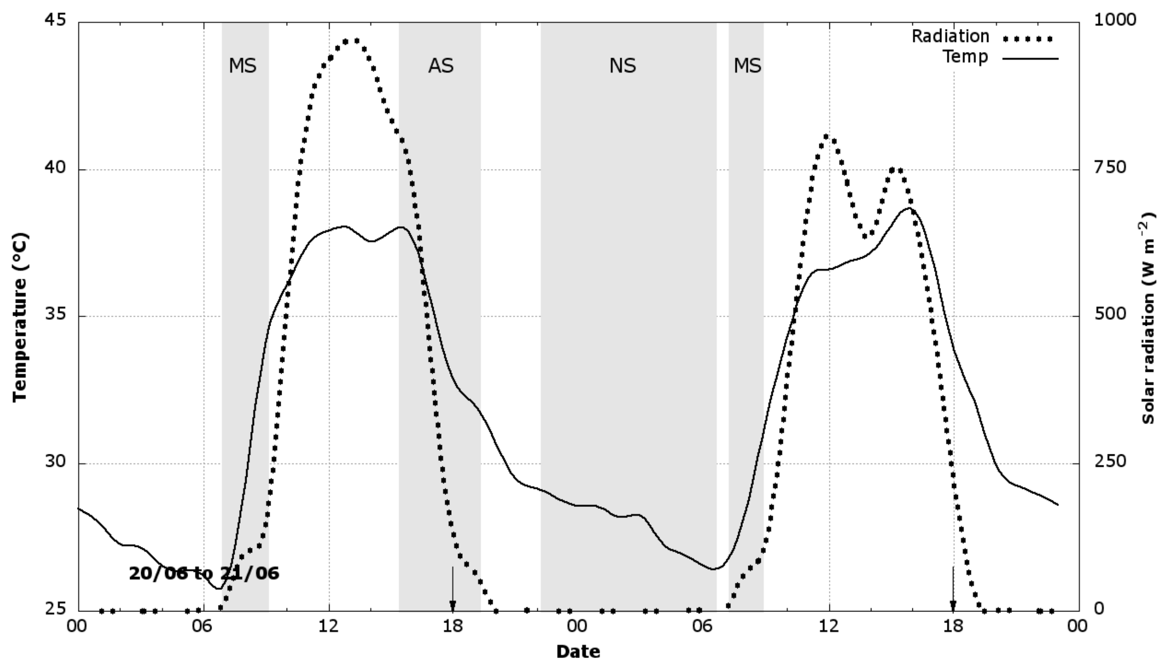

Figure 5 Radiation and air temperature nearby the trees during June 19th and 20th.

Solar radiation and air temperature were plotted and it can be appreciated that temperature increases as radiation does. Data from one sunny and one cloudy day were plotted, resulting the latter in radiation peaks (Figure 5). Stem morning slopes (MS) where MXD decreases abruptly are shown. After MS ended during the sunny day (June 20th), air temperature reached 35°C meanwhile the solar radiation was just over 200 W m^{-2}. On the cloudy day MS finishes when the radiation overpasses 75 W m^{-2} and air temperature is just over 31.3°C. Afternoon slope (AS) started with a radiation and air temperature of 800 W m^{-2} and 37.2°C, respectively (Figure 5). This slope finished at 19:50 during sunset with a radiation of 25 W m^{-2} and an air temperature 32.2°C. The night slope with null radiation started at 22:30, decreasing the air temperature from 29°C until 6:20 of June 21th.

Soil water availability under farmer skills was measured with a penetrometer-type technique using a stainless 40 cm steel rod marked every 5 cm. The farmer introduced the rod inside the wet soil and at dawn (12 hours after watering) the bar arrived easily to the mark at 30 cm. In the RDI treatment after the day with null watering, the rod still arrived to the 30 cm mark and the top of the clay-loam red soil was still humid. It took 3 days after the last watering to begin visualizing texture changes in the soil surface. After 5 and 8 days, rod penetration was of 20 cm and 10 cm, respectively, but at root depth water availability was present. Grass cover appeared after the first irrigation period causing less soil transpiration. Farmer observations were based on experience and wilt was appreciated by leaf color and inclination. Trees with proper canopy opening allowed maximum radiation income. Tree preparation is similar to the one used by cane-grape pruning and requires of shoot thread tightening by tutors.

Dendrometers monitor physiological activity, including the plant transpiration cycle and the plant water storage capacity (Coscozza *et al*., 2018). The majority of diurnal stem diameter changes result from elastic cambial and phloem tissues thickness fluctuations. Xylem diameter fluctuations are limited in size when compared against cambial or phloem variations. Daily exchange of water between phloem and xylem is affected by transpiration of water stored in the stem and by the rate of root water uptake from the soil. The majority of trees exhibit diurnal shrinkage but diurnal expansion and lack of a consistent pattern were also common as sampled the 17 and 18th of June (Figure 6). The wavelet analysis showed that most trees had a mean phase angle indicating daily shrinkage, whereas others exhibited daily expansion (Herrmann *et al*., 2016).

5.4.1 Trunk measurement events in ET treatments

Stem diameter measurements for each treatment during 4-day periods are plotted in Figure 6 for trees ETF, ETRC and ETLC. In the 100% ET treatment between April 27 and April 30, MXD increased during the last three days for all the trees and water was always available at the soil, Figure 6A. Arrows in the figure show irrigation scheduling. At sunrise, air temperature decreased to minimum values beneath 21°C, but during April 28th, night temperature remained in 23 causing MXD to drop in all trees. The morning slope MS of canopy-only trees was similar, but different from the ETF that presented inflorescences and seven fruits in growing stage. ETF morning slopes were of -515±10.2%, being the steeper on April 28th. ETF black line signal on the afternoon of April 27 shows a linear AS of 319.15 from 16:40 up to 20:00. ETF encounters its MND at the V inverted peak and matches with the maximum air temperature peak.

The ETRC trunk diameter shrinked to -46.7 µm (29th of April), taking the soil water available directly for plant evapotranspiration without any trunk water storage; This period lasted seven hours. The ETRC (pointed line) presented the lower MXD, but on days 28, 29 and 30 of April, its magnitude was close to the one of ETLC that had a greater canopy. As noon temperature decreased daily, plant evapotranspiration and MND declined also (VPD=2.32). On both 28 and 29 of April, night slope was present in all the trees, resulting in tree growth.

As soil water available remains for 3 or four days after water shortage, stress was monitored in trees from May 20 to May 23, corresponding to the second stress week. In this period, MXD values ranged between 23.7 and 35.76 µm for ETF, Figure 6B. On 20th and 23th of May, warmer nights dropped MXD to 23.84 µm. ETF morning slopes differed for the four days (- 476±22%), having the 20th and 21th day of May two different slopes between 7:00 and 10:00, with a peak between them; the average of the growing fruits 94.4±10% grams. At noon, ETF trunk diameter measured zero microns for the first three days. ETF maximum shrinkage MND (-25.72 µm) during May 21 and May 22, occurred at 15:50 and 15:00, respectively. From this point onwards, water moving through the trunk got stored as plant evapotranspiration decreased (2.23 to 2.64).

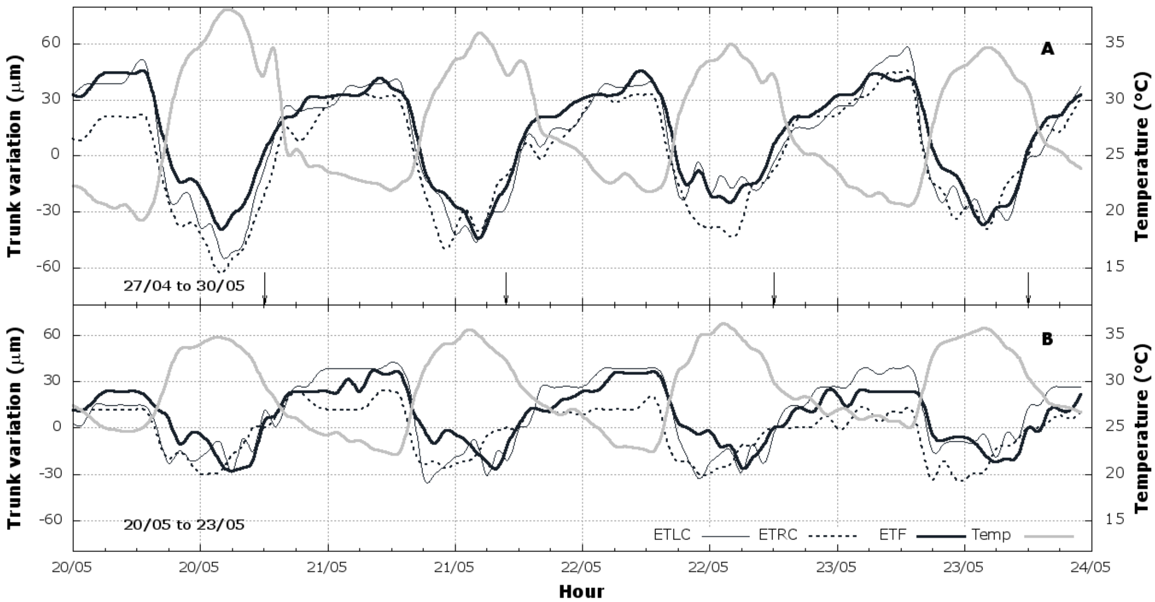

Figure 6 Trunk variations of ETLC —, ETRC --- and ETF ▬ tree and air temperature ▬ for (A) 100% ET0, and (B) stress treatments.

The tree with lower canopy (ETRC-pointed line) also presented the lower MXD in this stress period. On May 20th, with the dew temperature at 24.19°C, ETRC trunk diameter dropped to a (MXD) maximum value of 11.8 µm. Scarce soil water availability combined with high night air temperature of 24.75°C at 7:40 on May 23, limited trunk growth to 11.92 µm (Figure 6B). The afternoon slope differed all days and was only present until 17:40. The low soil water available was used during a 7-hour period to provide controlled plant evapotranspiration. By the 23th May, leaves started wilting and their inclination decreased.

Both trees having only vegetative cover (ETRC & ETLC) presented similar morning slopes; ETLC=-767±12.2%, and ETRC=-749±14.2%. However, the ETLC tree presented several peaks just after the morning slope. As the tree (ETLC-slim continuous line) has 810 leaves, trunk dimensions and branches vary due to their water distribution and storage throughout the 9:00 to 18:00 periods. This tree with the pivotal continuous stem provides higher MXD and lower MND; higher leaves in this branch suffered premature wilting compared to lateral branches fixed to the tutors. As air temperature increases for periods, stomatal conductance rises and trunk shrinks more. The difference in leaf cover is clearly noted during this stress period. The ETLC stressed tree showed on June 20th poor trunk shrinkage (oscillating between -8 and -14 µm) with the scarce soil water available.

Just after a period of 210 mm of rainfall up to June 5th the trial zone experienced, nights remained warm, and MXD decreased to 17.9 µm in the ETRC tree, from June 17 to June 19. The night temperature of July 18 was 26.53°C and the MXD of the fruit bearing tree (ETF) was of 41.7 µm. The next two days, dew temperature decreased to 24.3°C and MXD reached maximum values of 53.6 and 59.6 µm. The two morning slopes in the ETF stem are temperature dependent; in the first MS slope (-448±28%), temperature rises quicker (3.4°C hr^{-1}), meanwhile in the second MS temperature rises to a peak with a reduced gradient (0.6°C hr^{-1}). The maximum peak of 29.8 µm between the two MS indicates trunk water storage to provide water requirements to the growing fruits with an average of 104±8 grams. Stem diameter variations should be considered within the water balance and the sugar content of mango trees (Daudet et al., 2005); In mango trees the sugar content of woody tissues changes as a function of fruits. Trunk diameter plots find the MND value, according to the phenological stage tree considered. For example, the ETF tree always have the MND in the bottom point of the V graph being of -39.7 µm at 14:50. ETRC MXD varied between 18 and 41 µm, in the period from June 17 to June 20. The ETLC tree was the one that grew more, having two different slopes in the afternoon. During this period MXD varied from 50.7 to 74.5 µm in the ETLC tree.

Table 2 correlations found with the signals of figures 6 and 7. MXD and MND considerations of trees under ET and stress treatment.

		MXD Considerations	MND Considerations
ET	ETF	Two morning different slopes	Mostly before noon
	ETRC	MDX is temporized with T_{min}	MND is temporized with T_{max}
	ETLC	Trees are out of phase in stress and rain	
STRESS	ETF	Presents more NS than others.	MND at 14:10
	ETRC	Trees wilted after 7 day	ETRC to -10 in stress
	ETLC	Increasing T_{dew}, MXD rises	

5.4.2 Trunk measurement events in RDI treatments

RDIF & RDIC tree dendrometer and air temperature monitoring data obtained from each treatment were plotted in four-day periods (Figure 7). Watering took place at 18:00 on the 27 of April, and this moment was not plotted in Figure 7A. Similar morning slopes (-437±4.3%) during the four days were encountered in the RDIF tree, non-dependent if water was applied (Figure 7A). RDIF trunk growth on the 27th and 28th of April can be correlated to dew and minimum evening temperature. On April 27th, MXD and dew temperatures were of 50.66 µm and 18.91°C, respectively. The 28th of April, MXD decreased to 38.7 µm as dew temperatures increased to 20.73°C. After midnight, as the air temperature slope is gentle (0.5°C hr^{-1}), MXD remains constant up to 7:40 being the RDIF morning slope of -647. The sharp air temperature drops (-12.76°C hr^{-1}), coincides with the NS (165.6), that ends at 2:10 of April 29th. On April 30th dew temperature was of 19.89°C, the MXD 50.6 µm and the MS of -451. Previous NS was of 126.63 and the temperature night gradient was of -13.8°C hr^{-1}. MND values do not coincide with the maximum temperature peak.

The contraction on the day of the stem is an indicator of the loss of water absorbed overnight by elastic stem tissues, as a result of perspiration (Yazgan et al., 2006), and not yet replaced (Devine and Harrington, 2011). At night, stem radius growth can be induced by replenishing stem tissues with water, but also by newly formed cells (Zweifel *et al.*, 2016). Minimum stem diameter (MND) values corresponding to maximum shrinkage, were greater in the tree irrigated daily (ETRC) than in the tree with deficit irrigation (RDIC) during the period of April 27-30. Similar maximum diameter values (MXD) were found in the period, so MDC tend to be greater in the daily irrigated tree.

In both trees without vegetative growth and flushes, morning slopes presented similar magnitudes but the stem shrinked more in the daily watered tree, starting a higher transpiration process. MDC and MXD were similar in trees with only-canopy being subjected to stress. The main difference was the appearance of two peaks in the bottom of the curve of the RDI tree due to two factors: reduced soil water available and ants attack to 100 leaves in the early morning of May 22nd, resulting on a reduced stomata conductance. In periods when maximum daily stem size decreased notably over successive days, it can be concluded that insufficient soil water is available to recharge the stem overnight. After rainfall and a continuous ET watering, MDC increased all days, and the tree stem undergo an irreversible growth, losing its elasticity. Dry periods occur when the tree does not balance for 24 hours, the tree's stem tissues are not fully saturated and does not cease completely overnight. This is the potential of water before dawn, which decreases when a plant is not able to saturate its tissues at night (Larcher, 2003).

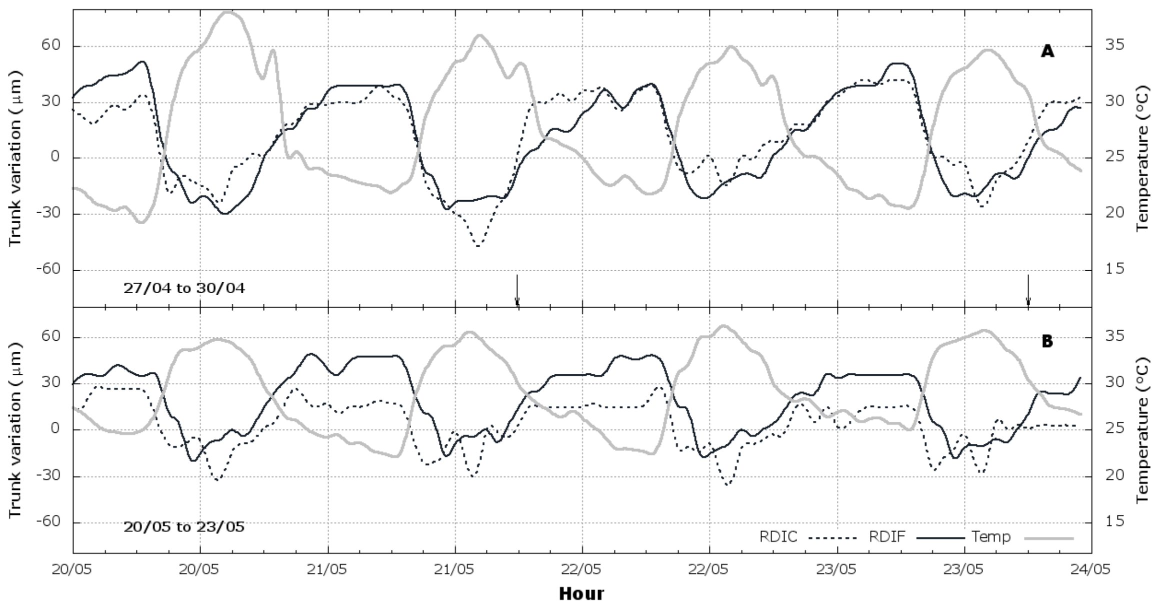

Figure 7 Air temperature —and trunk dendrometer measurements of RDIC --- and RDIF — trees for (A) RDI, and (B) stress treatments

RDIC morning slopes (pointed lines) are quite different from the RDIF ones and only were similar on April 30th with a value -460. RDIC tree presented MND peaks at 14:10 of variable magnitude, being the minimum value of -47.7 µm (most negative). These V shaped peaks coincided with the maximum temperature peak. Higher afternoon slopes (489) were encountered during watering days, being AS of 219 when irrigation was not applied. (HR=59.8%).

In the RDIF tree subjected to watering stress from May 20 to May 23, MXD values ranged between 35.76 and 47.68 µm (Figure 7B). A MXD value of 35.76 µm during May 20th and 23th resulted from 24.7°C warm early mornings. In the RDIF tree, two morning slopes were encountered. On May 20th and May 21th, the earlier MS average was of -345.5, meanwhile the later (10:15-11:30) had a MS of -514.5. MND values ranging between -19.5 and -23 µm in the RDIF tree, appeared just before noon and did not coincide with maximum air temperature. RDIF presented similar AS (-237±13%) on May 20 and 21th. The average value of the mango fruit 80.6 ± 5 grams.

The RDIC tree presented a MND of -34.8 µm just after rainfall, being its minimum value almost constant (-29.9 to -35 µm) and matched in time with the maximum air temperature peak. In this tree (RDIC) having only canopy, a higher tree evapotranspiration is noted as the stem shrinks, water goes directly from the soil available water to the leaves. As the trunk stores water, the dendrometer detects trunk expansion in middle-peaks or MXD. Trunk growth is not possible during periods of stem shrinkage, which has been attributable to rehydration of tissues (Zweifel *et al*., 2016).

After rain, the RDIF tree MXD presented an increase from 47.7 and 59.6 µm on June 19 and 20, respectively. Dew temperatures ranged from 24.3°C to 25.9°C, and the tree was watered on June 19th at 18:20, generating a longer and steeper AS of 2573 up to 18:10 and a NS of 187 during midnight and early morning. MS of the RDIF varied each day and the MND peak was not located in only one V peak. Except for June 18, all the signals showed two peaks and the second one at 17:20 coincided with the higher air temperature.

MXD tends to grow during all the days under ET and RDI tree treatments. However, under RDI treatment, MND shrinkage is smaller on day 29th April, as less minerals get stored in the trunk. During mango fruit growth, when carbohydrates demanded by the fruit are higher than the supplied by photosynthesis, the fruit may obtain assimilates from leaf and stem reserves (Léchaudel *et al*., 2005). Under natural conditions, the contribution of initial fruit dry mass was the highest for all sink variables, including fruit growth rate (89.8%), as well as stem reserve mobilization (67.6%). At noon the stem's water potential decreases as a result of soil water depletion in response to increased tree transpiration rates (Naor *et al*., 2008). Under such conditions, the increase in crop load is expected to result in a greater decrease in the midday potential of water stem at low irrigation rates than at high irrigation rates.

Weather did not represent a critical factor as leaf-to-fruit ratio (Léchaudel *et al*., 2005). In this experiment, stress days in May with no watering did not show stem growth, and several peaks were noted in the 10:00-15:00 interval. Almost one month later, after some raining days and rewatering, MXD and MDS values increased daily. Tree roots with deeper roots recovers within a period of few days from water stress. The period depends on the severity of the water stress suffered and the amount of water supplied to re-water. Stomatal conductance takes longer to recover (Fernández, 2014).

5.4.3 Trunk measurement analysis and correlations

MXD tree average having only vegetative growth is of 46.43 (Table 3), being 21.2% higher than trees under stress (38.3%). This value account for both RDI and 100% ET treatments. The MXD average value was 80% lower in fruit-bearing trees under stress than those ET and RDI irrigated. In the case of MND with only canopy-trees the shrink average value was of -25.4 against -17.5 of stress plants (Table 3).

Table 3 Average and standard deviations of MXD, MND and MCD for each treatment for fruit-bearing and only-canopy trees.

	100% ET0				RDI				STRESS			
	Canopy		Fruit		Canopy		Fruit		Canopy		Fruit	
	Avg	SD	Avg	SD	Avg	SD	Avg	SD	Avg	SD	Avg	SD
MXD	**46.89**	9.87	48.29	6.97	**45.96**	10	52.37	8	**38.3**	6.04	27.91	11.92
MND	-31	16.18	-26.9	8.11	-19.8	12.5	-30	7.5	-17.5	15.64	-33.8	13.45
MCD	77.9	16.1	75.19	10.68	64.21	13.51	70.27	8.87	55.78	18.33	61.74	19.96
AS	296	51.3	353.7	129	288	88	-431	64.3	262	51	410	132
MS	-608	249	-526	94	-513	159	280	137	-515	113	-450	138

An increment on plant shrinkage of 45.1% is noted when the plant is irrigated. MDC also shows a notable difference between the average values of well irrigated versus stressed plants. Although average values are good enough, daily decisions are difficult to obtain. This is evident due to the long standard deviations encountered in the analysis. Morning slopes have average values that do not differ greatly between canopy only stressed and

RDI trees. Also its standard deviation is so high that is difficult to consider it for an irrigation index.

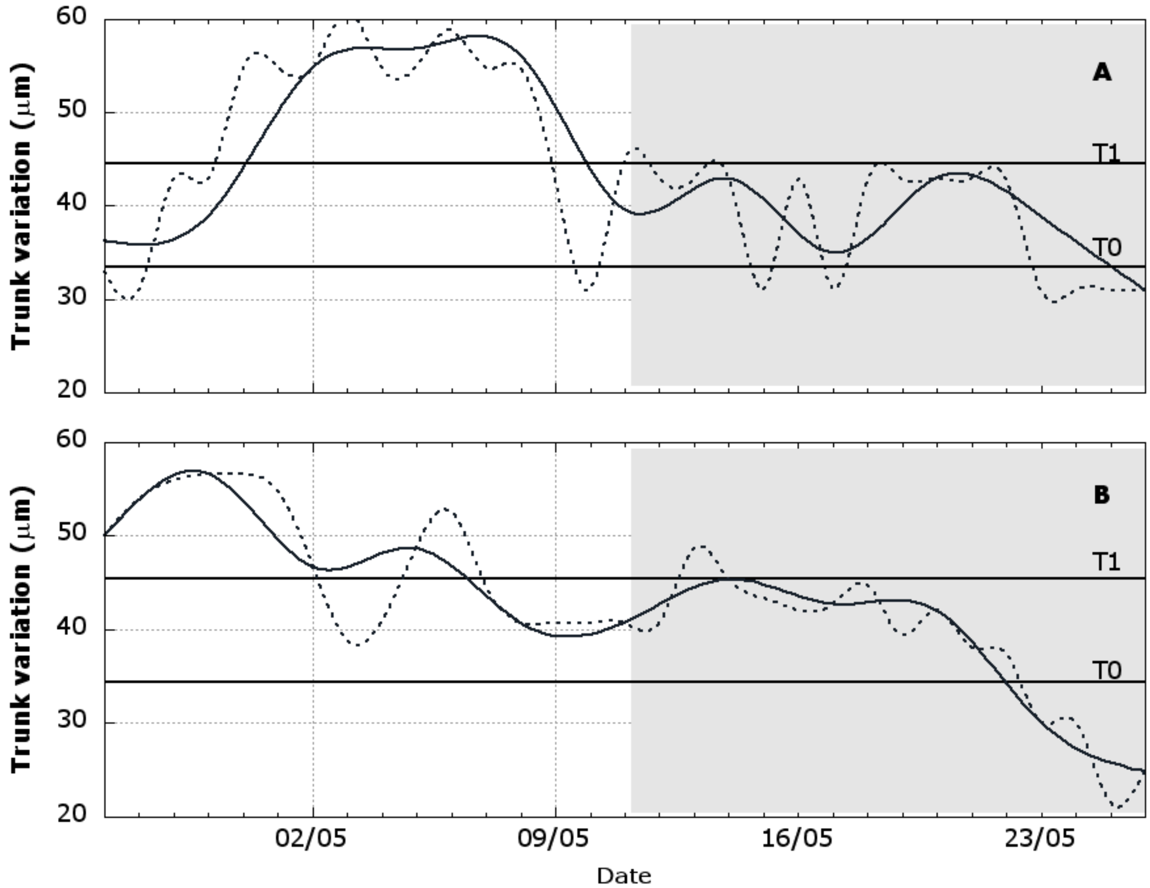

Figure 8 MXD trunk variation using daily ---and three-day average ▬ values for (A) ETRC and (B) RDIC trees.

MXD plotted values of the ETRC tree showed daily peaks which cannot be realistic (Figure 8A). The values in the pointed line that have a variation over 70% can be eliminated (Herrmann *et al*., 2016) or an average of three-day measurements can be considered as a strategy to take irrigation decisions. This continue line (Figure 8A) avoids peaks and can be used in RDI scheduling. Trunk measurement can provide irrigation scheduling. If the dendrometers give a value of T_1, the same irrigation stands, if $T_0 < T_1$, an additional 10% of watering is supplied, and if smaller than T_0 a 20% of additional water will be provided. Figure 8B shows the peak signal with all the data para tree ITRC. As the average responds in 3 days, a softer curve appears (Figure 8B continue line).

The environmental variable better related to MDC variation may change with species and cultural conditions. Positive values of stem diameter corresponded to negative values of air temperature (Cocozza *et al*., 2018). Time series highlight the potential to quantify time lags between physiological and meteorological events, (Figures 6 & 7). Environmental variables have been correlated against stem growth variables considering mainly two analyses: daily average environmental values and point measurements. In daily average measurements, the air temperature values sampled between 8:00 and 18:00 are averaged. A punctual air temperature measurement could be for example the predawn temperature acquired at 6:00.

In Table 4, punctual measurements were considered as they would be easier to obtain automatically. MXD, MND and MDC were correlated against T_{min} and T_8, which correspond to minimum temperature and temperature at 8:00, respectively. Canopy-only and fruit bearing trees punctual measurements show poor linear correlation R^2 for MND and MDC (Table 4). Fruit-bearing trees showed the best correlations of 0.77 between MXD and Tmin (Table 4). T8 against MXD presented R^2 correlation coefficients in fruit bearing trees but not in trees having only vegetative growth. After eliminating MXD values having a variation over 30%, the correlation MXD-T_8 increased to 0.68 in fruit bearing trees with a 100% ET.

MXD in tomato measurements occurred at 6:00 and was barely affected by climate factors such as solar radiation, vapor pressure deficit (VPD) and relative humidity (RH), but was affected by air temperature (T), where a linear correlation of 0.5 was obtained (Meng *et al*., 2017). Regression analysis used to establish relationships between the MXD and soil water content showed a coefficient of 0.9. After using the environmental variables with soil water content this regression analysis provided an R^2 of 0.97 (Meng *et al*., 2017). MND could be used as the operative parameter in irrigation scheduling protocols with young trees and MDS for mature trees (Orduño *et al*., 2004). Livellara et al., 2010, encountered a linear correlation of $R^2 = 0.69$ in cherry trees between stem water potential, SWP and maximum daily trunk shrinkage, MDS; SWP and trunk growth rate (TGR) correlation decreased to $R^2 = 0.57$.

Table 4 Punctual linear correlation R^2 of Tmin and T8 against MXD, MND and MDC for each treatment applied to fruit-bearing and only-canopy trees.

	100% ET0				RDI				STRESS			
	Canopy		Fruit		Canopy		Fruit		Canopy		Fruit	
	T_{min}	T_8	T_{min}	T_8	T_{min}	T_8	T_{min}	T_8	T_{min}	T_8	T_{min}	T_8
MXD	0.11	0.04	0.43	**0.58**	0.12	0.12	**0.61**	**0.58**	0.28	0.09	**0.77**	**0.62**
MND	0.08	0.32	0.001	0.06	0.006	0.03	0.12	0.08	0.24	0.19	0.14	0.001
MCD	0.24	0.47	0.19	0.47	0.11	0.01	0.16	0.19	0.41	0.21	0.49	0.2

Table 5 Average daily temperature and relative humidity correlation against MXD, MND and MDC for each treatment applied to fruit-bearing and only-canopy trees.

	100% ET0				RDI				STRESS			
	Canopy		Fruit		Canopy		Fruit		Canopy		Fruit	
	T_{avg}	HR	T_{avg}	HR	T_{avg}	HR	T_{avg}	HR	T_{avg}	HR	T_{avg}	HR
MXD	0.09	0.08	0.16	0.39	0.08	0.1	0. 1	0.47	0.15	0.33	**0.75**	**0.77**
MND	0.09	0.02	0.09	0.001	0.02	0.007	0.2	0.14	**0.55**	0.42	0.03	0.09
MCD	0.01	0.11	0.003	0.14	0.005	0.04	0.008	0.08	**0.58**	**0.56**	0.41	**0.54**

Trunk daily measurements were correlated against average air temperature and relative humidity (Table 5). Only stressed trees presented good correlations, being the better one between MXD and HR with an R^2 of 0.77 for the fruit bearing tree. Also MXD against T_{avg} provided a good correlation of 0.75. This values are higher than the ones reported by different researchers. In well irrigated lemon trees, day to day MDC values correlated against air temperature and global radiation were of 0.4 and 0.52, respectively (Velez *et al.*, 2007). This indicates that the absolute MDC values cannot be used as the only variable to schedule irrigation; Reference equations ratios help to increase the sensibility of the trunk diameter measured value. Air temperature against stem radius correlation was of 0.493. Correlation analysis between larch stem radius variations and environmental variables showed that air relative humidity presented high values (0.98) under different time windows (Tian *et al.*, 2018). As the time window became longer up to 21 days, certain hysteresis of the response was eliminated. The daily change in stem radius in 5 different trees in a forest (expressed in daily, 7-day and 21-day window values) showed the better correlation with daily mean relative air humidity. Pearson correlation coefficients reached values within 0.87 and 0.93 (Köcher *et al.*, 2012).

5.5 Conclusion

This work can conclude that dendrometers can help visualize plants health. It will move from the soil to the leaves passing through the stem. Daily shrinkage is a function of water loss through the leaves and water uptake by roots. Trees subjected to stress showed a smaller MNX, than daily irrigated trees and from RDI. However, for RDIF, MXD values were higher and the signals measured were out of phase. An event of ants eating leaves in a tree resulted in stem shrinkage as well. Trees well pruned and those with fruits had similar stem growth. When they were stressed every tree responded differently, as they had different topology. It took 5 days to recover with rain from the 12-day stress. MXD increased much more when the previous night was cooler.

Too many measurements provide the dendrometer per day and to reduce them we correlated against punctual and average temperature and relative humidity data. In this study it was able to detect stress fruit-bearing correlating MDX with Tmin with a r^2=0.77. The better correlation against average values was obtained between MDX and HR with a r^2=0.77. MND correlations were very poor as well as the different slopes encountered, but they will serve to detect different kind of insects that feed from plants. The thresholds T0 and T1 help as an irrigation index telling the system when the plant is stressed.

5.6 References

Alberts Organics. 2016. Organic Produce from Mexico. http://albertsorganics.com/resources/merchandising-tips/organic-produce-mexico.

Bosilovich, M.G., F.R. Robertson, L. Takacs, A. Molod, and D. Mocko. 2016. Atmospheric Water Balance and Variability in the MERRA-2 Reanalysis. Journal of Climate. 30(4): 1177-1196. doi: 10.1175/JCLI-D-16-0338.1.

Bustan, A., A. Dag, U. Yermiyahu, R. Erel, E. Presnov, N. Agam, D. Kool, J. Iwema, I. Zipori, and A. Ben-Gal. 2016. Fruit load governs transpiration of olive trees. Tree Physiol. 36(3):380-91. doi: 10.1093/treephys/tpv138.

Cocozza, C., R. Tognetti, and A. Giovannelli. 2018. High-Resolution Analytical Approach to Describe the Sensitivity of Tree–Environment Dependences through Stem Radial Variation. Forests. 9. 134. doi: 10.3390/f9030134.

Cohen, M., D. Goldhamer, E. Fereres, J. Girona, and M. Mata. 2001. Assessment of peach tree responses to irrigation water deficits by continuous monitoring of trunk diameter changes. J. Hortic. Sci. Biotechnol. 76:55–60. doi: 10.1080/14620316.2001.11511327.

Conejero, W., C.D. Mellisho, M.F. Ortuño, A. Moriana, F. Moreno, and A. Torrecillas. 2011. Using trunk diameter sensors for regulated deficit irrigation scheduling in early maturing peach trees. Environmental and Experimental Botany. 71(3):409–415. doi: 10.1016/j.envexpbot.2011.02.014.

Daudet, F.A., T. Ameglio, H. Cochard, O. Archilla, and A. Lacointe. 2005. Experimental analysis of the role of water and carbon in tree stem diameter variations. J. Exp. Bot. 56(409): 135–144. doi: 10.1093/jxb/eri026.

Devine, W.D., and C.A. Harrington. 2011. Factors affecting diurnal stem contraction in young Douglas-fir. Agric for Meteorol. 151: 414–419. doi: 10.1016/j.agrformet.2010.11.004.

Fereres, E. and M.A. Soriano. 2007. Deficit irrigation for reducing agricultural water use. J. Exp. Bot. 58(2): 147–159. doi: 10.1093/jxb/erl165.

Fernández, J.E. 2014. Understanding olive adaptation to abiotic stresses as a tool to increase crop performance. Environ. Exp. Bot. 103: 158–179. doi: 10.1016/j.envexpbot.2013.12.003.

Goldhamer, D.A., and E. Fereres. 2004. Irrigation scheduling of almonds trees with trunk diameter sensors. Irrig Sci. 23:11–19. doi: 10.1007/s00271-003-0088-0.

Goodwin, I., D. Whitfield, and D. Connor. 2006. Effects of tree size on water use of peach (Prunus persica L. Batsch). Irrig. Sci. 24: 59–68. doi: 10.1007/s00271-005-0010-z.

Herrmann, V., S.M. McMahon, M. Detto, J.A. Lutz, S.J. Davies, and C-H. Chang-Yang. 2016. Tree Circumference Dynamics in Four Forests Characterized Using Automated Dendrometer Bands. PLoS ONE 11(12): e0169020. doi: 10.1371/journal.pone.0169020.

Hu, L., and Z. Fan. 2016. Stem radial growth in response to microclimate in an Asian tropical dry karst forest. Acta Ecol. Sinica. 36: 401–409. doi: 10.1016/j.chnaes.2016.09.005.

Kleist, D.T., D.F. Parrish, J.C. Derber, V. Treadon, W. Wu, and S. Lord. 2009. Introduction of the GSI into the NCEPs Global Data Assimilation System. Weather Forecasting. 24: 1691–1705. doi: 10.1175/2009WAF2222201.1.

Köcher, P., V. Horna, and C. Leuschner. 2012. Environmental control of daily stem growth patterns in five temperate broad-leaved tree species. *Tree Physiology*. 32(8): 1021–1032, doi: 10.1093/treephys/tps049.

Larcher, W. 2003. Physiological plant ecology – ecophysiology and stress physiology of functional groups. Berlin, Germany: Springer.

Léchaudel, M, M. Génard, F. Lescourret, L. Urban, and M. Jannoyer. 2005. Modeling effects of weather and source-sink relationships on mango fruit growth. Tree Physiol. 25: 583-597. doi: 10.1093/treephys/25.5.583.

Levin, A.G., M. Peres, M. Noy, C. Love, Y. Gal, and A. Naor. 2018. The response of field-grown mango (cv. Keitt) trees to regulated deficit irrigation at three phenological stages. Irrigation Science, 36: 25. doi:10.1007/s00271-017-0557-5.

Livellara, N., F. Saavedra, and E. Salgado. 2011. Plant based indicators for irrigation scheduling in young cherry trees. Agricultural Water Management. 98:684–690. doi: 10.1016/j.agwat.2010.11.005.

Meng, Z., A. Duan, D. Chen, K.B. Dassanayake, X. Wang, and Z. Liu Z. 2017. Suitable indicators using stem diameter variation-derived indices to monitor the water status of greenhouse tomato plants. PLoS ONE 12(2): e0171423. doi:10.1371/journal.pone.0171423.

Moreno, F., W. Conejero, M.J. Martin-Palomo, I.F. Girón, and A. Torrecillas. 2006 Maximum daily trunk shrinkage reference values for irrigation scheduling in olive trees. Agricultural Water Management. 84: 290–294. doi: 10.1016/j.agwat.2006.03.005

Naor, A. 2014. Crop load and irrigation interactions—a new dimension of RDI. Acta Hortic. 1038: 113–119. doi:10.17660/ActaHortic.2014.1038.12.

Naor, A., S. Naschitz, M. Peres, and Y. Gal. 2008. Response of apple fruit size to tree water status and crop load. Tree Physiol. 28: 1255–1261. doi: 10.1093/treephys/28.8.1255

Neilsen, D., G. Neilsen, S. Guak, and T. Forge. 2016. Consequences of Deficit Irrigation and Crop Load Reduction on Plant Water Relations, Yield, and Quality of “Ambrosia” Apple. HortScience. 51(1): 98-106. doi:10.21273/HORTSCI.51.1.98.

Ortuño, M.F., W. Conejero, F. Moreno, A. Moriana, D.S. Intrigliolo, C. Biel, C.D. Mellisho, A. Perez-Pastor, R. Domingo, M.C. Ruiz-Sanchez, J. Casadesus, J. Bonany, and A. Torrecillas. 2010. Could trunk diameter sensors be used in woody crops for irrigation scheduling? A review of current knowledge and future perspectives. Agricultural Water Management. 97: 1–11. doi:10.1016/j.agwat.2009.09.008.

Ortuño, M.F., J.J. Alarcón, E. Nicolás, and A. Torrecillas. 2004. Comparison of continuously recorded plant-based water stress indicators for young lemon trees. Plant Soil. 267: 263-270. doi:10.1007/s11104-005-0108-3.

Salgado, E., and R. Cautín. 2008. Avocado root distribution in fine and coarse-textured soils under drip and microsprinkler irrigation. Agric. Water Manage. 95:817–824. doi: 10.1016/j.agwat.2008.02.005

Shah, N.H., I. Arshad, and Z.A. Khan. 2018. Effect of Different Levels of Water Stress on the Growth and Yield of Mango (Mangifera indica L.) by Using Drip Irrigation Technology. Int. J. Altern. Fuels Energy. 2(2): 3438.

Singh, Z. 2005. Embryo abortion in relation to fruit size, quality, and concentrations of nutrients in skin and pulp of mango. J. Plant Nutr. 28(10):1723–1737. doi: 10.1080/01904160500250771.

Tian, Y., Q. Zhang, X. Liu, and M. Meng. 2018. Stem Radius Variation in Response to Hydro-Thermal Factors in Larch. Forests. 9. 602. doi:10.3390/f9100602.

UNComtrade. 2016. World Mango Exports by All Reporters and Partners, 2005-2015 (based on HS80540). United Nations Statistics Division (UNSD).

Velez, J.E., D. Intrigliolo, and J. Castel. 2007. Scheduling deficit irrigation of citrus trees with maximum daily trunk shrinkage. Agricultural Water Management. 90(3): 197-201. doi: 197-204. 10.1016/j.agwat.2007.03.007.

Wei, J., G. Liu, D. Liu, and Y. Chen. 2017. Influence of irrigation during the growth stage on yield and quality in mango (Mangifera indica L). PLoS ONE 12(4): e0174498. doi:10.1371/journal.pone.0174498.

Yazgan, S., H. Buyukcangaz, C. Demirtas, and B. Candogan. 2006. Evapotranspiration for young cherry trees (Prunus avium) and growth responses to irrigation. Pakistan J. Biol. Sci. 9: 39–44. doi:10.3093/pjbs.2006.39.44.

Zweifel, R., H. Item, and R. Hasler. 2000. Stem radius changes and their relation to stored water in stems of young Norway spruce trees. Trees 15: 50–57. doi: 10.1007/s004680000072.

Zweifel, R., M. Haeni, N. Buchmann, and W. Eugster. 2016. Are trees able to grow in periods of stem shrinkage? New Phytologist. 211: 839-849. doi:10.1111/nph.13995.

6 PLANT BASED SENSORS DETECT F. OXYPORUM ON MANGO TREES

6.1 Abstract

Mexico has dominated the international mango trade and is doing research for optimizing water use without losing fruit quality and productivity. The use of soil, plant and environmental sensors helps to monitor plant water status. Pre-dawn, leaf or stem water potential are the most widely accepted methods for the direct sensing of plant water status. In this paper, plant based sensors such as dendrometers, leaf magnetic probes and infrared sensors were used to detect *Fusarium* infection in a mango orchard. The sensors helped to gain a deeper understanding on how water moves within the tree and how evapotranspiration takes place under *Fusarium* infection. Linear resistance dendrometers were developed and installed on the stem of a healthy and an infected mango tree. Every ten minutes, dendrometers, leaf turgor magnetic probes, and infrared leaf temperature sensors were sampled in both mango trees. Tree measurements were acquired under water-stress, watering and raining periods to encounter differences between the healthy and the infected tree. A soap powder solution was prepared with water and sulphur and applied three times to the infected tree, that became healthy and produced fruit. After analyzing data obtained from the sensors, the dendrometer plots provided reliable information on tree health, previous and after soap solution application. ZIM magnetic probes and leaf temperature sensors were unable to detect the disease. Although the micrometer leaf measurements were taken manually, leaf thickness proved to be a variable that sensed the infection effectively. Additionally, plotted trunk measurements indicated water storage for fruit growth and also when the fruit-bearing season was over.

Keywords: Dendrometer; *Fusarium*; Zim probe; thermal camera; leaf thickness.

6.2 Introduction

Mango is a popular product in tropical countries, but its global market has reached the last decade. Mango trade has increased significantly in both volume and geographic scope with the rapid expanding consumption in the US, China and the Netherlands. Mexico has dominated international mango trade from 2012-2016 with a 16% of market share, reaching US$328 million in 2015, four times higher than the fruit exported in 2005 (UNComtrade, 2016). However, 53% of world exports in 2015 are attributed to exporters such as Peru, Brazil, India, Thailand and Mexico. Mexico with an 8.98 MT/ha production is doing a good job of determining shifting market demands for different varieties that include Kent, Keitt, Tommy Atkins, Haden, Ataulfo, among others. An improved organic mango is offered, which satisfies a select group of consumers who are looking for healthy products, without chemicals and that protect the environment. More than 110,000 farmers in Mexico use organic practices, surpassing any other country in the world. (Alberts Organics, 2016).

La programación del riego implica determinar con precisión tanto la temporización del riego y la cantidad de agua a aplicar. Although mango trees are drought-tolerant plants they have to be irrigated mainly during the fruiting period. Water supply during the first six weeks of fruit development is critical, and a period of drought induces fruit fall and reduced fruit mass (Singh, 2005). Micro-sprinkling irrigation can effectively reduce water consumption (Levin et al., 2018). Since plant water status controls many physiological processes and crop productivity, this information is fundamental for irrigation scheduling. Many researchers are obtaining useful indicators based on stem diameter variations together with its threshold values for irrigation scheduling (Conejero et al., 2011; Goldhamer and Fereres, 2004; Livellara et al., 2011; Moreno et al., 2006; Ortuño et al., 2004).

In most mango producing areas there is a phytosanitary problem called "witch's broom" (Michel et al., 2013), which in Mexico is distributed in all producing states and can reduce 60% its production (Noriega et al., 1999). Research considers as causal agents of the disease *Fusarium oxysporum* and *F. subglutinans* (Freeman et al., 2000). In addition, a new species reported as *Fusarium mangiferae*, is related to strains that were previously identified as *F. subglutinans* (Britz et al., 2002). The symptoms of the disease include the loss of the apical domain, swelling of the vegetative shoots, proliferation of the leaves and the lack of fruiting, extensive abortion of the fruit (Noriega et al., 1999).

Leaf measurements can also provide information for irrigation scheduling. New magnetic ZIM-probes detect relative changes in leaf hydration and turgidity (Zimmermann et al. 2008). This technology uses miniature pressure sensors that are clamped to leaves via magnets, to measure cell leaf pressure that declines during transpiration and responds to drought (Kramer and Boyer, 1995). ZIM-probe technology has been used to monitor the water status of trees (Ehrenberger et al. 2012; Martinez et al., 2017; Rüger et al. 2010).

Plants exposed to pathogens, react with physiological mechanisms and reduces the photosynthetic rate. This photosynthetic rate reduction, induces an increase of fluorescence and heat emission (West et al. 2003). Infected plants chlorophyll content drop is detected by spectral reflectance (Hahn, 2009; Krezhova et al., 2017). Remote sensing can detect early or chronic changes in plants by analyzing the total energy absorbed by the plant (Meroni et al. 2010). This absorbed photosynthetic active radiation on a healthy plant is used for photochemical reactions (0–20 %) and dissipates the rest as heat (75– 90 %). Leaf or canopy temperatures obtained by thermal imaging systems, can be used as an indicator of plant stress and stomatal closure (Jones et al., 2009). Inexpensive thermal cameras as the FLIR- ONE have been connected to smartphones to assess grapevine and mature almond trees water status (García et al., 2018; Petrie et al. 2019). Net radiation absorbed by the leaf or canopy is a critical variable causing linear increments on leaf temperature (Grant et al., 2007).

The objective of this work was to evaluate plant based sensor´s measurements on healthy and “witch broom” infected trees. This research helps to understand if *Fusarium* causes evapotranspiration problems in the tree, and its response after applying a soap solution to the trees. Stem dendrometers, leaf ZIM-probes, infrared temperature sensors, a micrometer and an infrared thermal camera were evaluated as disease detectors; data analysis should be considered for each sensor.

6.3 Materials and methods

The experiment was established in a high density commercial mango orchard located at the town of Loma Bonita, Guerrero, Mexico (17° 25' 47" N, -101° 11' 19" W, 17 m ASL). The region is influenced by a subtropical arid climate, having a weather station at the orchard. The station recorded a mean annual rainfall of 1570 mm in 2018 and an average of 1470 mm during the last five years. Scarce rainfall occurs between January to May and rains heavily from September to November.

6.3.1 Field site for experiment trial

The experiment was run from the 20^{th} of April 2019 to end of harvest on August 20^{th} 2019 (Fig. 1). Two mango trees variety 'Kent' were selected within the same site having basaltic clay-loam red soil. Its bulk density was obtained from 30 soil cores taken randomly from depths between 10 to 40 cm, being its average density of 1.1 gcm^{-3}. The six-year-old mango trees had an 8 m between row and 4 m in-row spacing, having the tree rows an east-west direction.

Preliminary soil moisture studies indicated that micro-sprinkler watering maintained the soil beneath the trees wet. Three hours after irrigation at sunset, water inside the retaining well was still present, so null soil transpiration occurred. Excavations were also carried out to assess effective root depth. It was observed that the highest root density at a soil depth of 0.4 m, with fewer roots observed at a depth of 0.6 m. No plant roots were found to occupy the space below the canopy tree edges.

The trees received irrigation for an initial period of 17 days ending on May 13^{th} when a twelve-day stress period continued. According to tree size and age, 100% evapotranspiration (ET) watering was recommended to the farmer, corresponding to 55 l day^{-1}. Irrigation was controlled by automatic timers set to run for 20 min at

18:00 just before sunset to avoid soil transpiration. Water was delivered via one 120 L h^{-1} micro sprinkler installed at a distance of 0.5 m from the tree trunk. Stressed trees cycles resulted from withholding irrigation water until plants began to wilt. From June 5th raining events were present and combined with irrigation when showers failed.

Mango tree is considered a woody trunk plant with primary branches departing at a certain height from the main trunk. Secondary branches grow from primary branches. The tree structure was pruned and secondary branches strapped with threads to soil-fixed tutors. Pruned trees with strapped secondary branches presented slower vegetative growth and higher fruiting rates. The healthy tree (HT) started inflorescence in April and continued fruit production during June and July (Fig. 1). This tree presents a height of 1.7 m, three main branches and 1200 leaves and never got infected. Its canopy diameter measures 3.37 m being almost twice its height. The main bifurcation was found at a height of 0.83 m, having a stem diameter of 8.21 cm, 10 cm below. The IT (Infected Tree) presented a canopy diameter of 1.9 m, having 670 leaves shared within 3 main branches. The tree with a height of 1.8 m never showed vegetative growth, being its diameter of 8 cm.

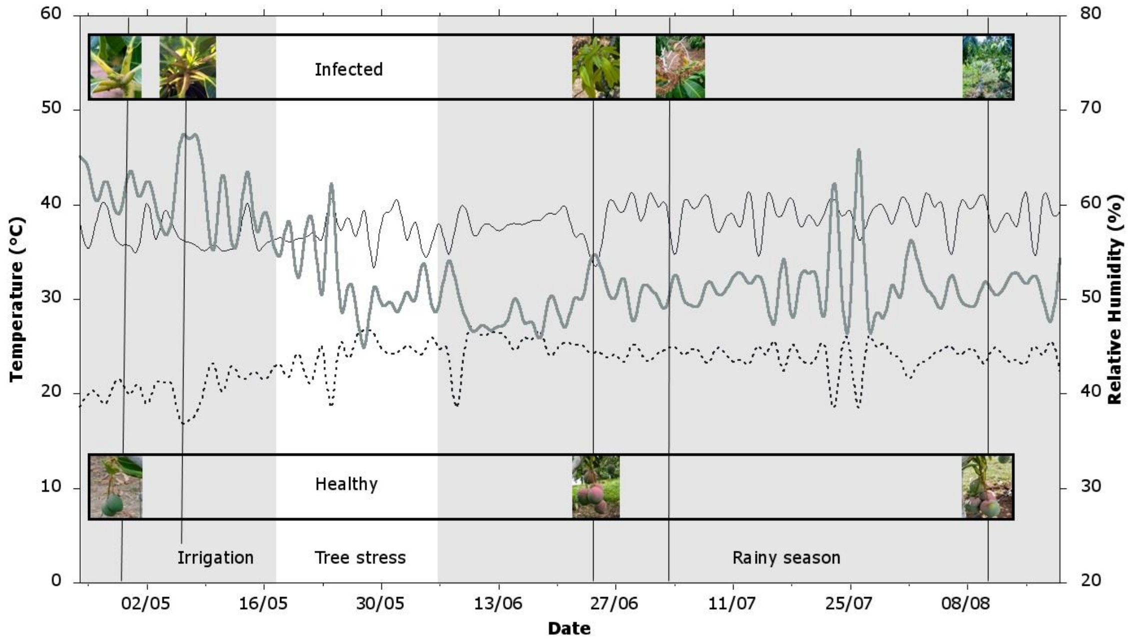

Fig. 1 Maximum temperature (Tmax—), minimum air temperature (Tmin---) and relative humidity (RH—) sampled during the mango production season in an infected (IT) and a healthy (HT) tree.

Fig. 2 Fungal infection (A) in vegetative buds, (B) affecting inflorescence, (C) in wilted inflorescence with fruit set, and (D) fruit panicle strains.

6.3.2 Disease symptoms and control

The infection caused by *Fusarium subglutinans* and *Fusarium oxysporum* affects vegetative and floral shoots. In vegetative shoots when sprouting appears, shoots proliferation causes a marked reduction in internode length and leaf area. When the bud of a mature sprout has already been damaged (Fig. 2A), the new sprout can result in either vegetative or floral malformation depending on the environmental conditions. The floral malformation has abnormal inflorescences, where the primary and secondary axes of the panicle shorten, thicken and produce many branches strongly grouped together.

The major symptom of inflorescence malformation consists of copious panicles (Fig. 2B), that produce many branches grouped together; These panicles are producing up to three times the normal number of flowers. however, these flowers are unusually enlarged, sterile and bear no fruit (Kumar et al., 1993). The affected inflorescences continue their growth even after fruit set, remaining green for long periods. Subsequently they wilt and remain as compact dark-colored masses that remain attached to the tree (Fig. 2C). As fruit grow strains of the infecting fungi remain with their panicles (Fig. 2D).

In the presence of *Fusarium* the symptoms may be accompanied with gills. It is possible that the infection subsequently occurs in outbreaks previously damaged by the *A. mangiferae* mite. It can occur simultaneously with the mite infestation in outbreaks that occur at the beginning of the rainy season. The infection caused to shoots and inflorescences in trees and its response after applying soap + wettable sulphur to the trees was evaluated with plant based sensors. Soft soaps made from potassium compounds for pest control can add useful minerals to the soil and leaves during spraying. A solution of one tablespoon of Roma soap powder together with 5 grams of sulphur per liter of water was applied to the mango leaves and inflorescences with an atomizer. It was applied on May 18th, on July 1st and on August 1st of 2019 to the infected tree.

6.3.3 Plant based sensors

Trunk measurements were taken daily with dendrometers, leaf turgor with ZIM-probes (Yara plant sensor, Yara International, Oslo, Norway) and canopy temperature with a Flir camera mounted to a smartphone. Air temperature and relative humidity were measured with environmental sensors. The dendrometer (Fig. 4A) was placed at a height of 0.15 m below the main bifurcation with a N-S direction to avoid direct incidence from the sun.

6.3.4 Dendrometer trunk measurements

Dendrometers measure trunk diameter growth in the order of microns using linear variable transducers attached to the trunk by a special bracket (Zweifel et al., 2000). Our assembled dendrometer used a linear resistor transducer to convert a linear displacement into a proportional electrical signal. A linear current source fed the resistance to avoid sampling errors caused by the discharge of the lithium battery. A microcontroller with real time clock acquired the voltage at the resistor pin ten times every ten minutes; The values were averaged and the result saved in a MSD memory. Data was transmitted wirelessly, introduced to a computer and plotted (Fig. 3). MXD corresponds to the maximum trunk diameter, meanwhile MND the minimum trunk diameter after stem shrinkage (Fig. 3). MXD and MND daily values occur just before sunrise and sometime during the afternoon, respectively.

A trunk morning slope (MS) results from stem shrinkage, as water and carbon compounds stored in trunk cells flow upwards. As ambient air temperature increases, stomata open and evapotranspiration (ET) starts, reducing trunk maximum diameter. An afternoon slope (AS) results when stomata close and water gets stored in the trunk; this slope starts as air temperature decreases. Temperature continues dropping through the night and when the temperature slope changes, a new night slope (NS) is produced. The daily plot was centered at zero with the dendrometer value obtained at the irrigation time of 18:00.

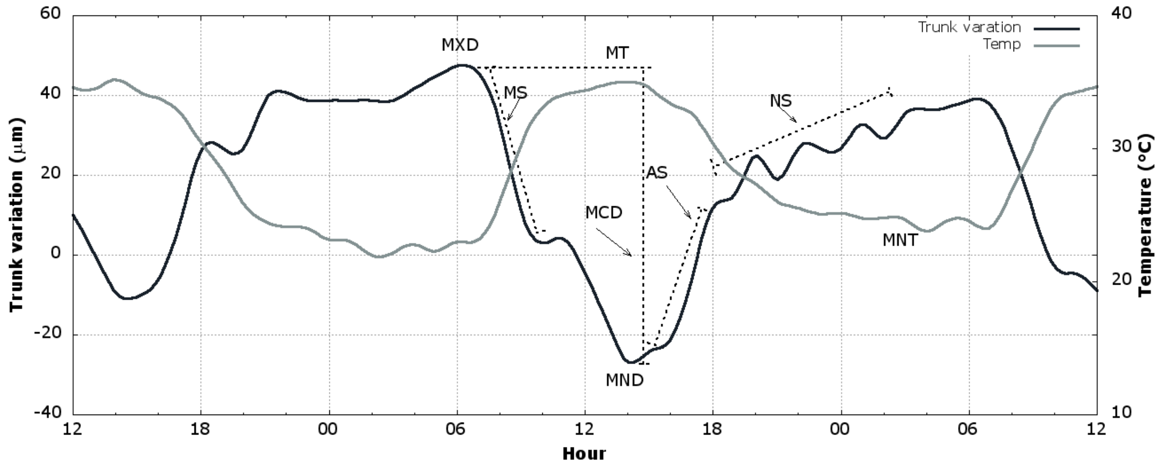

Fig. 3 Daily temperature (—) and stem growth (—) variables plotted, being MXD the maximum diameter, MND the minimum diameter, MS the morning slope, AS the afternoon slope, NS the night slope, MCD the daily trunk growth, MT the maximum temperature, and MNT the minimum temperature.

6.3.5 Environmental measurements

Air relative humidity and temperature were measured with a Sensirion DTH22 sensor (Fig. 4B). A temperature and humidity sensor was placed just over the canopy of a second branch in each tree, approximately at a height of 1.5 m over the soil. The CMOSens sensors, signal magnifier, A/D switch and 12C bus interface are integrated in one chip; This chip was installed by one side of the tree canopy and connected to the microcontroller. Data are acquired every 10 minutes and saved in a MSD memory.

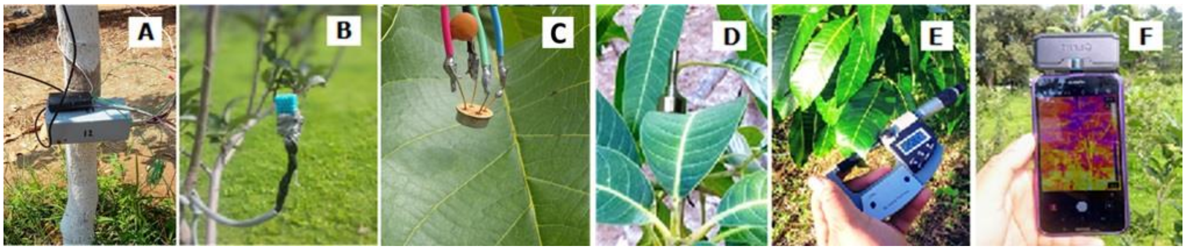

Fig. 4 Plant based sensors including (A) dendrometer, (B) DTH22, (C) MLX90614 infrared sensor, (D) ZIM-Probe, (E) IP65 digital micrometer and (F) Flir One camera.

Fig. 5 Thermal infrared and color image of (A) fruit, (B) infected leaves, and (C) healthy leaves on a mango tree.

6.3.6 Infrared thermography

A FLIR-ONE Pro (Flir Systems Inc., Wilsonville, OR, USA) camera had its emissivity set at 0.95. This low-cost camera uses a thermal sensor (8–14 µm, 80 × 60 pixels) and a digital sensor (1440 × 1080 pixels) connected to a smartphone (Fig. 4F). This fact allows overlapping two images (a false-colored with a digital image) for subsequent analysis. The images taken with the FLIR-ONE Pro camera, were captured by using the free software “Flir One” and analyzed with the Flir-Tool application. The Android smartphone acquired a mango tree color image together with its thermal image, being the leaves and fruit temperature of 39.2°C and 40.8°C, respectively (Fig. 5A). Each pixel corresponds to an effective temperature reading, varying from 20° C to 120° C with an accuracy of ±3°C (García et al., 2018). Leaf inclination with respect to the horizontal caused variation in heat absorption, so measurements were taken at an inclination of 30°. The temperature from ten leaves were taken daily from each tree every three hours during the period from June 17th to June 22th and from August 12th to August 17th. Stiff infected leaves were darker in color with a low temperature of 36.4°C (Fig. 5B); healthy tree canopy was of 40.6°C (Fig. 5C).

An infrared non-contact thermometer (mod. MLX90614, Melexis Technologies, Belgium) for punctual leaf measurements was used (Fig. 4C). The IR sensitive thermopile detector chip, with a 17-bit ADC signal conditioning unit are integrated in a TO-39 can. Temperature can be measured in the -20°C to 120°C range with an output resolution of 0.14°C. Measurements were sampled by the microcontroller every ten minutes and saved in a MSD.

6.3.7 Leaf thickness and turgor measurements

Turgor measurements in real time are provided by Yara ZIM-probes (Fig. 4D) consisting of two magnets that exert an external pressure to a patch of a leaf covering an area of 87 mm^2 (Zimmermann et al., 2008). The sensor measures patch pressure (P_p), and the distance between the magnets can be regulated in order to set up P_p between 10 and 60 kPa. ZIM-probes weigh only 5.5 g (Ehrenberger et al., 2012) and were clamped with the sensor facing the abaxial leaf surface. Turgor was measured on one east-directed leaf every ten minutes, at a height of 1.5 m of each tree. The infected leaf measurements of May 16th previous to soap application and on May 20th after soap application were analyzed. In order to measure leaf thickness ten leaves were taken per tree and measured with a digital micrometer (mod IP65, Mitutoyo, Japan) every three hours. Leaf measurements were taken in both trees from June 20th to June 22th and afterwards from August 14 until August 17. The ratchet thimble micrometer measures from 0 to 25 mm with a resolution of 0.001 mm and an accuracy of ±2 µm. Values were averaged and the standard deviation obtained.

Statistical analysis

Every tree dendrometer provided a huge quantity of data as 144 measurements were taken daily. In a month having 30 days, 4320 stem diameter values were acquired and saved in the MSD. The same quantity of data was obtained from the both ZIM-probes, air temperature and relative humidity sensors. If two sensors are considered for sampling, a total of 1,152 measurements were acquired per day. A macro program in Excel was generated to obtain the MXD, MND, MS, AS, P_p, maximum and minimum air temperatures. Average and standard deviations were obtained by variable for each irrigation treatment, and soap application; both IT and HT trees were considered. Average daily air temperature and relative humidity also were obtained. Canopy temperature measurements were taken with the FLIR-ONE Pro camera and the leaf temperature measurements averaged. If the canopy presented three leaves, all the measurements inside the image were averaged. Simple regression curves were adjusted using the least squares technique in order to correlate thermal canopy temperature of the MLX90614 sensor against the thermal image for both trees.

6.4 Results

Plant based sensors were installed to measure water transport through the mango tree. As water passes through the trunk it gets sampled, before arriving to the leaves that are also measured. The sensors to be used most be practical and easy to handle, avoiding the use in the field of complicated laboratory equipment. Trunk and leaf measurements of a healthy and an infected tree were compared during stress and watering conditions. It is important to mention that microbiological tests were not carried out to know the degree of infection in the tree. Tree classification as healthy or infected depended on inflorescence quality, fruit set and its growth.

6.4.1 Trunk measurements

Continuous air temperature and trunk diameter measurements under stress and watering conditions during 3-day periods are plotted for the HT and the IT tree (Fig. 6 dotted line). As soil water available remains for 3 days after water shortage, trunk growth was plotted from May 21th to May 23th (Fig. 6A), corresponding to the second stress week (Fig. 1). A watering period from June 17th to June 19th and a wet August period were also plotted.

Trunk MXD measurements were averaged for the healthy and the infected tree under irrigated and stressed days (Table 1). The average value was obtained from all the monitored data from each tree under stress and irrigated conditions during the periods shown by Fig. 1; it does not consider only data plotted by Fig. 1 and

Fig. 7. Average MXD and MND was similar between HT and IT, during watering days. Healthy tree average MXD decreased by 45.5% under water stress conditions, meanwhile MXD in the infected tree decreased only by 19.7%. Minimum diameter average (MND) in the healthy tree was higher during stress as the tree shrinked 24.6% more. In the infected tree, its behavior was different as the tree shrinked 52% less during water stress conditions, than under irrigation. Independent of the water treatment, MCD average values are always higher in the healthy tree than in the infected tree.

Table 1 Healthy, infected and soap reaction to tree measured in the trunk with dendrometers.

	HEALTHY				INFECTED				SOAP			
	Irrigated		Stress		Irrigated		Stress		Irrigated		Stress	
	Avg	SD	Avg	SD	Avg	SD	Avg	SD	Avg	SD	Avg	SD
MXD	48.4	7.05	26.4	8.52	47.7	11.17	38.3	6.03	74.5	5.95	39.51	5.81
MND	-26.8	7.94	-33.4	13.35	-29.4	15.19	-14.1	11.04	0.99	10.51	-18.11	4.248
MCD	79.2	10.68	59.76	17.2	77.17	14.9	52.42	13.42	73.51	11.86	57.62	6.283

In the plotted stress period, MXD values ranged between 23.7 and 35.76 µm for the healthy tree, (Fig. 6A-dark line), being its average MXD value of 26.4 µm (Table 1). The warmer night of May 23th dropped MXD to 23.84 µm and leaves started to wilt. HT morning slopes differed in the three days (- 0.264±13% µm min^{-1}), having the 21th of May two different slopes between 7:00 and 10:00, with a peak between them. Fruit absorb water and growth take place within these periods. At noon of May 21th and May 22th, HT trunk diameter shrinked until -2.2 microns (Fig. 6A). Maximum HT shrinkage MND (-25.72 µm) during May 21 and May 22, occurred at 16:50 and 17:00, respectively.

The infected tree (dot line) presented the lower MXD in this stress period (Table 1). Scarce soil water availability combined with dew temperature of 24.75°C at 7:40 on May 23, limited trunk growth to 11.92 µm (Fig. 6A). The afternoon slope differed all days and only was present until 17:40. The soil water flows to the leaves during 7 hours, providing controlled plant evapotranspiration (ET); The same ET period was noted when the trunk shrinked from May 21th to May 23th.

Later in each afternoon, water flowing through the trunk got stored as plant evapotranspiration decreased.

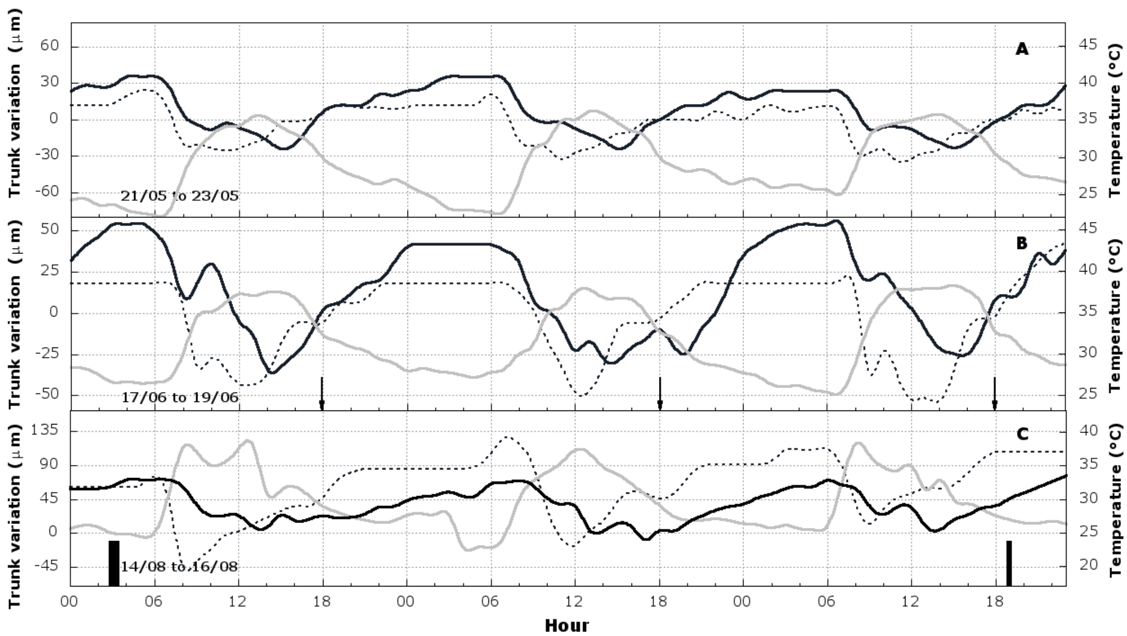

Fig. 6 Air temperature (—), trunk variations of healthy (—) and infected tree (…) during (A) stress, (B) watering, and (C) rain conditions.

Measurements after soap application only considered 3 days at the infected trunk, being the values acquired from May 18th to May 20th for the stressed condition (Table 1). Average values after applying soap to the infected tree during May were 3.16% and 28.4% higher for MXD and MND, respectively.

In the period between June 17th and June 19th, daily 100% ET watering was applied where the arrows are shown (Fig. 6B). Although water was always available at the soil during the three days, warm nights caused a constant MXD of 17.9 μm in the infected tree (Fig. 6B). June 17th night temperature was of 26.5°C, and June 19th dew temperature decreased to 24.3°C. Trunk shrinkage noted by MND peaks in Fig. 6B can be attributed to tissue rehydration (Zweifel *et al.*, 2016) and do not allow trunk growth. Infected tree trunk shrinkage increased from -48 μm on June 17th to -53 μm in June 19th. MND peaks occurred close to noon and matched maximum air temperature.

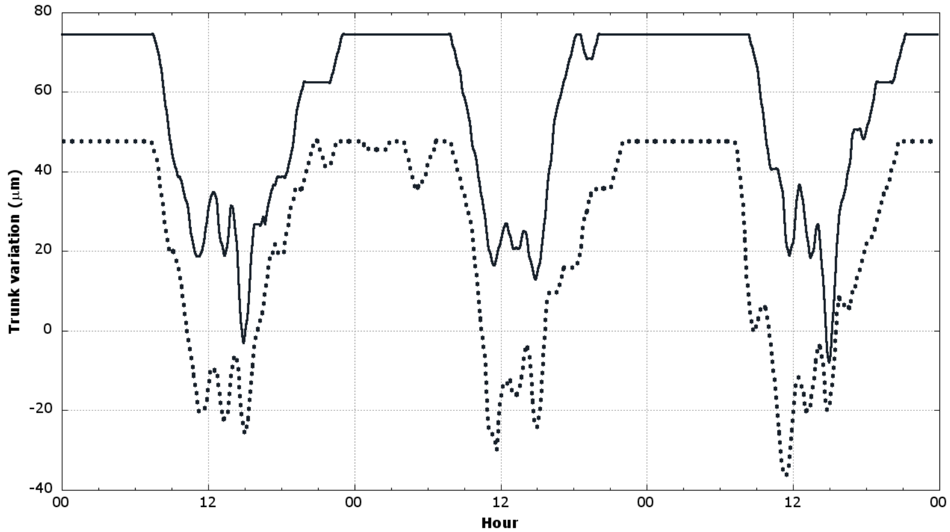

Fig. 7 Trunk variations of tree just --- before and — after soap treatment.

Infected tree trunk measurements between June 27th and June 29th were plotted (Fig. 7-dot line). The solution of soap dissolved in water was applied to inflorescences and leaves of the infected tree (IT) on the afternoon of July 1st. Dendrometer measurements were also plotted from July 5th to July 7th as mango fruit curdled and began to grow showing peaks between 11:30 and 16:00 (Fig. 7-dark line). Constant MXD values of 74.6 µm were sampled during the three July days. Morning slopes of June 27th and July 5th were similar (-0.285 µm min^{-1}) as were the ones of June 28th (-0.387 µm min^{-1}) and July 6th. The morning slope of June 27th finished at 11:30 with a value of 20.03 µm. Morning slopes of June 29th and July 7th present a phase shift of 70 minutes. MS ended at 11:40 on June 28th, being the MND of -32.89 µm. June 29th was the day showing greater infection, and MND was -38.85 µm at 11:30. Afternoon slopes presented several steps when the tree was infected.

After soap application, trunk MXD in the period from July 5th to July 7th increased 56% with respect the one obtained by the IT under the normal irrigation period (Table 1). July 5th maximum peak of 33.8 µm between the two morning slopes (MS) indicates trunk water storage to provide water requirement for fruit growth. Trunk diameter variations should be considered within the water balance and the sugar content of mango trees (Daudet et al., 2005) as sugar content of woody tissues changes as a function of fruits. A strong shower was present on July 7th between 5:00 and 8:00 and ET started later. After soap application maximum shrinkage (MND) was obtained on July 7th at 14:50 with a value of -6.95 µm.

After the soap solution with sulphur was applied to the infected tree on July 1st and August 1st, the tree was blooming and fruit started to grow (Fig. 1C). MDC increased all days with continuous irrigation and rain, and the IT tree trunk undergo an irreversible growth, losing its elasticity. MDX on August 15th and August 16th increased to 131.13 µm and 111.26 µm, respectively. The tree presented a MND of -49.6 µm seven hours after rainfall, and matched in time with the maximum air temperature peak of 37.9°C (Fig. 6C). Tree morning slopes varied significantly every day during August sampling. The MND peaks were located in the V bottom point and matched with the maximum temperature peak magnitude.

6.4.2 Leaf measurements

Leaf measurements consider canopy temperature measurements, leaf thickness and leaf turgor. Leaf temperature was measured within the June 17th to June 22th period, using the infrared thermal camera on both trees under irrigation. Leaf temperature varied according with the inclination, being higher in leaves having a smaller angle with respect to the horizontal (Table 2). Temperature increased from sunset to 15:00 and decreased afterwards. Infected leaves had similar temperatures for inclinations of 30° and 45°.

Table 2 Canopy temperature of healthy and infected leaves having inclinations of 30° and 45°.

	Healthy leaf temperature (°C)						Infected leaf temperature (°C)					
	6:00-10:00		12:00-16:00		17:00-21:00		6:00-10:00		12:00-16:00		17:00-21:00	
	Avg	SD	Avg	SD	Avg	SD	Avg	SD	Avg	SD	Avg	SD
30°	31.2	2.12	38.11	3.06	28.8	0.83	31.56	1.45	37.18	1.46	29.02	0.57
45°	29.6	1.33	38	1.94	28.6	1.37	31.33	1.65	37.34	1.9	29.18	0.58

Air and canopy temperature measured during the stress period from May 13th to May 25th in the healthy tree were compared in table 3. Air temperature was measured with the DTH22 sensor and the infrared MLX90614 sensor sampled leaf temperature at the top flat leaf surface. Air and leaf temperature differences were of 6%, 6.9%, and 5.9% at the 6:00-10:00, 12:00-16:00 and 17:00-21:00 periods, respectively. Canopy temperature standard deviation during the 12:00-16:00 period was higher as leaves absorb less radiation after 15:00. With the disease leaves are darker and stiffer decreasing leaf heat absorption, so a smaller standard deviation is obtained during this period.

Table 3 Canopy and air temperature of healthy tree measured during watering and stress periods from April 24th to May 12th.

	Air temperature						Canopy temperature					
	6:00-10:00		12:00-16:00		17:00-21:00		6:00-10:00		12:00-16:00		17:00-21:00	
	Avg	SD	Avg	SD	Avg	SD	Avg	SD	Avg	SD	Avg	SD
Stress	24.98	2.39	32.73	0.92	28.25	1.93	26.71	3.35	34.95	0.76	29.73	2.17
Irrigat	22.8	3.13	32.4	0.9	27.38	2.26	24.17	3.64	34.64	0.99	29.01	2.84

When the healthy tree was water-stressed, removed average canopy and average air temperature increased by 2°C in the morning (Table 3). At midday, average air temperature at the stressed healthy tree was 0.3°C higher than during watering. Average canopy temperature was 2.22°C higher than average air temperature.

Leaf temperature correlations between the MLX90614 sensor and the infrared camera temperature shows a linear tendency behavior (Fig. 8). When both trees are healthy in August, tendency lines are parallel (Fig. 8b), but when the disease is present during June the dark line changes its slope (Fig. 8a). Pointed tendency lines of the healthy tree have lower punctual leaf temperatures during June and August.

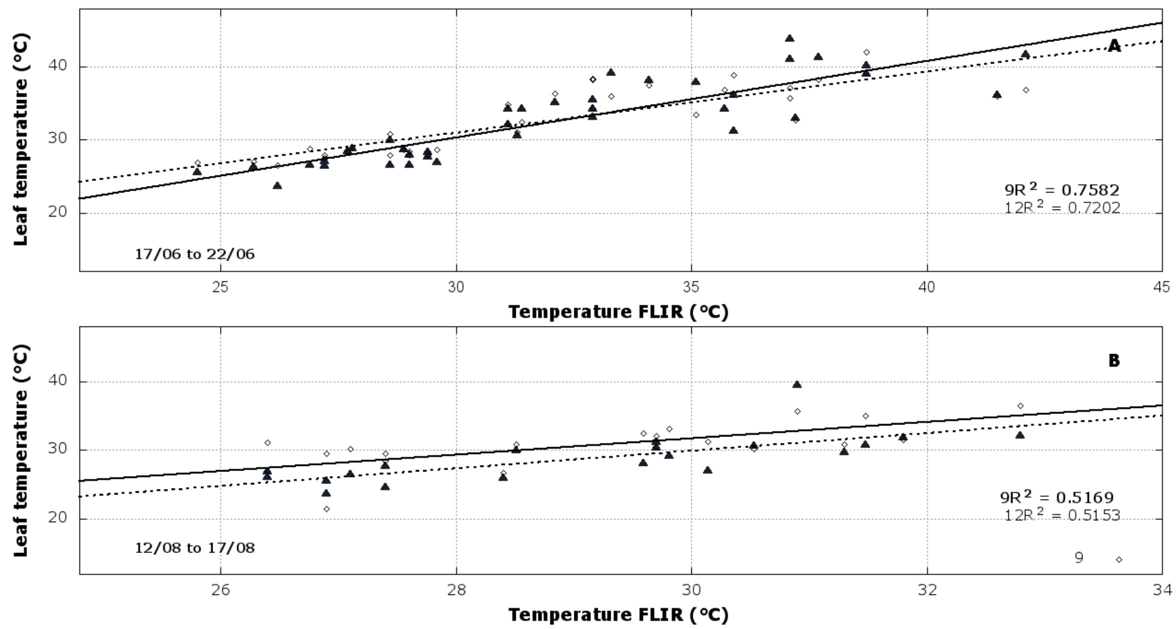

Fig. 8 Flir thermal leaf temperature versus punctual MLX90614 leaf infrared temperature in (A) June and (B) August for HT (▲) and IT (○) trees.

Previous to soap solution application in July 1st and August 1st the infected tree shows a R^2 of 0.758 between both temperature detectors (Fig. 8a). The tendency line of the healthy tree intercepts the infected tree line at a FLIR camera temperature of 32.8°C. The healthy tree tendency shows a lower R^2 of 0.72. Although tendency lines are parallel during the August 12th to August 17th period, R^2 decreased to 0.51 in both trees.

Magnetic-based probes attached to the mango leaf presented a peak patch pressure (P_p) of 86 kPa after 13:00 in the non-watered infected tree on May 16th of 2019. Simultaneously the dendrometer showed a trunk morning slope (MS) starting at 7:30 and finishing at 9:00 (Fig. 9A). Leaf turgor and trunk measurements increased from 9:00 to 11:00 due to stomatal conductance closing (Rüger et al., 2010). P_p starts decreasing at 13:00 until 20:00 when the pressure falls to 37.9 kPa (Fig. 9A). This unhealthy leaf measured on May 16th shows a turgor P_p peak; simultaneously the dendrometer MND measures 0.2 µm.

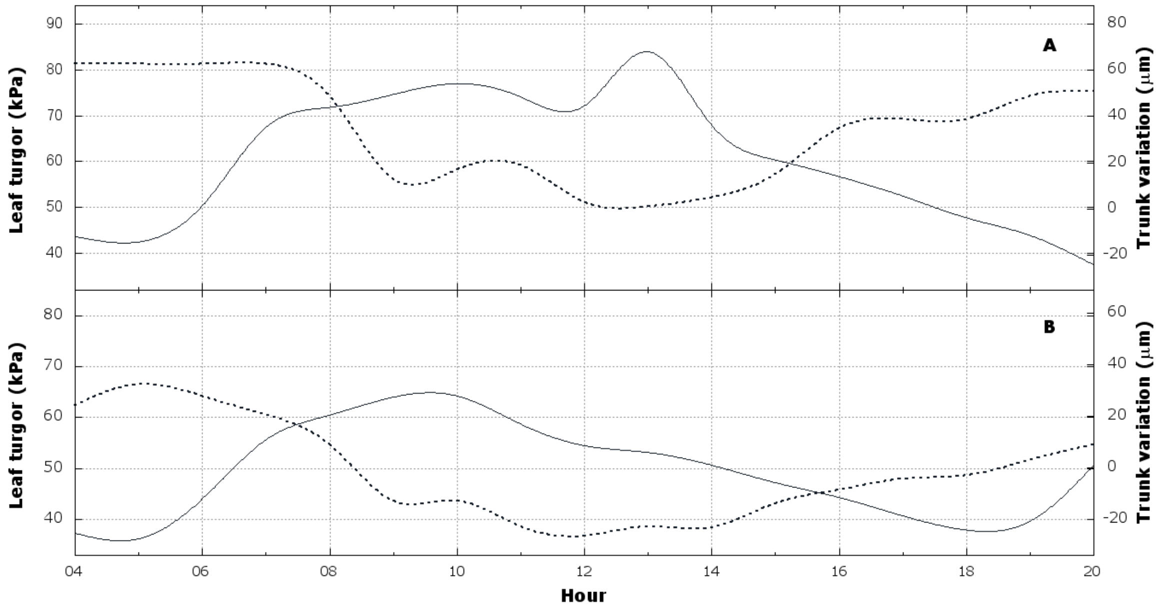

Fig. 9 Trunk variation --- and leaf turgor — two days (A) before, and (B) after soap application.

Two days after applying soap on May 18th, P_p decreased to 55 kPa at noon and the peak value was achieved at 10:00. Trunk diameter decreased from 7:00 until 9:00, obtaining a MND value of -27 µm on May 20th (Fig. 9B). A dendrometer peak was found from 9:00 to 11:00 starting trunk water storage at 11:45; at this time leaf turgor decreased.

Leaf thickness sensors can monitor leaf water content. but cannot stay on the leaf continuously. Micrometer measurements taken on the same place of the leaf, damaged the tissue. Canopy temperature during June 20-22 on the infected tree varied from 38 to 25°C, meanwhile thickness variations ranged from 0.28 to 0.31 mm (Table 4). In the same days, the healthy tree presented thickness variations from 0.239 to 0.29 mm. Maximum leaf thickness in the healthy leaf did not occur synchronously with canopy temperature, that decreased from 44°C to 23°C in those days. Maximum and minimum leaf thickness on the infected leaf occurred at 23:00 and 12:00, respectively.

Table 4 Maximum and minimum leaf thickness and thermal temperature for healthy and infected tree in June and August periods.

	Infected				Healthy			
	Thickness (mm)		Leaf temperature (°C)		Thickness (mm)		Leaf temperature (°C)	
	Max	Min	Max	Min	Max	Min	Max	Min
June	0.31	0.28	38	25	0.29	0.239	44	23
August	0.302	0.279	37.5	20.3	0.261	0.24	39.42	22

After applying soap to the inflorescences, fungal activity ceased and on August 14th the infected tree had several 200 g fruit hanging. Fifty mm of rain on this day, occurred from 3:00 to 4:00 causing minimum low IT canopy temperature of 24°C and 0.284 mm thickness at 8:00. Canopy temperature during August 14-17 on the infected tree varied from 20.3 to 37°C, meanwhile thickness variations ranged from 0.279 to 0.302 mm (Table 4). The heathy tree presented a leaf temperature ranging from 22°C to 39.4°C with a lower thickness varying between 0.24 and 0.26 mm.

6.5 Discussion

Average values measured by sensors in plants do not represent and explain daily behavior, that includes floral infection and lack of fruit set deformed inflorescences. Dendrometers (Meng et al., 2017; Ortuño et al., 2010) and leaf turgor (Martinez et al., 2017; Rodriguez et al., 2019) have been used as plant sensors for irrigation scheduling. However, disease detection by plant sensors has to be investigated, so in this study plant based sensors analyzed the signals provided by water-stressed and disease-stressed mango trees.

6.5.1 Plant infection

Environmental and soil factors are essential for *Fusarium* plant infection and disease severity has been found to be optimum at 28 ℃ which is within most of night temperature. As temperature increases above 34 ℃ and falls below 17℃ its severity decreases (Zitter 1999). The infection caused by *Fusarium* affected vegetative and floral shoots. Producers detect floral malformations as the major symptom of the disease which produce abnormal inflorescences. The copious panicles produce up to three times the normal number of flowers, however they are sterile and do not bear frui (Kumar et al., 1993). Little research on mature leaves behavior after infection has been reported. These apical buds produce deformed buds and brittle leaves being smaller compared to healthy plants. Under water stress conditions after May 21th, night temperature and maximum day temperature were within 24 ±1°C and 36±1.5°C, respectively. Temperatures together to an average RH over 58%, lead to the absence of floral shoots. The high dew temperature affected plant health.

6.5.2 Leaf sensing

Magnetic-based probes can be used for long-term measurements in the field as leaf patches do not show any lesions, and no P_p data interruption was present even with strong winds. Yara-magnet probes have been successfully used to monitor leaf water status in fruit trees (Martínez et al., 2017; Rüger et al., 2010). After evaluating peak Pp values daily in the healthy and infected leaf variations between them were not considerable. Also it was found that when the solution was applied and the sensors were not removed, no changes were noted later.

Infected leaves were thicker than healthy leaves as more water remained absorbed within the tissue. Minimum infected leaf thickness of 0.28 mm was slimmer only in 5% of the measurements than the maximum thickness of 0.29 mm from healthy leaves during the June 20-22th period. The same effect was noted in August when healthy leaves were slimmer than infected leaves. Although the tree was bearing fruit and look healthy, water in damaged tissues remained trapped (Table 4). Leaf temperature and relative humidity operate on leaf thickness by their effects on transpiration rates (Bùrquez, 1987). Canopy temperatures in August arrived to 39.4°C meanwhile in June its maximum value was 44°C. In the raining season average air temperature reached 38°C and the average RH arrived to 52%. At the end of June when infection is critical air temperature increased to 41.5°C and RH decreased to 48%.

Vegetation temperature is related to stomatal conductance and transpiration-associated evaporative cooling and is used as an indicator of vegetation health (Hernandez et al., 2019). Under water stress conditions, stomatal conductance decreases as stoma closes and vegetation temperature increases; as a result, transpiration rate decreases. El cierre de las aberturas de los estomas es un mecanismo de defensa que impide la entrada de microbios y la colonización de tejido huésped. El aumento resultante en la hoja y la temperatura de la cubierta a menudo se puede detectar por imagen térmica en el plano de la hoja en una etapa temprana de la infección (Jones, 1999; Lindenthal et al., 2005).

Punctual infrared MLX90614 sensor and thermal infrared image presented a linear correlation and when both leaves were healthy, parallel tendency lines were encountered (Fig. 8). The plot between MLX90614 and thermal infrared image for an infected leaf shows a different slope than a healthy leaf as the thermal image value is obtained after averaging several points over the leaf. Canopy temperature was always higher than air temperature under stress and irrigation conditions (Table 3). Infrared thermal images provided canopy temperatures within four-hour spans. Standard deviations were below 4 (Table 3), and the 12:00-16:00 span presented the lowest standard deviations beneath one. Further temperature studies can measure from 10:00-16:00 without having huge measurement variations if no clouds are present. However, as a disease detector, canopy temperature differences vary throughout the day. Maximum difference of 0.94°C was found at midday, being lower in the infected leaf (Table 2). During sunrise and sunset, the infected leaf was hotter than the healthy leaf by a 0.35°C or less.

6.5.3 Trunk measurements

Dendrometers monitor physiological activity, including the plant transpiration cycle and the plant water storage capacity (Cocozza et al., 2018). The majority of diurnal stem diameter changes result from elastic cambial and phloem tissues thickness fluctuations. Daily exchange of water between phloem and xylem is affected by the perspiration of water stored in the trunk of the tree and by the rate of water absorption from the root in the soil. The wavelet analysis showed that most trees had a mean phase angle indicating daily shrinkage, whereas others exhibited daily expansion (Herrmann et al., 2016). Although (Scalisi et al., 2017), mentioned that stem diameter variations do not reveal useful information on fruit and leaf status in this case the information was valuable. The different phenological stages of the tree, together with water application changes helped to understand better the dendrometer response.

In this experiment, stress days in May with no watering in the healthy tree did not show stem growth, and several peaks were noted in the 10:00-15:00 interval. Trees with deeper roots recover within a period of few days from water stress. The period depends on the water stress severity and on the amount of water supplied for rewatering. Stomatal conductance takes longer to recover (Fernández, 2014).

Dendrometer measurements explain how the tree reacts against the infection after analyzing MXD and MND average values under water stress (Table 1). Under this condition, MND shrinkage is lower in the infected tree than in the healthy tree, reducing even more water transport for evapotranspiration. Under scarce water in the soil, MXD in the infected tree is higher than in the healthy tree, to store more water for plant operational activities and disease control. Under this state, new floral sprouts did not produce any inflorescence.

In trees, higher evapotranspiration is noted as trunks shrink, and water flows directly from soil to leaves. As trunk stores water, the dendrometer detects trunk expansion in middle-peaks or MXD. Trees exhibit diurnal shrinkage, but diurnal expansion and lack of a consistent pattern were apparent during June 17th and June 18th (Fig. 1B). The healthy tree presented a higher MXD than the IT, but a lower MND value. Morning slopes were steeper in the infected tree, so MND peak timings occurred earlier in the IT than in the healthy tree.

The healthy tree trunk presented water peaks in the morning providing water to its fruits weighting between 250 and 500 grams. The infected tree did not present a single fruit. During mango fruit growth, when carbohydrates demanded by the fruit are higher than the supplied by photosynthesis, the fruit may obtain assimilates from leaf and stem reserves (Léchaudel et al., 2005). Under natural conditions, the contribution of initial fruit dry mass from stem reserve mobilization is 67.6%.

Almost one month later, after some raining days and rewatering, MXD and MCD values increased daily, resulting in a trunk irreversible growth in the healthy tree. After comparing both trees IT and HT, MXD average values under watering conditions show similar values (Table 1). As soil water is always available for evapotranspiration, IT and HT present MND average values of -29.4 and -26.4, respectively, being a difference of 11%. Stomata conductance is affected by the disease and causes MND variations which can be observed by NIR (near infrared) spectral analysis. In the NIR spectral range, infected leaves present lower values than healthy leaves, caused by cell structure changes (Hahn, 2009; Krezhova et al., 2017). Cell structure changes in infected leaves are detected by NIR spectroscopy, presenting lower spectral values than those of healthy leaves (Hahn, 2009; Krezhova et al., 2017).

Although MXD, MND and MCD are the main dendrometer variables reported by researchers, morning slopes help to diagnose when the flower-fruit period of the trees is over. The slope becomes more gentle (dark line), meanwhile the dot line in Fig. 6C shows the tree without infection and bearing fruit in August.

6.5.4 Sampling trees after soap solution

Dendrometer measurements after May, July and August soap solution application presented different responses. Average values after applying soap to the infected tree during May were 3.16% and 28.4% higher for MXD and MND, respectively. Water evapotranspiration increased after attacking the disease, although trunk water storage remained almost constant. The healthy tree presented a lower average MXD being 49.7% less than the obtained by the treated infected tree.

HR and maximum temperature between June 27th and June 29th were of 52% and 41.2°C, respectively. Infected tree showed Fusarium infection symptoms mainly in panicles, that disappeared after soap solution with sulphur application on July 1st afternoon. The first days after solution application, MCD was smaller as MND decreased and MXD remained constant. ET decreased, being easily observed by the leaf thickness and color cover. After soap application maximum shrinkage (MND) increased daily having a value of -6.95 µm on July 7th, reaching

-25.6 µm one week after. MXD remained with a constant value and MND value changed one week after solution application. Based on these values, trees take one week before entering the healthy stage. Several steps appear in the afternoon slope when the pathogen was present (Fig. 7).

July 5th showed less shrinkage, but the big peaks in the morning revealed fruit set. July 6th had no such big peaks, but on July 7th the peaks returned. Afternoon slope was steeper after soap application, so water within the trunk cambium re-saturated earlier in the night (Larcher, 2003). Larcher (2003) also stated that dry periods occur when tree water is not balanced over 24 hours and related it to predawn water potential.

6.6 Conclusions

As stomata close under water deficits, leaf temperatures rise and water gets stored in the trunk. In this paper, dendrometers help to visualize plants health, not only by checking its MXD and MND values. Steep morning slopes characterize a tree without fruit bearing; morning peaks in the MS show water provided for fruit growth. Dendrometer data analysis requires of plot examination and not from data average.

From all the plant based sensors, tree infection was better detected with the dendrometer morning slope (MS) and minimum diameter (MND). Also, leaf thickness with the micrometer provided a reliable measurement, but the micrometer did not provide continuous values and damage leaf tissue.

Leaf temperature and canopy were not as effective to determine leaf infection, as temperatures between infected and healthy leaves was small. Leaf turgor sensor can remain in leaves but changes in plant health were not appreciated.

Application of the solution of soap powder + sulphur dissolved in water was effective during the irrigation and raining seasons, but its operation was poor for trees under water stress condition. The magnetic probe and leaf temperature sensors did not provide proper results after the solution was applied. Dendrometer

MXD and MND values show that one week after the solution has been applied under irrigation or rain periods, tree health changes.

6.7 Acknowledgments

We would like to acknowledge Mr. Luis Lombera who took many measurements on the trees and to the Universidad Autonoma Chapingo for lending the sensors and helping us to develop the project.

6.8 References

Alberts Organics. 2016. Organic Produce from Mexico. http://albertsorganics.com/resources/merchandising-tips/organic-produce-mexico.

Britz, H., Steenkamp, E.T., Coutinho, T.A., Wingfield, B.D., Marasas, W.F.O., Wingfield, M.J., 2002. Two new species of Fusarium section Liseola associated with mango malformation. Mycologia. 94, 722-730. doi:10.1080/15572536.2003.11833199.

Bùrquez, A., 1987. Leaf thickness and water deficit in plants: a tool for field studies. J Exp Bot. 38(1), 109-114. DOI: 10.1093/jxb/38.1.109.

Cocozza, C., Tognetti, R., Giovannelli, A., 2018. High-Resolution Analytical Approach to Describe the Sensitivity of Tree–Environment Dependences through Stem Radial Variation. Forests. 9, 134. doi: 10.3390/f9030134.

Conejero, W., Mellisho, C.D., Ortuño, M.F., Moriana, A., Moreno, F., Torrecillas, A., 2011. Using trunk diameter sensors for regulated deficit irrigation scheduling in early maturing peach trees. Environmental and Experimental Botany. 71(3), 409–415. doi: 10.1016/j.envexpbot.2011.02.014.

Daudet, F.A., Ameglio, T., Cochard, H., Archilla, O., Lacointe. A., 2005. Experimental analysis of the role of water and carbon in tree stem diameter variations. J. Exp. Bot. 56, 135–144. doi: 10.1093/jxb/eri026.

Ehrenberger, W., Rüger,V., Rodríguez-Dominguez, C.M., Díaz-Espejo, A., Fernández, J.E., Moreno, J., Zimmermann, D., Sukhorukov, V.L., Zimmermann, U., 2012. Leaf patch clamp pressure probe measurements on olive leaves in a nearly turgorless state. Plant Biol. 14, 666–674. doi: 10.1111/j.1438-8677.2011.00545.x.

Fernández, J.E., 2014. Understanding olive adaptation to abiotic stresses as a tool to increase crop performance. Environ. Exp. Bot. 103, 158–179. doi: 10.1016/j.envexpbot.2013.12.003.

Freeman, S., Maimon, M., Pinkas. Y., 2000. Etiology of mango malformation disease using GUS transformants of Fusarium subglutinans. Acta Horticulture. 509, 731-758. doi: 10.17660/ActaHortic.2000.509.88.

García, I. F., Ortega, C. J., Iglesias, M., Moreno, J. M., Souza, L., Tavira, S.C., Duran, V.H., 2018. Assessing the crop-water status in Almond (Prunus dulcis Mill.) trees via thermal imaging camera connected to smartphone. Sensors, 18(4), 1050. doi:10.3390/s18041050.

Goldhamer, D.A., Fereres, E., 2004. Irrigation scheduling of almonds trees with trunk diameter sensors. Irrig Sci. 23, 11–19. doi: 10.1007/s00271-003-0088-0.

Grant, O.M., Tronina, L., Jones, H.G., Chaves, M.M., 2007. Exploring thermal imaging variables for the detection of stress responses in grapevine under different irrigation regimes. Journal of Experimental Botany. 58, 815–825. doi: 10.1093/jxb/erl153.

Hahn, F., 2009. Actual Pathogen Detection: Sensors and Algorithms - a Review. Algorithms. 2, 301-338. doi:10.3390/a2010301.

Hernandez, R., Hornero, A., Mottus, M., Penuelas, J., Gonzalez, V., Jimenez, J., Alonso, L., Zarco, P., 2019 Early Diagnosis of Vegetation Health from High-Resolution Hyperspectral and Thermal Imagery: Lessons Learned from Empirical Relationships and Radiative Transfer Modelling. Curr Forestry Rep. 5(3), 169-183. Doi:10.1007/s40725-019-00096-1.

Herrmann, V., McMahon, S.M., Detto, M., Lutz, J.A., Davies, S.J., Chang-Yang, C-H., 2016. Tree Circumference Dynamics in Four Forests Characterized Using Automated Dendrometer Bands. PLoS ONE. 11(12): e0169020. doi: 10.1371/journal.pone.0169020.

Jones, H.G., Serraj, R., Loveys, B.R., Xiong, L., Wheaton, A., Price, A.H., 2009. Thermal infrared imaging of crop canopies for the remote diagnosis and quantification of plant responses to water stress in the field. *Funct Plant Biology*. *36*(10), 978-989. doi:10.1071/FP09123.

Jones, H.G., 1999. Use of infrared thermometry for estimation of stomatal conductance as a possible aid to irrigation scheduling. Agric. For. Meteorol. 95, 139–149. doi: 10.1016/S0168-1923(99)00030-1

Kramer, P.J., Boyer, J.S., 1995. Water relations of plants and soils. Academic, San Diego.

Krezhova, D., Velichkova, K., Petrov, N., Maneva, S., 2017. The effect of plant diseases on hyperspectral leaf reflectance and biophysical parameters. Doi: 10.21175/RadProc.2017.55.

Kumar, J., Singh, U.S., Beniwal, S.P.S., 1993. Mango malformation: One hundred years of research. Annual Review of Phytopathology. 31, 217–232. Doi: 10.1146/annurev.py.31.090193.001245.

Larcher, W., 2003. Physiological plant ecology – ecophysiology and stress physiology of functional groups. Berlin, Germany: Springer.

Léchaudel, M., Génard, M., Lescourret, F., Urban, L., Jannoyer, M., 2005. Modeling effects of weather and source-sink relationships on mango fruit growth. Tree Physiol. 25, 583-597. doi: 10.1093/treephys/25.5.583.

Levin, A.G., Peres, M., Noy, M., Love, C., Gal, Y., Naor, A., 2018. The response of field-grown mango (cv. Keitt) trees to regulated deficit irrigation at three phenological stages. Irrigation Science. 36(1), 25-35. doi:10.1007/s00271-017-0557-5.

Lindenthal, M., Steiner, U., Dehne, H.W., Oerke, E.C., 2005. Effect of downy mildew development on transpiration of cucumber leaves visualized by digital infrared thermography. Phytopathology. 95, 233–240. Doi: 10.1094/PHYTO-95-0233.

Livellara, N., Saavedra, F., Salgado, E., 2011. Plant based indicators for irrigation scheduling in young cherry trees. Agricultural Water Management. 98, 684–690. doi: 10.1016/j.agwat.2010.11.005.

Martínez, M.A., Castiella, M., Rüger, S., Intrigliolo, D.S., Ballester, C., 2017 Evaluating the usefulness of continuous leaf turgor pressure measurements for the assessment of Persimmon tree water status. Irrig Sci. 35 (2), 159-167. doi:10.1007/s00271-016-0527-3.

Meng, Z., Duan, A., Chen, D., Dassanayake, K.B., Wang, X., Liu, Z., 2017. Suitable indicators using stem diameter variation-derived indices to monitor the water status of greenhouse tomato plants. PLoS ONE 12(2), e0171423. doi:10.1371/journal.pone.0171423.

Meroni, M., Rossini, M., Colombo, R., 2010. Characterization of leaf physiology using reflectance and fluorescence hyperspectral measurements. In: Maselli F, Menenti M, Brivio PA (eds): Optical observation of vegetation properties and characteristics. Research Signpost, Trivandrum, pp 165–187.

Michel, A.C., Sánchez, M.A., Díaz, A., Martínez, R.D., Ariza, R., Barrios, A., 2013. Biocontrol de la "Escoba de Bruja" del Mango, con Trichoderma spp., en Condiciones de Campo. Revista mexicana de fitopatología. 31(1), 1-12.

Moreno, F., Conejero, W., Martin-Palomo, M.J., Girón, I.F., Torrecillas, A., 2006 Maximum daily trunk shrinkage reference values for irrigation scheduling in olive trees. Agricultural Water Management. 84, 290–294. doi: 10.1016/j.agwat.2006.03.005.

Noriega, D.H., Téliz, D., Mora, G., Rodríguez, J., Zavaleta, E., Otero, G., Campbell, C.L., 1999. Epidemiology of mango malformation in Guerrero, México, with traditional and integrate management. Plant Disease. 83, 223-228. doi:10.1094/PDIS.1999.83.3.223.

Ortuño, M.F., Conejero, W., Moreno, F., Moriana, A., Intrigliolo, D.S., Biel, C., Mellisho, C.D., Perez-Pastor, A., Domingo, R., Ruiz-Sanchez, M.C., Casadesus, J., Bonany, J., Torrecillas, A., 2010. Could trunk diameter sensors be used in woody crops for irrigation scheduling? A review of current knowledge and future perspectives. Agricultural Water Management. 97, 1–11. doi: 10.1016/j.agwat.2009.09.008.

Ortuño, M.F., Alarcón, J.J., Nicolás, E., Torrecillas, A. 2004. Comparison of continuously recorded plant-based water stress indicators for young lemon trees. Plant Soil. 267, 263-270. doi:10.1007/s11104-005-0108-3.

Petrie, P.R., Wang, Y., Liu, S., Lam, S., Whitty, M.A., Skewes, M.A., 2019. The accuracy and utility of a low cost thermal camera and smartphone-based system to assess grapevine water status. Biosystems Engng. 179, 126-139. doi:10.1016/j.biosystemseng.2019.01.002.

Rodriguez, V., Hernandez, V., Buckley, T.N., Fernández, J.E., Diaz-Espejo, A., 2019. Sensitivity of olive leaf turgor to air vapour pressure deficit correlates with diurnal maximum stomatal conductance. Agricultural and Forest Meteorology. 272, 156-165. Doi: 10.1016/j.agrformet.2019.04.006.

Rüger S, Ehrenberger, W., Arend, M., Geßner, P., Zimmermann, G., Zimmermann, D., Bentrup, F.W., Nadler, A., Raveh, E., Sukhorukov, V.L., Zimmermann, U., 2010. Comparative monitoring of temporal and spatial changes in tree water status using the non-invasive leaf patch clamp pressure probe and the pressure bomb. Agr Water Manag 98, 283– 290. doi: 10.1006/j.agwat.2010.08.022.

Scalisi, A., Bresilla, K., Grilo, F., 2017. Continuous determination of fruit tree water-status by plant-based sensors. Italus Hortus. 24, 39-50. doi: 10.26353/j.itahort/2017.2.3950.

Singh, Z., 2005. Embryo abortion in relation to fruit size, quality, and concentrations of nutrients in skin and pulp of mango. J. Plant Nutr. 28(10), 1723–1737. doi: 10.1080/01904160500250771.

UNComtrade., 2016. World Mango Exports by All Reporters and Partners, 2005-2015 (based on HS80540). United Nations Statistics Division (UNSD).

West, J.S., Bravo, C., Oberti, R., Lemaire, D., Moshou, D., McCartney, H.A. 2003. The potential of optical canopy measurement for targeted control of field crop diseases. Ann Rev Phytopathol. 41, 593–614. Doi: 10.1146/annurev.phyto.41.121702.103726.

Zimmermann, D., Reuss, R., Westhoff, M., Gessner, P., Bauer, W., Bamberg, E., Bentrup, F.W., Zimmermann, U., 2008. A novel, non-invasive, online-monitoring, versatile and easy plantbased probe for measuring leaf water status. J Exp Bot 59:3157–3167. doi: 10.1093/jxb/ern171.

Zitter, T.A., 1999. Fusarium wilt of melon, a worldwide problem in temperate and tropical regions. Acta Horticulturae. 492, 157–161. doi: 10.17660/ActaHortic.1999.492.18.

Zweifel, R., Haeni, M., Buchmann, N., Eugster, W., 2016. Are trees able to grow in periods of stem shrinkage? New Phytologist. 211, 839-849. doi:10.1111/nph.13995.

Zweifel, R., Item, H., Hasler, R., 2000. Stem radius changes and their relation to stored water in stems of young Norway spruce trees. Trees. 15, 50–57. doi: 10.1007/s004680000072.

7 ANEXOS

7.1 Gestión de energía

Para lograr el objetivo de consumo de energía bajo, el cual brinde los 8 días de autonomía de las baterías, no se quiso depender de que cada dispositivo (como la tarjeta MSD, el reloj, la resistencia y el bluetooth) tenga poca energía inactiva. Entonces en lugar de eso la placa cuenta con una línea normal de GND para alimentar el microcontrolador y luego una línea conmutada de GND_sw, que alimenta a los sensores. GND_ se puede activar o desactivar a través del uso de un pin digital (Pin_D0) del microcontrolador (Figura 1).

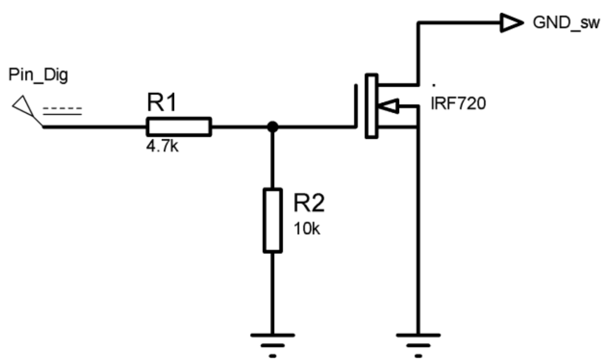

Figura 1 Diagrama de conexión del Mosfet IRF720

Un MOSFET de canal N se usa para proporcionar una interrupción de “lado bajo”. Para activar un MOSFET de canal N, la terminal de la puerta puede ser más positiva que la fuente. Al poner el Pin_D0 en alto la terminal de la puerta obtendrá 5V, el MOSFET conducirá, lo que significa que ahora pasa el GND_sw en el drenaje.

La resistencia de 4.7 k Ω limita la corriente para proteger el pin de salida. La resistencia de 10 kΩ proporciona un pull-down fuerte que garantizar que la puerta tenga un valor lógico bajo cuando el procesador esta encendido.

La funcion para encender los periféricos es:

```
void Prender(int PIN){
  digitalWrite(PIN, HIGH);
```

```
}
```

Siendo la función para apagar los perifiericos:

```
void Apagar(int PIN){
   digitalWrite(PIN, LOW);
}
```

7.1.1 Consumo de energía

Las pruebas que se revelaron en el capítulo 5 del el uso del Mosfet, combinada con el microcontrolador en modo de suspensión, mostraron que durante el uso del temporizador de vigilancia (necesario para activar el procesador y tomar lecturas) se consume alrededor de 4 mA de corriente. Sin embargo, si no se usara el modo ahorro de energía el microcontrolador consumiría alrededor de 26 mA. Al tomar 10 lecturas cada 10 minutos la mayor parte del tiempo estará en modo de bajo consumo de energía (Figura 2).

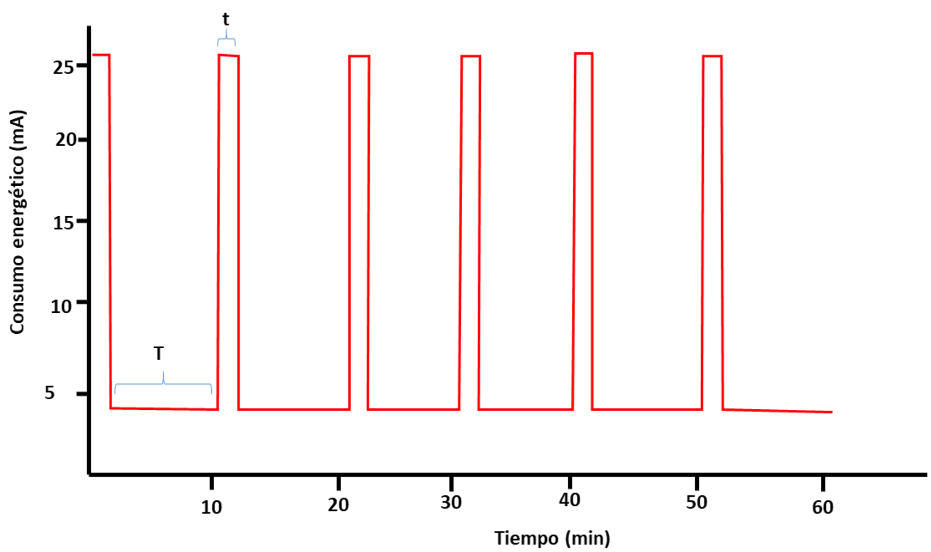

Figura 2 Ciclo de consumos con respecto al tiempo. T=Consumo bajo; t=consumo alto

Una batería de LiOn de 4.2 V modelo 18650, tiene una capacidad de 2200 mAH. Es decir, que puede proporcionar un mA durante 2200 horas, a continuación se muestra el cálculo del consumo promedio durante una hora de medición y el número de días capaz de proporcionarnos la batería al estar completamente cargada:

$$Consumo\ energetico = \ (duracion * ciclos * consumo\ de\ funcion)$$

$$Consumo\ bajo = \ \left(\frac{590\ s}{3600\ s} * h * \frac{6\ ciclos}{h} * 4\ mA\right) = 3.93\ mA$$

$$Consumo\ anto = \ \left(\frac{10\ s}{3600\ s} * h * \frac{6\ ciclos}{h} * 26\ mA\right) = 2.77x10^{-3}\ mA$$

$$Consumo\ total = 3.93 + 2.77x10^{-3} \ = 3.9327\ mA$$

$$\frac{2200\ mAh * día}{3.9327\ mA * 24\ h} = 23.30\ días$$

Claramente la batería pasa del supuesto estimado como óptimo. Por su puesto escribir en la tarjeta MSD y el uso del Bluetooth se consume energía, por lo que las cifras no serán tan buenas, al igual que la edad de la batería es un factor que va afectando a la retención de energia

7.2 Código

El diagrama de flujo (Figura 3) muestra la representación gráfica que desglosa el proceso realizado por el dendrómetro durante la toma de decisiones. Al encenderse el arduino se ejecutara el código del setup() y luego el bucle infinito loop() el cual se repite de forma indefinida hasta que se apague o reinicie el microcontrolador. Sin embargo para este caso en particular, la rutina del microcontrolador inicia con la definición de las librerías que serán ocupadas por los distintos sensores y sistemas de comunicación. Posteriormente iniciamos el void setup(), que es la primera funcion de la programación en arduino y que queremos que se ejecute solo una vez. Aquí, básicamente establecemos los criterios con los que trabajara el microcontrolador arduino: comunicación serial, determinación de pines de entrada y salida, detección y ajuste de sensores.

Como tercer paso, iniciamos la funcion loop(), esta se estará ejecutando un número infinito de veces haciendo la comparación de la hora en tiempo real, proporcionada a través de la funcion *DateTime now = RTC.now()* que proporciona la librería *RTClib*, guardando el valor en una variable llamada “*min*”, el cual en una sentencia de “*If*” se compara si el valor es múltiplo de 10, que representa a realizar la medición cada 10 minutos. Si la sentencia resulta negativa el microcontrolador dormirá durante 8 segundos. Cumplido ese tiempo se llama a una interrupción “*watchdog*” para despertar el microcontrolador e inicie el programa de comparación.

Por otro lado, si la variable “min” tiene un múltiplo de 10 entra a la funcion “*tomar_lecturas()”* en la cual se llaman funciones por separado de cada sensor en particular (estas funciones y su funcionalidad se detallan posteriormente) y de la memoria micro SD. Al finalizar esta funcion se guardan los datos en la memoria micro SD y se entra en el estado de sueño del microcontrolador.

El programa utiliza las siguientes librerías:

- **watchdog**, para interrupciones software,
- **softwareserial** para añadir puertos serie adicionales (para bluetooth),
- **LowPower** para utilizar el modo de bajo consumo donde más partes de nuestros micro están desactivadas, dejando solo interrupciones hardware para sacarlo de ese estado el cual es "sleep mode power down",
- **SD/SPI**, para la memoria SD
- **WIRE/RTClib** para reloj RTC,
- **DHT** para sensor de temperatura/humedad relativa.
- **Adafruit_MLX90614** para el sensor infrarrojo

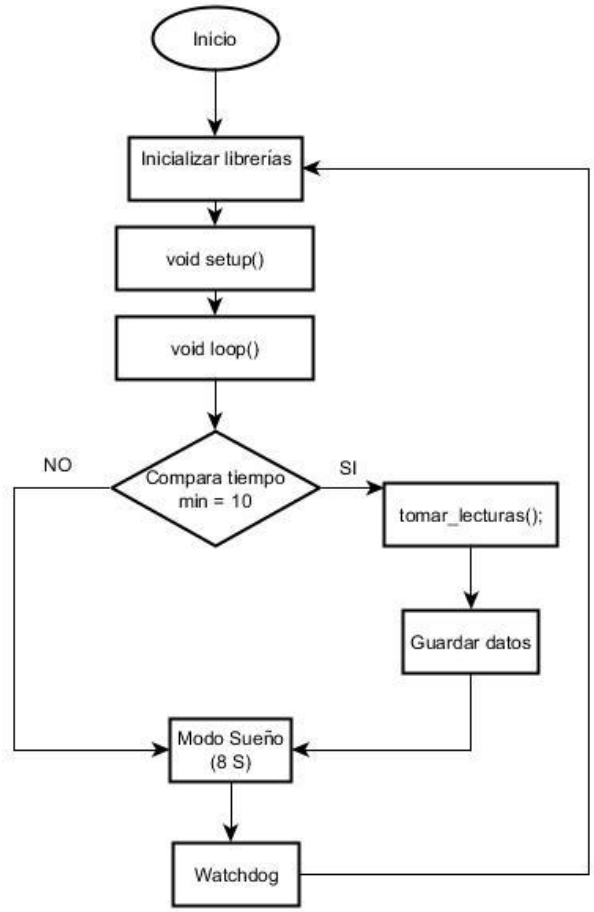

Figura 3 Diagrama de flujo del programa

Posteriormente el programa está compuesto por una serie de rutinas de código, las cuales brindan la funcionalidad al dendrómetro, la función principal loop() describe el proceso de comparación de tiempo para realizar las mediciones de las diferentes variables estudiadas, se describe a mayor detalle esta funcion:

loop()

En el loop, se toma la hora actual del RTC, se guarda el minuto actual en la variable minute. Posteriormente se compara si esta variable es múltiplo de 10, en caso de serlo, el microcontrolador dispara el proceso de medición llamado “tomarlecturas ()” donde se realizan las mediciones y el almacenamiento de los datos (Figura 4). En caso contrario, se pone en modo ahorro de energía durante 6 ciclos de 8 s, dando 1 minuto en modo de bajo consumo, después de este minuto se vuelve a comparar el minuto actual. El microcontrolador despierta a través de una interrupción por software (watchdog). Esto es así, debido a que cuando se utiliza este modo de sleep, los timer como la función millis (), microsecond (), etc, se paralizan debido a que se apagan al entrar en modo power_down.

```
void loop() {
wdt_reset();
Wire.begin();
DateTime now = RTC.now();
counter++;
if (counter >= 6){
getTime ();
if((minute %TIEMPO_ENTRE_LECTURA) == 0){
tomarlecturas();
        }
counter = 0;
}
serialEvent();
delay(100);
flashLED (1);
Apagar(PinTransistor);
LowPower.powerDown(SLEEP_8S, ADC_OFF, BOD_OFF);
}
```

La funcion tomarlecturas (), inicia dando una señal lumínica a través de la funcion flasLED (), prendiendo el MOSFET que alimentara a los sensores y comprobando que la memoria SD esté conectada, esto se comprueba con la funcion iniciaSD (). Posteriormente hace una búsqueda de la existencia del archivo donde se guardaran los datos, de no encontrarlo llama a la funcion names (), que crea el archivo y le da los nombres a los encabezados. Al comparar que si existe el archivo, ya sea que ya estaba o que fue creado, se procede a abrirlo. La apertura del archivo permite guardar los datos adquiridos por las funciones: writeDateTime (); leerDHT22 (); leerMLX (); voltimetro (); LM35 (). Estas funciones se describen a mayor detalle posteriormente. Cuando se llega a la última funcion, que en este caso es la LM35 (), se procede a dar un salto de línea en el archivo (\n) y luego a cerrarlo. La culminación de la funcion viene dada por la llamada nuevamente de la funcion flasLED ().

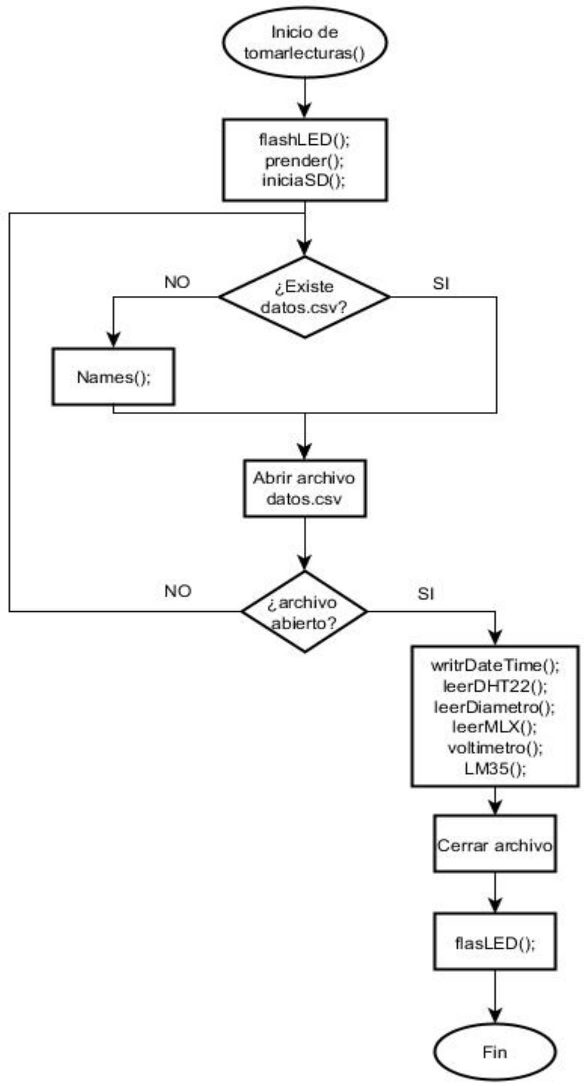

Figura 4 Diagrama de flujo de la funcion tomarlecturas ().

El archivo creado durante la apertura de la funcion tomarlecturas () tiene el formato de tabla de calculo, es decir una extencion “CSV”. El archivo de salida es “Datos.csv” en el directorio raíz (Figura 5). Los ficheros CSV, si se exportan a Excel, utilizan la primera línea para indicar los nombres de las columnas, y el resto de filas, son los datos adquiridos a lo largo de la temporada de mediciones.

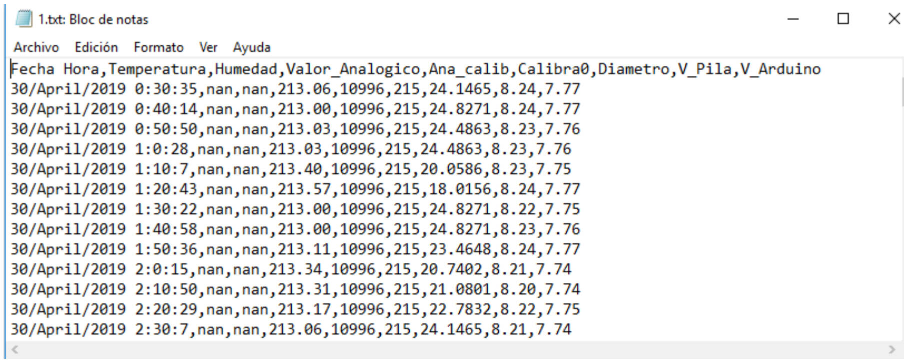

1.txt: Bloc de notas

Archivo Edición Formato Ver Ayuda

```
Fecha Hora,Temperatura,Humedad,Valor_Analogico,Ana_calib,Calibra0,Diametro,V_Pila,V_Arduino
30/April/2019 0:30:35,nan,nan,213.06,10996,215,24.1465,8.24,7.77
30/April/2019 0:40:14,nan,nan,213.00,10996,215,24.8271,8.24,7.77
30/April/2019 0:50:50,nan,nan,213.03,10996,215,24.4863,8.23,7.76
30/April/2019 1:0:28,nan,nan,213.03,10996,215,24.4863,8.23,7.76
30/April/2019 1:10:7,nan,nan,213.40,10996,215,20.0586,8.23,7.75
30/April/2019 1:20:43,nan,nan,213.57,10996,215,18.0156,8.24,7.77
30/April/2019 1:30:22,nan,nan,213.00,10996,215,24.8271,8.22,7.75
30/April/2019 1:40:58,nan,nan,213.00,10996,215,24.8271,8.23,7.76
30/April/2019 1:50:36,nan,nan,213.11,10996,215,23.4648,8.24,7.77
30/April/2019 2:0:15,nan,nan,213.34,10996,215,20.7402,8.21,7.74
30/April/2019 2:10:50,nan,nan,213.31,10996,215,21.0801,8.20,7.74
30/April/2019 2:20:29,nan,nan,213.17,10996,215,22.7832,8.22,7.75
30/April/2019 2:30:7,nan,nan,213.06,10996,215,24.1465,8.21,7.74
```

Figura 5 Fichero Datos.CSV creado en la funcion tomarlecturas ().

A continuación se da una explicación más detallada de funciones del programa:

iniciaSD():

Inicia la comunicación del módulo SD con el microcontroladora a través de un pin de comunicación y la librería "*SD.h*".

```
void iniciaSD(){
if (!SD.begin(SDPIN)){
  pinMode(SDPIN, OUTPUT);
  }
}
```

existe():

Comprueba si el fichero existe en la memoria SD, en caso de no existir se crea el fichero y se envía la línea de nombres (name).

```
 void LeerDatos(){
  if (!SD.begin(SDPIN)) {
Serial.println (F("Fallo lectura de memoria!"));
name();
while (1);
  }
  Serial.println(F("Archivo Datos..."));
}
```

names():

Escribe la línea de nombres de encabezado de las columnas la cual identifica a todos nuestros valores a guardar.

```
void names(){
//            ESCRIBIENDO DATOS EN LA MEMORIA SD DE ARDUINO
  //Se abre el documento sobre el que se va a leer y escribir.
  Archivo = SD.open("datos.csv", FILE_WRITE);
  //Se comprueba que el archivo se ha abierto correctamente y se procede a escribir
  if (Archivo){
Archivo.println(F("Fecha,Hora,Temperatura,Humedad,Valor_analogico,Analog_Calibra0,Calibra0,Diametro,MLX_Ambiente,MLX_Hoja,V_Pila,V_Arduino,LM35"));
    Archivo.close();
  }
  //            FIN DE LA ESCRITURA DE DATOS EN LA MEMORIA SD DE ARDUINO
}
```

leerDHT22():

El sensor utilizado para monitorear la temperatura y la humedad relativa es el DTHT22. Integra un sensor capacitivo de humedad y un termistor para medir el aire circulante. Muestra los datos mediante el pin de datos de manera digital. Este sensor requiere una pequeña resistencia de pull-up de 10 k entre el pin de datos y el Vdd, por que usa una configuración de drenaje abierto para cambiar entre el procesador que envía el pulso y recibe la respuesta.

El sensor está conectado a la línea GND_sw y requiere una lectura de aproximadamente de 2 segundos después de ser encendido, por lo que hay un retraso de 2 segundos incorporados en el código. La funcion lee la temperatura y humedad relativa del sensor. Esos datos leídos se guardan en el “Archivo” creado.

```
void leerDHT22(){
//Leyendo datos sensor DHT22
  //Serial.println(F("DHT"));
  float temp = dht.readTemperature(); //Se lee la temperatura
  float hum = dht.readHumidity(); //Se lee la humedad

  // El archivo se encuentra abierto
  Archivo. print (temp);
  Archivo.print(F(","));
  Archivo.print(hum);
  Archivo.print(F("," ));
}
```

writeDateTime():

Para el registro del tiempo, se incorporó el chip DS1307RTC. Tiene un circuito inter-integrado (I^2C) con el fin de controlar varios chips de manera sencilla. Es un protocolo de comunicación síncrono vía SDA, sincronizado por una señal de reloj vía SCL. El RTC utiliza como batería modelo CR2032 de 3 V, como la batería de respaldo. El chip está conectado a la línea GND_sw por lo que se apaga cuando no es necesario. La funcion escribe la fecha y hora completa en el fichero de la SD cada que se entra en un ciclo de medición.

```
void writeDateTime(){
  //Serial.println(F("tiempo"));
  Archivo.print(day);
  Archivo.print(F("/"));
  Archivo.print(month);
  Archivo.print(F("/"));
  Archivo.print(year);
  Archivo.print(F(" "));
  Archivo.print(hour);
  Archivo.print(F(":"));
  Archivo.print(minute);
  Archivo.print(F(":"));
  Archivo.print(second);
  Archivo.print(F(","));
}
```

flashLED ()

Esta funcion concretamente realiza la acción de prender y apagar un led durante intervalos preestablecidos en la programación, recibiendo el número de parpadeos que el pin LED dará.

```
void flashLED (const byte Tiempos)
  {
  // flash LED
  for (int i = 0; i < Tiempos; i++)
    {
    digitalWrite (LED, HIGH);
    delay (20);
    digitalWrite (LED, LOW);
    delay (300);
```

```
  }
}  // fin de flashLED
```

LM35()

La funcion LM35(), mide la temperatura del ambiente a través de es un sensor de temperatura analógico LM35. La temperatura es proporcionada en el momento que inicien las mediciones, su precisión es de 1 °C. Se hace ***n*** cantidad de mediciones y se promedian entre sí, para tener un valor de la temperatura media en el instante. Este valor final es guardado en el archivo creado en la SD.

```
void LM35(){
  int n = 10;
  float valor_analogico_LM35 = 0;
  for(int i =0; i<n;i++){
    valor_analogico_LM35 += analogRead(PIN_LM35);

  }
  valor_analogico_LM35 = (valor_analogico_LM35/n);
  float Valor_Temperatura_Suelo = (5.0*valor_analogico_LM35*100.0)/1024.0;
  Archivo.println(Valor_Temperatura_Suelo);
}
```

Voltimetro()

La funcion voltímetro() se ocupa para verificar el valor de voltaje que posee la batería, al igual que el voltaje que el arduino proporciona a los sensores, esto con el fin de almacenar en el archivo creado las variaciones y posteriormente hacer correcciones por picos de voltaje en las medicines de los sensores. Esta funcion hace uso de un divisor de voltaje, donde el voltaje de salida es una fracción al voltaje de entrada. De manera física está constituido por dos resistencias en serie de 1 MΩ aproximadamente. Esto con el fin de evitar consumos altos de energía por pérdidas de calor en las mismas resistencias.

```
void Voltímetro(){
float v1 = 4.95; // valor real de la alimentación de Arduino, Vcc
  float r1 = 997000;
  float r2 = 1018000;
  float R1 = 997000;
  float R2 = 1018000;//1018000;
```

```
float Volt1 = 0;
float Volt2 = 0;
int n = 100;
for (int i=1; i <=n; i++){
  Volt1 += (analogRead(1) * v1) / 1024.0;
  delay(2);
  Volt2 += (analogRead(2) * v1) / 1024.0;
  delay(2);
}
float voltaje1= Volt1/n;
float voltaje2 = Volt2/n;
float V_Pila = (voltaje1 / (r2 / (r1 + r2)));
float V_Arduino = (voltaje2 / (R2 / (R1 + R2)));
Archivo.print(V_Pila);
//Serial.print(V_Pila);
Archivo.print(F(","));
Archivo.print(V_Arduino);
Archivo.print(F(","));
//Serial.println(V_Arduino);
}
```

leerMLX()

En esta funcion se hace uso del sensor infrarrojo Melexis 90614, el cual es un termómetro infrarrojo para mediciones de temperatura sin contacto de la hoja y del ambiente. Posee una resolución de medición de 0.02 °C y una precisión de 0.5 °C. Los valores de la hoja y el ambiente son almacenados en el archivo de la SD

```
void leerMLX(){
   float T_MlxAmbient = mlx.readAmbientTempC();
   float T_MlxHoja = mlx.readObjectTempC();
  Archivo.print(T_MlxAmbient );
  Archivo.print(F(","));
  Archivo.print(T_MlxHoja);
  Archivo.print(F(","));*/
}
```

leerDiametro()

Consta de una resistencia variable (BEI sensors 9605R1.7KL2.0), conectada a través de una fuente de corriente constante (LM334) que se alimentó directamente de la batería. Después de este arreglo, la resolución de la resistencia aumento. Sin embargo, proporciono un voltaje de 0-7 V, sin embargo se adaptó un diodo Zener para ajustar el voltaje a un máximo de 4.7 V, que es adecuado para el microcontrolador. En esta funcion inicializamos la variable donde se almacenaran los valores obtenidos de la resistencia variable, estos valores serán medidos y promediados ***n*** número de veces para después ser almacenados en el archivo de la SD

```
void leerDiametro(){
 float Sensor = 0;
 int n = 35;
  for(int i = 0; i<n; i++){
     int Valor_analogico = analogRead(PinHall);
     Sensor += analogRead(PinHall);
     delay(50);// tiempo de reaccion del sensor en milisegundos
  }
  float Valor_sensor = Sensor / n;
  um =  (-11.921*Valor_sensor + 13560);
  Archivo.print(Valor_sensor, 5);
  Archivo.print(F(","));
  Archivo.print(um, 5);
  Archivo.print(F(","));
```

tomarlecturas():

Esta funcion se inicializa cuando el tiempo de medición se cumplió, en ella se llaman las funciones que poseen sensores o están en coexistencia con ellos. Primero se inicia el módulo SD para trabajar con él, comprueba si el fichero donde se almacenaran los datos medidos existe, para escribir los valores tomadas, de lo contrario creara el fichero. Posteriormente entra a cada una de las funciones necesarias para la medición.

```
void tomarlecturas(){
 flashLED (3);
 Prender(PinTransistor);
 iniciaSD();
 if(!SD.exists("datos.csv")){
  names();
 }
 else{
    Serial.println(F("Escribiendo datos"));
 Archivo = SD.open("datos.csv",FILE_WRITE);
```

```
if (Archivo){
  delay(3000);
  writeDateTime(); //Escribimos la hora de la medicion
  leerDHT22();
  leerDiametro();
  leerMLX();
  Voltimetro();
  LM35();
  Archivo.close();
  Serial.println(F("Guardado 1"));
  flashLED (3);
}
//En caso de que haya habido problemas abriendo datos.csv, se muestra por pantalla.
else{
  Serial.println(F("El archivo de datos no se abrio correctamente"));
}
}
```

serialEvent()

En esta funcion verificamos si en la comunicación serial existe algún intento de petición de acción de algún equipo (computadora o teléfono). Si encontramos algún dato, lo verificamos en la base de datos y comprobamos que petición se realizó.

```
// Si esta disponible el puerto serial leemos los datos
while (Serial.available()) {
  // Obtiene el siguiente byte que se recibió, este es un carácter
  char comando = (char)Serial.read();
  // Dependiendo del carÃ¡cter recibido ejecutamos una acción
  switch (comando) {
    case 'A':
      LeerDatos();
      break;
    case 'B':
      LeerCalibracion();
      break;
    case 'C':
      Borrar_Archivo_Datos();
      break;
    case 'D':
      Borrar_Archivo_Calibracion();
      break;
    default:
```

```
      // Si no es ningún carácter de comando regresamos el siguiente mensaje
      Serial.print(comando);
      Serial.println(F(": Comando no reconocido"));
      break;
    }
  }
}
```

LeerDatos()

En esta funcion se envían de manera serial los datos almacenados en el archivo creado o un error si es que no existe el archivo slicitado

```
void LeerDatos(){
  if (!SD.begin(SDPIN)) {
    Serial.println(F("Fallo lectura de memoria!"));
    while (1);
  }
  Serial.println(F("Archivo Datos..."));

  // re-open the file for reading:
  Archivo = SD.open(F("datos.csv"));
  if (Archivo) {
    Serial.println(F("datos.csv:"));

    // read from the file until there's nothing else in it:
    while (Archivo.available()) {
      Serial.write(Archivo.read());
    }
    // close the file:
    Archivo.close();
  } else {
    // if the file didn't open, print an error:
    Serial.println(F("error abriendo datos.csv"));
  }
}
```

Borrar_Archivo_Datos()

En eta funcion se ejecuta la eliminacion del archivo seleccionado, el cual se pierde definitivamente a menos de haber hecho una copia de seguridad.

```
void Borrar_Archivo_Datos(){
    Serial.println(F("Borrando Archivo Datos.txt..."));
  SD.remove("datos.txt");
```

```
  if (SD.exists("datos.csv")) {
    Serial.println(F("datos.txt aun existe."));
  } else {
    Serial.println(F("datos.txt no existe."));
  }
}
```

void fijarHora ()

Esta funcion solo se usa una vez, cada que le cambiamos la batería de respaldo al RTC, ya que aunque desconectemos el microcontrolador el RTC no perderá la hora debido a su batería. Posteriormente esta funcion se tiene que volver comentario para que el RTC no este en continua programación de la hora.

```
void fijarHora(){
  //SI hace falta configurar la hora real en el RTC
  rtc.setDOW(WEDNESDAY);        // Set Day-of-Week to FRIDAY
  rtc.setTime(21, 52, 0);     // Set the time to 12:00:00 (24hr format)
  rtc.setDate(6, 3, 2018); // Set the date to August 6th, 2010
}
```

7.3 Solicitud de Patente

Instituto Mexicano de la Propiedad Industrial

INSTITUTO MEXICANO DE LA PROPIEDAD INDUSTRIAL
Dirección Divisional de Patentes

[X] Solicitud de Patente [ ] Solicitud de Registro de Modelo de Utilidad [ ] Solicitud de Registro de Diseño Industrial, especifique cuál: [ ] Modelo Industrial [ ] Dibujo Industrial	Uso exclusivo Delegaciones y Subdelegaciones de la Secretaría de Economía y Oficinas Regionales del IMPI Sello Folio de entrada Fecha y hora de recepción

Solicitud
Expediente: MX/a/2018/007965
Fecha: 27/JUN/2018 Hora: 13:01:37
Folio: MX/E/2018/047701 656062

Antes de llenar la forma lea las consideraciones generales al reverso

I DATOS DEL (DE LOS) SOLICITANTE(S)

El solicitante es el inventor [ ] El solicitante es el causahabiente [X]

1) Nombre (s):
UNIVERSIDAD AUTÓNOMA CHAPINGO
2) Nacionalidad (es):
MEXICANA
3) Domicilio; calle, número, colonia y código postal: KM.38.5, CARRETERA MÉXICO-TEXCOCO, SN, CHAPINGO, C.P. 56230
Población, Estado y País: TEXCOCO, ESTADO DE MÉXICO, MÉXICO
4) Teléfono (01595) 95-21500 EXT. 6080 Y 5209 5) Fax (clave):

II DATOS DEL (DE LOS) INVENTOR(ES)

6) nombre (s):
DR. FEDERICO FÉLIX HAHN SCHLAM e ING. JESÚS ANTONIO GARCÍA MARTÍNEZ
7) nacionalidad (es):
MEXICANA
8) Domicilio; calle, número, colonia y código postal: CALLE PARASITOLOGÍA No. 1, Col. de Profesores Chapingo, C.P. 56230
Población, Estado y País: TEXCOCO, ESTADO DE MÉXICO, MÉXICO
9) Teléfono (clave): (01595) 95-21500 EXT. 6080 Y 5209 10) Fax (clave):

III DATOS DEL (DE LOS) APODERADO (S)

11) Nombre (s): LIC. JUAN LUIS MORENO ARELLANO 12) R G P:

13) Domicilio; calle, número, colonia y código postal:
CALLE IRRIGACIÓN, 28, CHAPINGO C.P. 56230
Población, Estado y País: TEXCOCO, ESTADO DE MÉXICO, MÉXICO 14) Teléfono (clave): (01595) 95-21500 EXT. 6080 Y 5209 (15) Fax (clave):
16) Personas Autorizadas para oír y recibir notificaciones:
LIC. PAOLA CAROLINA FERNÁNDEZ REYES

17) **Denominación o Título de la Invención:**

SISTEMA PARA DETERMINAR LA CONDICIÓN HÍDRICA DE UN HUERTO PARA SER USADO POR PRODUCTORES SIN CONOCIMIENTOS EN EL ÁREA

18) **Fecha de divulgación previa** Día Mes Año
19) **Clasificación Internacional** uso exclusivo del IMPI
20) **Divisional de la solicitud** Número Figura jurídica
21) **Fecha de presentación** Día Mes Año

22) **Prioridad Reclamada:**

País	Fecha de presentación Día	Mes	Año	No. de serie

Lista de verificación (uso interno)

No. Hojas		No. Hojas	
X 1	Comprobante de pago de la tarifa	X 2	Documento de cesión de derechos
X 35	Descripción y reivindicación (es) de la invención		Constancia de depósito de material biológico
X 10	Dibujo (s) en su caso		Documento (s) comprobatorio(s) de divulgación previa
X 1	Resumen de la descripción de la invención		Documento (s) de prioridad
X 1	Documento que acredita la personalidad del apoderado		Traducción
		50	TOTAL DE HOJAS

Observaciones: 14 Hojas de copia de Acta Constitutiva

Bajo protesta de decir verdad, manifiesto que los datos asentados en esta solicitud son ciertos.

JUAN LUIS MORENO ARELLANO
Nombre y firma del solicitante o su apoderado

CHAPINGO, ESTADO DE MÉXICO A 25-JUNIO-2018
Lugar y fecha

Página 1 de 2 IMPI-00-009